AIAA 2000-1772

Contributions of the NASA Langley Transonic Dynamics Tunnel to Launch Vehicle and Spacecraft Development

Stanley R. Cole, Donald F. Keller, and David J. Piatak

NASA Langley Research Center
Hampton, VA 23681

AIAA Dynamics Specialists Conference
April 5-6, 2000
Atlanta, GA

CONTRIBUTIONS OF THE NASA LANGLEY TRANSONIC DYNAMICS TUNNEL TO LAUNCH VEHICLE AND SPACECRAFT DEVELOPMENT

Stanley R. Cole,* Donald F. Keller,† and David J. Piatak‡
Aeroelasticity Branch
NASA Langley Research Center
Hampton, VA 23681

ABSTRACT

The NASA Langley Transonic Dynamics Tunnel (TDT) has provided wind-tunnel experimental validation and research data for numerous launch vehicles and spacecraft throughout its forty year history. Most of these tests have dealt with some aspect of aeroelastic or unsteady-response testing, which is the primary purpose of the TDT facility. However, some space-related test programs that have not involved aeroelasticity have used the TDT to take advantage of specific characteristics of the wind-tunnel facility. In general, the heavy gas test medium, variable pressure, relatively high Reynolds number and large size of the TDT test section have made it the preferred facility for these tests. The space-related tests conducted in the TDT have been divided into five categories. These categories are ground wind loads, launch vehicle dynamics, atmospheric flight of space vehicles, atmospheric reentry, and planetary-probe testing. All known TDT tests of launch vehicles and spacecraft are discussed in this report. An attempt has been made to succinctly summarize each wind-tunnel test, or in the case of multiple, related tests, each wind-tunnel program. Most summaries include model program discussion, description of the physical wind-tunnel model, and some typical or significant test results. When available, references are presented to assist the reader in further pursuing information on the tests.

INTRODUCTION

The NASA Langley Transonic Dynamics Tunnel (TDT), which became operational in late 1959, has long been dedicated to aeroelasticity research and development. The TDT has many features that make it particularly suitable for aeroelastic testing including subsonic to transonic Mach number capability, variable density, very low operating pressures, and the capability of rapidly reducing aerodynamic loads during testing. The TDT also has the ability to use either air or a heavy gas as its test medium. The heavy gas is particularly suitable for aeroelastic scaling of wind-tunnel models. In addition to providing for extensive contributions to aircraft-related testing, these features have allowed the TDT to support many significant research and development activities for launch vehicles and spacecraft.

The TDT has been used many times throughout its history to support aeroelastic research and development of space vehicles to simulate the transition through the earth's atmosphere for launch vehicles and "flying" spacecraft. The facility has also been used to study similar atmospheric transitions for spacecraft on other planets. Additionally, ground-wind studies have been carried out in the TDT simulating launch vehicles on the launch pad and for a Viking lander on the Martian surface. Figure 1 illustrates the relative amount of space-related testing conducted in the TDT over the past 40 years compared to all tests conducted in the facility. As shown in the figure, approximately 17 percent of all testing in the TDT has been in support of space-related activities.

The TDT space-related tests have been grouped in this paper into five categories; launch vehicle ground-wind loads, launch vehicle dynamics, atmospheric flight of space vehicles, atmospheric reentry, and planetary-probe model tests. Although launch vehicles transition through Earth's atmosphere, TDT launch vehicle studies (i.e. Saturn V) have been categorized in this paper separately from more conventional lifting-surface space vehicles (i.e. Space Shuttle) that rely substantially on fluid-dynamic lift for vehicle flight control. Figure 2 illustrates the distribution of TDT space-related testing based on the test categories used in this paper. Figure 2 also breaks down the test distribution for each decade of TDT operation.

* TDT Facility Manager, Senior member AIAA, Member AHS.
† Aerospace Research Engineer.
‡ Aerospace Engineer, Member AIAA, Member AHS.

A significant amount of launch vehicle ground-wind loads testing has taken place in the TDT. Ground-wind loads testing deals with the steady and unsteady loads that a launch vehicle experiences while erected on the launch pad due to the natural wind environment. These loads can result in dynamic response of a launch vehicle that can cause structural damage if the launch system is not properly designed. Ground-wind loads studies in the TDT have involved vehicles such as Apollo-Saturn, the Titan III, the Space Shuttle, and the Atlas-Centaur launch vehicle. Figure 2 shows that approximately one quarter of all TDT space-related testing has involved assessment of ground-wind loads.

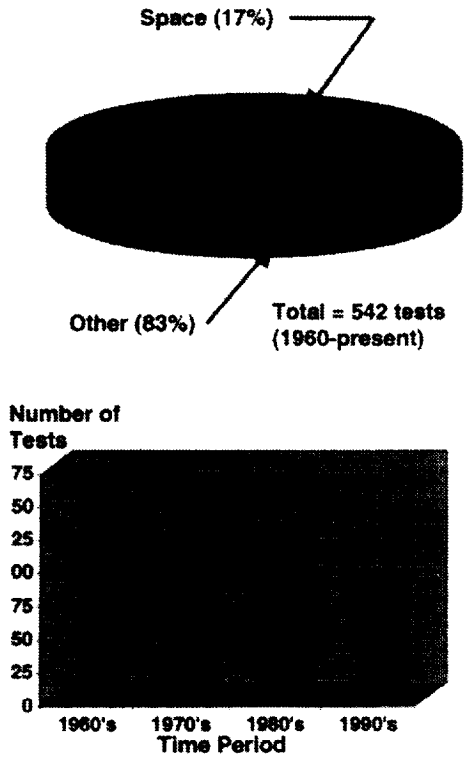

Fig. 1- Portion of TDT testing related to space activities.

Launch vehicle studies in the TDT have generally centered on buffet measurements, although a few tests in the 1960's are thought to have been conducted primarily to measure static pressures. Over the years, buffet and general dynamic response studies have been carried out for vehicles such as the Apollo-Saturn, Atlas-Centaur, and Delta-series launch vehicles. The models used for these tests have ranged from partial-vehicle rigid models used for making unsteady pressure measurements to full-vehicle, aeroelastic models that provide scaled dynamic response measurements. Figure 2 shows that 14 percent of TDT tests associated with space vehicles have involved launch vehicle dynamic response measurements.

Atmospheric space-vehicle-flight studies conducted in the TDT have generally involved flutter clearance and flutter research activities. However, other studies for aerodynamic performance, buffet, buzz, and panel flutter have also been performed for space vehicles with lifting surfaces, such as the Space Shuttle. Of the five space-related test categories, the atmospheric-flight category is most typical of TDT testing in that atmospheric-flight studies closely match typical TDT aircraft tests. In recent years, extensive research was conducted in the TDT as part of the National Aerospace Plane (NASP) program. This work included wing-alone, vertical-tail-alone, full-vehicle, and engine-related buzz, divergence, and flutter studies. In addition to Earth atmospheric flight testing, a recent development has been the proposed atmospheric flight on Mars of the conceptual NASA "Mars flyer". In the early planning stages for this program, the TDT was identified to support tests of this conceptual vehicle, primarily because of the very low pressure (and therefore low Reynolds number) capability of the TDT. Atmospheric-flight studies have accounted for nearly 36 percent (see Fig. 2) of all TDT space-related tests. The large percentage of tests in this category is somewhat exaggerated in the sense that an unusually high number of very simplistic, preliminary model tests were conducted for the NASP vehicle program.

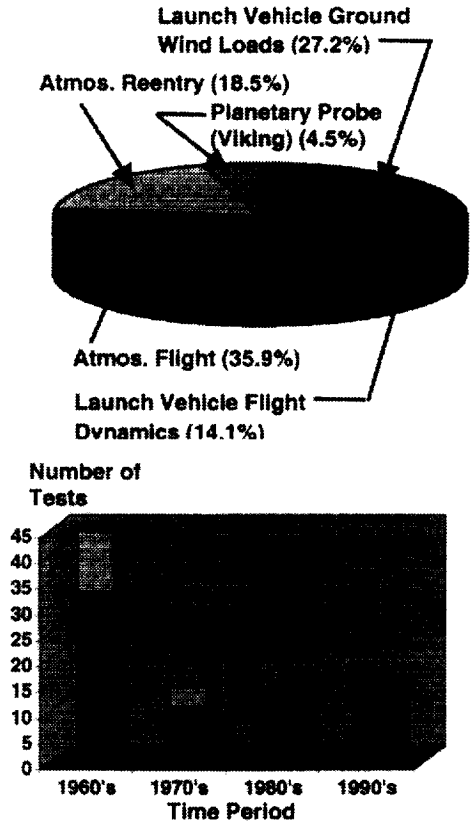

Fig. 2- Breakdown of space-related testing in the TDT according to test categories.

The TDT has also made significant contributions to research studies associated with unpowered atmospheric transition. Most of these tests involved Earth atmospheric reentry concepts; some associated with the NASA manned space-flight program. A number of these research tests involved conceptual reentry vehicles, or decelerators. The TDT contributed significantly to understanding the capabilities of these concepts; however, most of the tested ideas were never use in flight. Other reentry (or more appropriately, atmospheric-entry) tests have been conducted in the TDT for vehicles entering planetary atmospheres. Several tests have been conducted for entry into the Mars atmosphere. The Galileo probe parachute system, successfully used for entry into the Jupiter atmosphere, was also tested in the TDT. The TDT was used to more appropriately simulate these planetary atmospheres through combinations of heavy gas or air test mediums at various pressure levels. The wind-tunnel models have generally been aeroelastically scaled to match the dynamic properties of the actual vehicle. These models have been used to help assure that the entry configuration will function without undue dynamic response during its nominal trajectory or upon encountering gusts. Atmospheric entry models tested in the TDT have included several parachute concepts, deployable hot-air-balloon-type vehicles, a number of drag brake configurations, and inflatable decelerators. Figure 2 shows that approximately 19 percent of all TDT space-related tests involved atmospheric reentry studies.

The final category of TDT space-related tests involves ground-wind tests of planetary probes. This category is not large, comprising only about five percent of TDT space-related tests (Fig. 2). These tests concerned testing of the Mars-lander vehicles Viking 1 and Viking 2. These tests were not ground-wind loads tests per se; rather, they involved studying the effects of ground winds on the precision of instrumentation on the Mars Viking landers. These tests were done in the TDT in large part because the very low pressure capability of the TDT gives it the ability to match densities and/or Reynolds numbers suitable to simulate the Martian ground-level environment, albeit in an air test medium in the TDT.

This paper summarizes the various types of tests conducted in the TDT throughout its history related to launch vehicles and spacecraft, including several fairly unique tests. The tests will be discussed in categories as introduced above. Table 1 (last page of this report) is a complete tabulation of all known space-related tests that have been conducted in the TDT. Specific test-summary information could not be found for every individual test in this list. However, general program information was found that correlated with the test subject area, test titles, and/or the test time period for every test in this table. The test titles and the test categories listed will help the reader correlate test information in the table with test-summary discussions in this paper. This paper will attempt to more thoroughly explain the unique nature of the TDT that made it suitable to the types of space-related studies that have been accomplished. Also, the paper will serve as a bibliographic summary of this type of testing in the TDT and, as such, an attempt will be made to summarize significant technical contributions of the TDT testing to space activities. The authors hope that the paper will ultimately point to the continued viability of the TDT in supporting research related to space vehicles.

WIND TUNNEL

The NASA Langley Research Center (LaRC) Transonic Dynamics Tunnel (TDT) has operated for over forty years, supporting fixed wing, rotorcraft, spacecraft, and other miscellaneous research testing throughout its history. The TDT is a continuous-flow wind tunnel capable of testing at total pressures from about 0.1 to 1.0 atmospheres and over a Mach number range from zero to 1.2. The test section of the TDT is 16.0 ft. square with cropped corners.

The TDT is specifically designed for studying aeroelastic and other unsteady flow phenomena. The wind tunnel is capable of operating at both subsonic and transonic speeds. The TDT has a variable fluid density capability, which is particularly helpful in structural scaling of aeroelastic models. Testing can be conducted in the TDT using either air or a heavy gas as the test medium. Testing in a heavy gas provides advantages in aeroelastic model scaling. Prior to 1997, the TDT heavy gas was dichlorodifluoromethane, known as R-12. The density of R-12 is approximately four times that of air. This means that scaled models can be made heavier relative to a scaled model for testing in air. This generally makes the task of building a scaled model with sufficient strength easier. After 1997, the TDT began operating in a heavy gas known as 1,1,1,2-Tetrafluoroethane (CH_2FCF_3), or R-134a. This gas is approximately 3.5 times denser than air for identical pressure, temperature, and volume, making it a reasonably equivalent replacement for the previous R-12 heavy gas. All of the tests discussed in this report actually used air or the initial TDT R-12 heavy gas test medium. The TDT also has several unique features that are particularly useful for aeroelastic tests. One of these features is a group of four bypass valves connecting the test section area (plenum) of the tunnel to the return leg of the wind-tunnel circuit. In the event of a model instability, such as flutter, these quick-actuating valves are opened. This causes a rapid reduction in the test section Mach number and dynamic pressure, which may result in stabilizing the model. A more complete description of the TDT can be found in reference 1.

GROUND-WIND LOADS TESTING

During the rapid pace of ballistic missile and launch vehicle development of the late 1950's and early 1960's, it was realized that a critical design point of the vehicle's structure was that of a class known as ground-wind loads (GWL). Ground wind loads refer to both steady and dynamic loads imparted to a launch vehicle while it is erected on its launch pad and fully exposed to the natural wind environment, which can be quite unpredictable and severe at times. The dynamic response of a flexible launch vehicle to ground-wind loads can cause design problems with regard to structural strength, guidance platform alignment prior to launch, and clearance between adjacent umbilical towers. Steady and dynamic loads due to wind drag and wind induced oscillations impart large bending moments to the first stage structure of launch vehicles and are typically the maximum bending loads that the first stage will be subjected to even while in flight. It was then, and still is today, important to design the thin-walled, tank structure of the first stage such that it would endure vehicle response due to a wide range of expected ground winds at a particular launch site.

Figure 3 illustrates the factors contributing to ground-wind loads. This diagram shows a launch vehicle on a flexible support structure standing beside an umbilical tower and is subjected to a steady wind that results in both static and dynamic loads on the vehicle. The predominant aerodynamic force associated with launch vehicle ground-wind loads is a result of flow separation and shed vortices from the bluff body of the vehicle. The resulting unsteady aerodynamic forces are perpendicular to the wind direction and referred to as oscillating lift. The steady and oscillating aerodynamic drag forces act primarily in the direction of the mean wind. Prediction of these steady and unsteady aerodynamic loads is critical to the design success of any launch vehicle.[2]

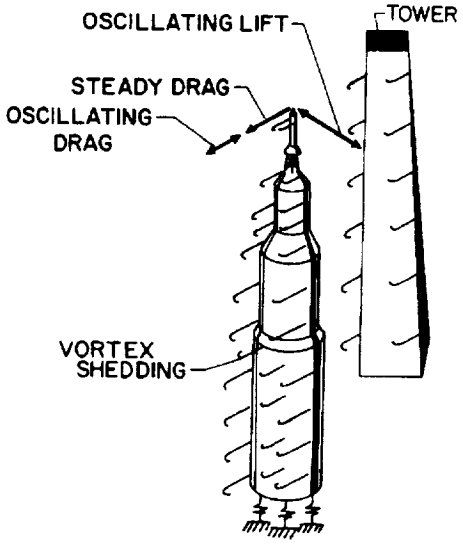

Fig. 3- Load conditions caused by ground-wind loads.

Even today, it is very difficult to accurately predict the response of a vehicle to ground wind loads. Therefore, the accepted method for determining the design ground wind loads has been to perform wind-tunnel tests of aeroelastically-scaled models of the launch vehicle. Research conducted at the Transonic Dynamics Tunnel (TDT) played a key role in the early understanding of ground-wind loads and the development of many launch vehicles which occurred in the 1960's, 70's, and 80's.

Because flow separation and the resulting shed vortices are highly dependant on Reynolds number and Strouhal number, these non-dimensional parameters are important to match in the design of any GWL wind-tunnel model and wind-tunnel test in order to ensure that results are scalable to the actual vehicle. The TDT was the facility of choice for many launch vehicle ground-wind load test because of its large test section (16ft-by-16ft) and the variable density test capability that combined allow for reasonable simulation of full-scale Reynolds numbers in a sub-scale wind-tunnel test. By using R-12 as the test medium, which has a kinematic viscosity of about one-fifth that of air, Reynolds number simulation was approximately achieved during ground-wind loads tests for all launch vehicles tested in the TDT except for the Saturn V. Additionally, the TDT has the capability of remote azimuth positioning of a ground-wind loads model in its test section using a unique ground-plane turntable.

The following sub-sections will capture the full breadth of ground-wind loads testing performed in the TDT since its inception in the late 1950's. From early tests of Jupiter ballistic missiles for the U.S. Army to Saturn launch vehicles and the Space Shuttle, each test took advantage of the unique capabilities of the TDT to determine the particular ground-wind loads response of the vehicle. Throughout the 1960's, 70's, and 80's the TDT proved itself as one of the nations premier facilities for performing ground-wind loads testing of launch vehicles.

Model Design

The most reliable means of obtaining quantitative data on ground-wind loads on a launch vehicle, once the design is finalized, is from wind-tunnel studies of dynamically and elastically scaled models. Such models that simulate both the aerodynamic and structural dynamic properties are referred to as aeroelastic models. Scaling laws are used to determine the nondimensional parameters to be duplicated by the model if the response of the model to tunnel-simulated ground winds is to simulate accurately the response of the full-scale vehicle to ground winds.

For ground-wind loads testing, it is required that the following parameters be the same for model and full-scale vehicle: external shape, Reynolds number, Strouhal number based on vehicle first bending mode and the

diameter of the lower stage, mass ratio based on the generalized mass of the first bending mode, damping ratio of the first bending mode, and surface roughness. From the dimensionless parameter design requirements specified above and from a knowledge of TDT test capabilities, the fundamental scale factors (model-to-full-scale ratios) for scaling length, mass, and time are readily obtained. It is also important to geometrically model the launch vehicle umbilical tower and place it at the scaled location relative to the vehicle in order to capture the effects of the tower on the wind profile. Figure 4 shows an aeroelastic ground-wind loads model of the Scout launch vehicle and its umbilical tower as tested in the TDT.

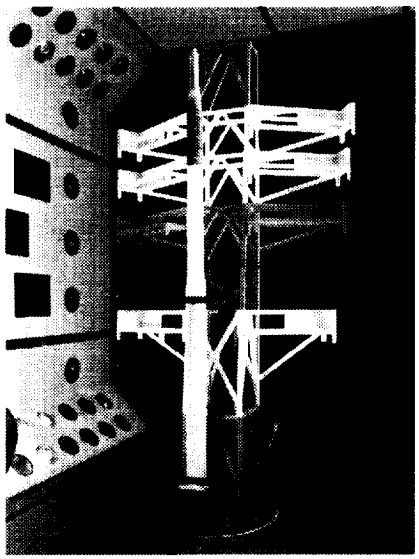

Fig. 4- 0.15-scale Scout launch vehicle ground-wind loads model.

Model construction typically consisted of a center spar structure with lead weights attached at various points, which is representative of the scaled stiffness and mass distribution of the vehicle. Cylindrical shells representing the geometric shape and axial stiffness were then attached to the to the spar. Most ground-wind load tests at the TDT included the ability to vary the payload fairing shape, vary the vehicle's fueled condition, and vary the booster configuration (for instance, strap-on boosters). It was important for the model to be configurable in order to allow every conceivable vehicle configuration to be tested for ground-wind loads since many launch vehicles were erected in stages on the pad (Jupiter, Titan, Atlas, and Saturn I) and all were fueled in stages on the pad.

Another important aspect of model design includes matching the vehicle first bending mode damping. Structural damping has been found to be one of the key parameters that governs the susceptibility of a vehicle to wind-induced oscillations. Early ground-wind load tests in the TDT such as the Scout and Jupiter, relied on the model construction to provide structural damping which was representative of the full-scale vehicle. This method proved troublesome because structural damping is very difficult to control in a scale model compared to other model design parameters. A solution was found in the application of viscous dampers that can be used to vary the amount of damping in a model and thus provide for the precise regulation of structural damping in a scale model. The device used in ground-wind loads tests, shown in Figure 5, consists of a series of lead slugs that are free to slide on concave trays inside of a cylinder filled with viscous oil. Motion of the lead slugs in the viscous oil dissipated energy and thus increasing the damping. Changing the number of lead slugs or the viscosity of the oil could then change the degree of damping.

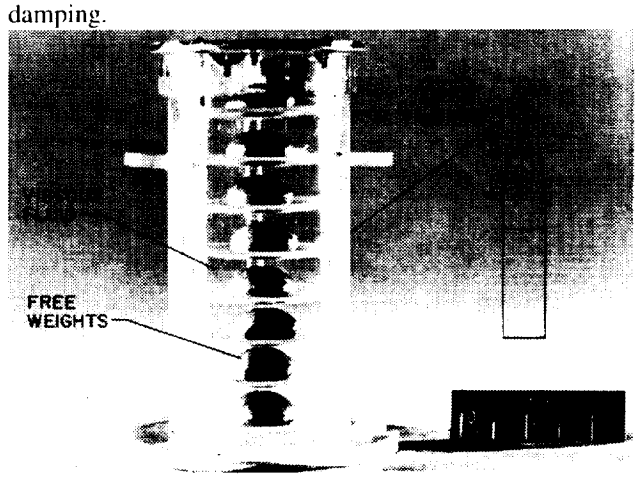

Fig. 5- Viscous damper used in ground-wind loads models.

The primary instrumentation for ground-wind load tests at the TDT consisted of two strain-gage bridges mounted near the model base in planes 90° apart around the circumference of the first stage and two accelerometers mounted on the model near the nose in the same two reference planes. This instrumentation was used to obtain time histories of the bending moment and deflection responses of the model to simulated ground winds in the TDT. Recording and display mediums for this instrumentation varied as technology progressed, but most ground-wind load tests at the TDT used strip-charts, oscilloscopes, and digital computer data acquisition systems as they came into use. One method of data readout which proved useful to early ground-wind loads tests was the use of time exposure photographs of an oscilloscope set up to display the response from two strain gages (on opposite model reference planes) on two axes. Figure 6 shows such a photograph and schematic. As the model responds both statically and dynamically, the outputs from these strain gages trace an elliptical pattern on the oscilloscope since the lift response is greater than the drag response. The borders of the ellipse thus formed represent the curve of maximum dynamic bending

moment response and the distance the center of the ellipse has shifted from the no-wind position yields the magnitude and direction of the static bending moment.[2-4]

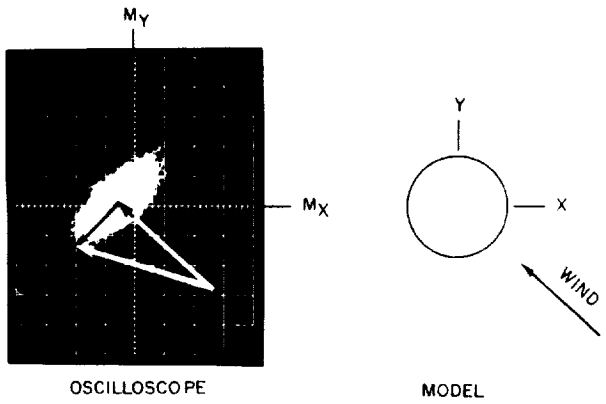

Fig. 6- Oscilloscope time exposure of bending moment.

Test Techniques

Ground-wind loads testing would begin by first setting the desired tunnel condition. This would include the desired density of R-12 heavy gas for Reynolds number and Strouhal number simulation and also setting of the tunnel speed. Because of model size, some tests such as the Saturn V could not be tested at higher simulated wind velocities due to compressibility effects of operating above Mach 0.3 at low pressures in R-12. At each desired tunnel velocity, one to two minute samples of data of the model response were recorded. After data has been recorded for each desired tunnel velocity, the model azimuth would be changed such that the model and umbilical tower were subjected to simulated wind conditions from a different azimuth or angle.

Early ground-wind loads tests relied on technicians to enter the test section and unbolt the model from the test section floor and relocate it at the desired azimuth. This proved very costly with regard to test time since each model azimuth change require hours of R-12 heavy gas processing to clear the test section for personnel entry. In mid-1962 an agreement was made between NASA and the Martin Company of Baltimore to perform ground-wind loads test of the Titan III at the TDT. One requirement was that the azimuth of the model be easily changed remotely from the TDT control room. This requirement resulted in the ground-loads floor turntable being built by the Martin Company specifically for the Titan III test at the TDT. After the test the turntable and floor-fairing structure remained and became a standard capability of the TDT for all subsequent ground-wind load tests. Figure 7 shows a model mounted to the ground-wind loads floor turntable.

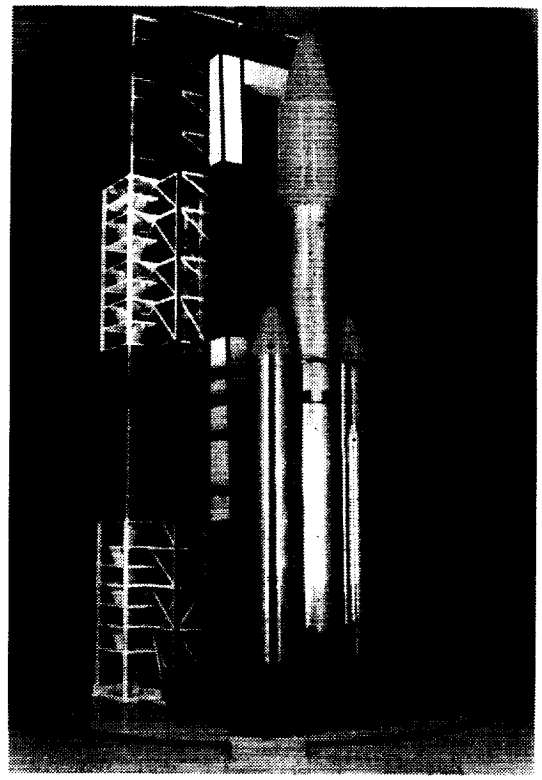

Fig. 7- Model mounted to TDT ground-wind loads floor turntable.

TDT Ground-Wind Loads Test Summaries

Scout launch vehicle (TDT Test 12): The Scout launch vehicle was developed by NASA specifically for orbital and sub-orbital research and had a useful career that spanned over 30 years. In October of 1960, testing began at the TDT of a 0.15-scale ground-wind loads model of the Scout launch vehicle and its service/umbilical tower. Testing was performed with both air and R-12 as a test medium in order to precisely match full-scale Reynolds number. The Scout was tested in the fueled configuration. Figure 4 shows the Scout ground-wind loads model and its umbilical tower in the TDT test section. A second Scout test was conducted in the TDT in August 1961.

Saturn I Block I (TDT Test 18): The first ground-wind loads test of NASA's Saturn family of launch vehicles was a test of the Saturn I Block I, which was a single-stage, sub-orbital launch vehicle. The Saturn I Block I was the first US launch vehicle to qualify the concept of clustering many rocket engines in the first stage, in this case eight, and paved the way for the Saturn IB and Saturn V. The successful first flight of the Saturn I Block I occurred on October 27, 1961 (SA-1). Results from the test at the TDT resulted in increased confidence in the vehicle's ability to withstand wind-induced

oscillations while exposed to the environment before and during launch from Launch Complex 34 at Cape Canaveral.[5]

During this test, the response of a 7.5 percent aeroelastically scaled model of the Saturn I Block I (SA-1) vehicle was measured at simulated ground winds up to 80 ft/s (48 knots) at full-scale Reynolds numbers using R-12 as the test medium. TDT testing of the SA-1 vehicle began in March of 1961. A photograph of the model is shown in Figure 8. The SA-1 gantry tower was not modeled because the full-scale tower was pulled back 200 yards from the vehicle prior to launch and did not cause any aerodynamic interference.

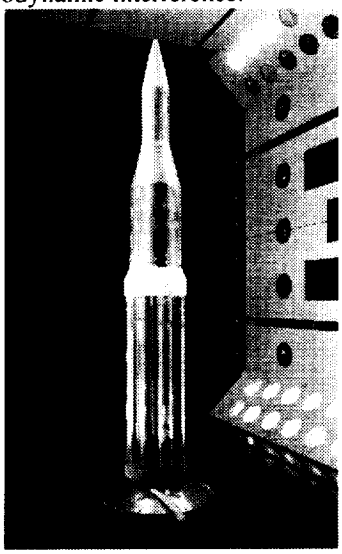

Fig. 8- 7.5 percent Saturn I Block I model.

Figure 9 shows the steady-drag and maximum oscillatory bending moment measured at the base tie-down location. The oscillatory bending moment shown was measured perpendicular to the wind direction. The response represented by these data was due to the oscillating lift force of vortex shedding. At high velocities the steady-drag moment becomes several times larger than the oscillatory moment and approaches the static overturn moment for the unfueled vehicle resting unclamped on the launch arms. Thus, tests at the TDT showed that for the Saturn SA-1 vehicle the critical load from ground winds is the moment due to steady-drag rather than the oscillatory response lateral to the wind, which was the critical loads for other launch vehicles tested up to that time.[6]

Jupiter IRBM (TDT Test 28): Tests of a 1/5-scale Jupiter missile aeroelastic model were conducted at the TDT in October 1961. Once again, R-12 heavy gas was used as the test medium to match full-scale Reynolds numbers. The model was tested to full-scale wind velocities up to 95 knots. Figure 10 shows the Jupiter model mounted to the test section floor of the TDT.

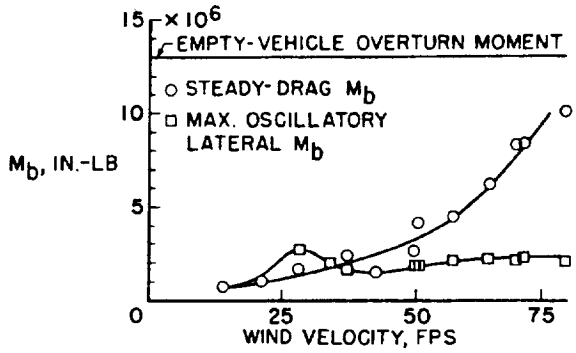

Fig. 9- Saturn I Block I ground-wind-induced loads.

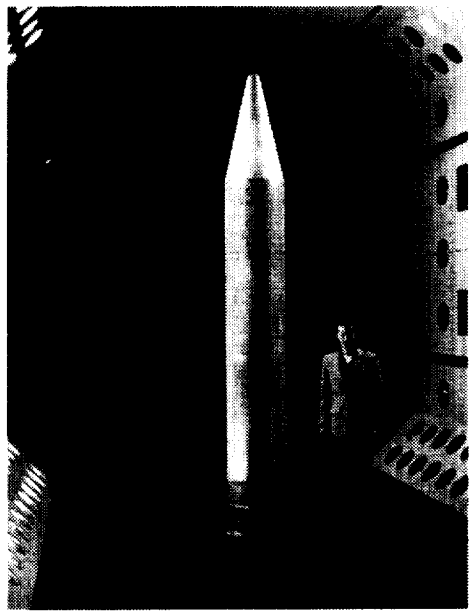

Fig. 10- 1/5-scale Jupiter IRBM.

Configurations of the Jupiter missile included a clean nose and with strake-type spoilers mounted to the nose as shown in Fig. 11. It was shown during this test that the spoilers had a pronounced ground-wind load alleviation effect and can prove a useful tool in reducing a launch vehicle's susceptibility to wind-induced oscillations. These results are shown in Fig. 12 as a plot of the maximum resultant bending moment against wind speed.[2,7]

Wind-induced loads research model (TDT Tests 37 and 40): These tests were part of a basic research program for determining the sensitivity of a generic launch vehicle's ground-wind response to two different nose shapes. Figures 13 and 14 show two configurations of the research model mounted to the test section floor of the TDT. Other test hardware included a wind anemometer used to measure wind speed and a turbulence grid used to create a wind profile that better simulates the natural turbulence of ground winds. The

conical base of the model was fixed to the floor while the upper portion was mounted to leaf springs that provided different stiffness values in two principal directions. The springs allow the upper portion of the model to sway back and forth in all directions, thus simulating the side-to-side motion typical of wind-induced oscillations of upright launch vehicles. The generic model could be rotated in azimuth to change the alignment of the spring mount principal directions with the wind direction. These tests were conducted only in air as a test medium.

Results from this generic ground-wind loads model proved to be inconsistent due to the fact that model damping was highly dependent on azimuth. This was a shortcoming of the design of the model. No results were published due to these problems with the program.

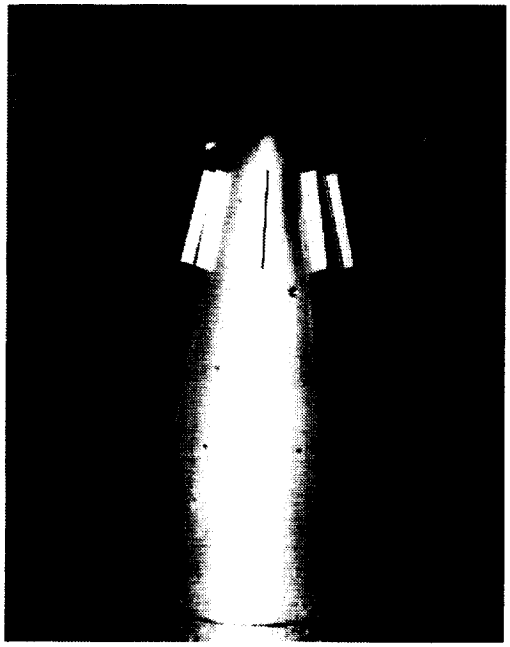

Fig. 11- Spoilers on 1/5-scale Jupiter IRBM.

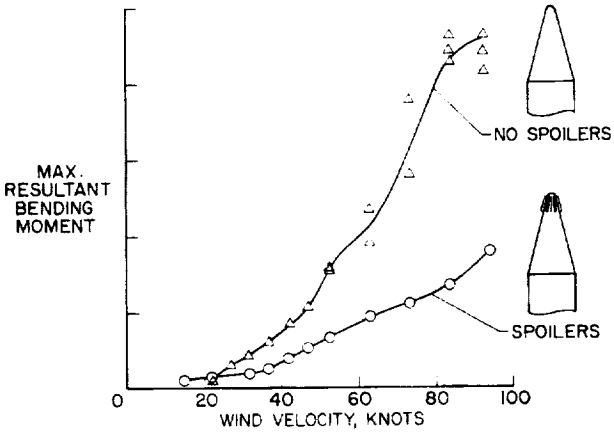

Fig. 12- Effect of nose spoilers on bending moment response of 1/5-scale Jupiter IRBM model.

Fig. 13- Generic ground-wind loads model in TDT.

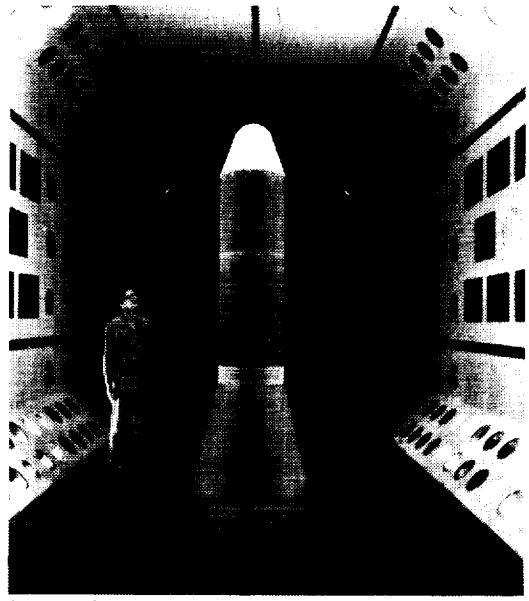

Fig. 14- Generic ground-wind loads model in TDT.

Titan III (TDT Test 52): Ground-wind loads testing was conducted on a 7.5 percent aeroelastically-scaled Titan III launch vehicle with a geometrically scaled model of its umbilical tower. Testing was conducted in R-12 heavy gas and full-scale Reynolds number was matched. For this test, the Martin-Marietta Corporation agreed to design and fabricate a ground-wind loads turntable to be used to remotely change model azimuth from the TDT control room. At the end of this test, this turntable was turned over to NASA for use in future ground-wind loads tests at the TDT.

There were three configurations tested by Martin-Marietta and NASA engineers during this test. These included a conical and a Dyna-soar payload, which at the time were firmly established payloads, and a bulbous shape that was of general interest but at the time not a scheduled flight payload. Soon after, the Dyna-soar program was cancelled by the Air Force and only the conical and bulbous payload fairings actually flew on Titan. Figures 15 and 16 show the bulbous and Dyna-soar Titan model configurations mounted on the TDT floor ground-wind loads turntable. Results from this test showed that the flow behind the umbilical tower could cause a large model response under certain conditions.

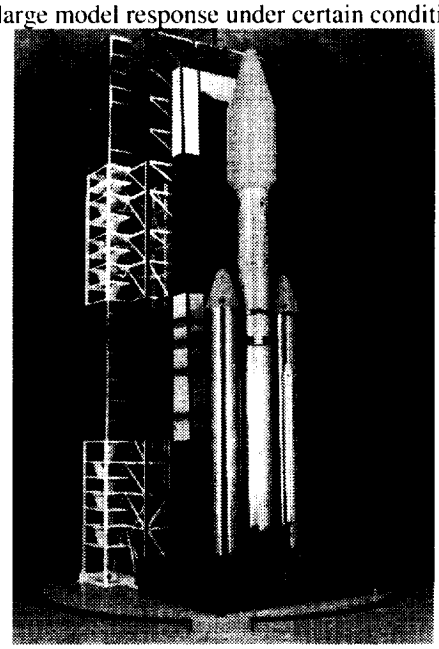

Fig. 15- Titan III bulbous payload.
(Same photograph as used in Fig. 7).

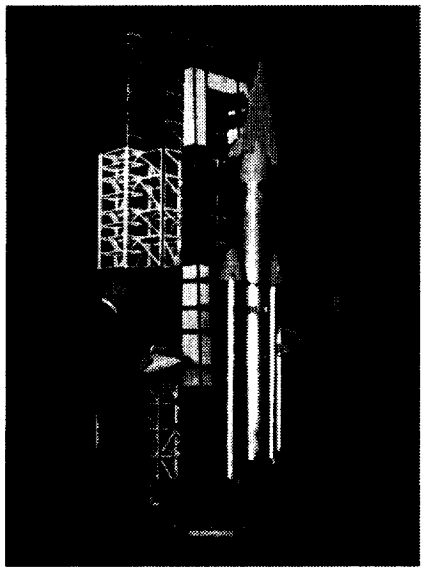

Fig. 16- Titan III Dyna-soar payload.

Saturn I Block II (TDT Test 53): Immediately following the Titan III test, the Saturn I Block II vehicle was ground-wind loads tested at the TDT in support of the upcoming first flight of the vehicle in January of 1964 (SA-5). Figures 17 and 18 show the 7 percent Saturn I Block II aeroelastic ground-wind loads model as tested in the TDT with Jupiter and Apollo payloads and with a geometrically accurate model of Launch Complex 37B (LC-37B). The Block II vehicles are differentiated from the Block I vehicles by the inclusion of a live S-IV second stage capable of providing orbital insertion of payloads, by taller S-I first stage to provide more propellants, and by eight aerodynamic fins for enhanced stability.[5]

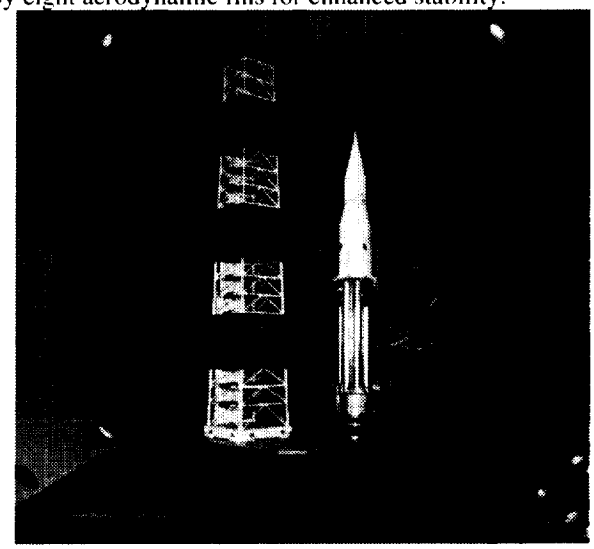

Fig. 17- 7 percent Saturn I Block II with Jupiter payload fairing.

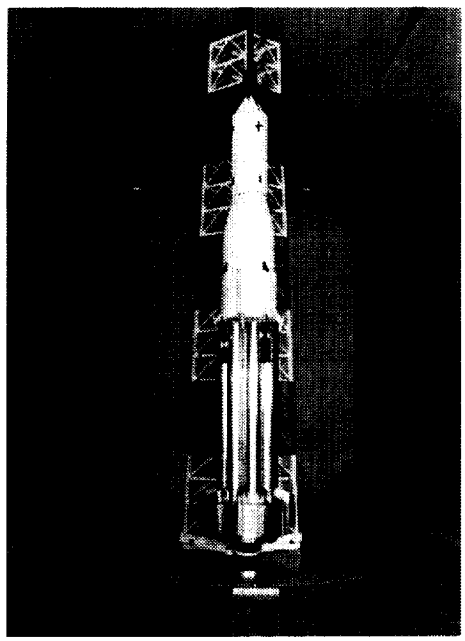

Fig. 18- 7 percent Saturn I Block II with Apollo spacecraft.

The main objective of this test was to provide ground-wind loads data to be used to establish ground handling procedures in the event a Saturn I Block II vehicle was exposed to high winds while erected on the launch pad. Both fueled and unfueled configurations were tested and various protuberances such as retrorockets for staging, telemetry antenna, ullage rockets, and service module thrusters were included. Testing was conducted at many wind azimuth directions using the TDT ground-wind-loads turntable, at full-scale wind velocities up to 50 mph (44 knots), and at full-scale Reynolds numbers using R-12 heavy gas as the test medium. Figure 19 shows the maximum resultant base bending moment obtained at the most critical wind azimuth angle for the Saturn I Block II, Saturn IB, and Saturn V for values of damping ratio greater than or equal to 0.01. As shown, the Saturn I Block II vehicle was found to possess no ground-wind load problems over the range of steady wind velocities of the test at the TDT. Thus, testing at the TDT cleared all Saturn I Block II flights (SA-5 through SA-10) from ground-wind loads problems.[4,8]

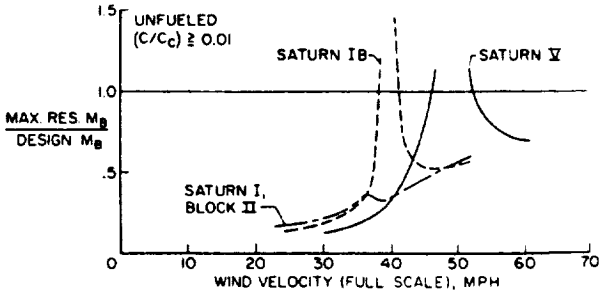

Fig. 19- Maximum resultant base bending moment at most critical wind azimuth for Saturn I Block II, Saturn IB, and Saturn V vehicles.

Saturn V (TDT Tests 55, 62, 79, and 106): Early in the development of the Saturn V, it was realized that ground-wind loads would play a role in the design of the vehicle and launch configuration. In response to this, NASA relied on both model-scale, wind-tunnel tests at the TDT and full-scale tests of a Facilities Integration Vehicle. There were several TDT tests in March and July 1963, June 1964, and May 1966 of a 3-percent, aeroelastically-scaled model of the Saturn V launch vehicle to determine its response to wind-induced loads. Since the first two tests took place when the Saturn V design was still in its infancy, the mass and stiffness of the vehicle and the base stiffness of the launcher was likely to change significantly as the design matured. Therefore, it was decided that a simplified 3-percent-scale Saturn V ground-wind loads model would be designed such that only scaled bending frequency would be matched to full-scale. This model was modified for the later tests to represent changes to the vehicle, hold-down structure, and umbilical tower as the design matured.

The principal variables of the investigation were wind velocity, wind direction, flexibility of the support structure, structural damping, and fueled/unfueled configuration. As in the Saturn I Block II tests, many protuberances were included in the Saturn V to provide a very complete model from a geometric standpoint. Because of the enormity of the Saturn V launch vehicle (more than twice the size of previous Saturn configurations), full-scale Reynolds number could not be matched in the TDT at the 40 knot design wind speed of the vehicle without exceeding a Mach number where compressibility effects become significant (Mach=0.35-0.40). Therefore, the model Reynolds number was approximately one-third that of full scale. Figure 20 shows the Saturn V model and umbilical tower mounted to the TDT ground-wind loads turntable. The Saturn V mobile service tower was also included in testing at the TDT.

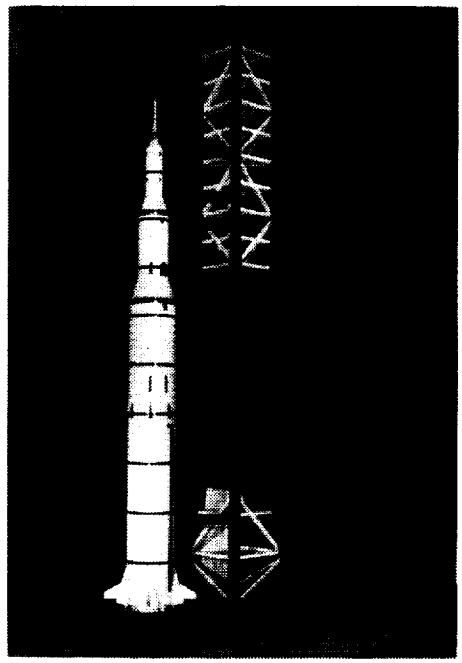

Fig. 20- 3 percent Saturn V model and service tower.

Sub-critical Reynolds number testing at the TDT of the Saturn V model in the unfueled configuration yielded an undefined peak (the model had inadequate load capability to define the peak) near 50 knots which exceeded the design bending moment of the vehicle. This is shown in Fig. 19. The response of the unfueled Saturn V model was found to be significantly affected by the presence of nearby tower structures. Figure 21 illustrates the effects of the nearby structures on the azimuth angles at which peak dynamic loads were measured. Since the Saturn V was to be fueled as near to the time of launch as possible, the vehicle would be subjected to winds in the unfueled configuration during its transport from the Vehicle Assembly Building to the

launch complex. Testing of the model in the fueled configuration showed that the design bending moment was not exceeded. Using the tunable viscous damper in the nose of the Saturn V model, it was found that when the damping of the vehicle's first bending mode was increased to 3 percent of critical, the bending moment response peaks were practically eliminated.

From past experience, it was expected that the damping of the first mode of the Saturn V would not exceed 2 percent critical. Therefore, two solutions were investigated for improving the Saturn V's ground-wind loads response. These included an external support that would effectively stiffen the vehicle and the addition of an external damper to increase the damping of the vehicle's first bending mode. It was found that the first solution would submit the vehicle to very high load conditions. Therefore, the accepted solution was to utilize an external viscous damper to increase the first mode damping as testing at the TDT suggested. A motion damper arm mounted to the S-II/S-IVB interstage was developed for the Saturn V Facilities Integration Vehicle (SA-500F), which was a facility checkout and ground-wind test vehicle (not a flight vehicle). During vibration testing of SA-500F in the Vehicle Assembly Building at Cape Canaveral, the motion damper arm increased the first mode damping from 1.5 percent critical to 4.5 percent critical.

Rollout of SA-500F with the motion damper arm occurred on May 25, 1966 and ground-wind loads testing showed no problems with the vehicle. On all subsequent Saturn V vehicles, the motion damper arm was connected to the launch escape tower. As discussed, the TDT played a key role in the testing and development of the Saturn V launch vehicle used to send man and machine to the moon.[2,8,9]

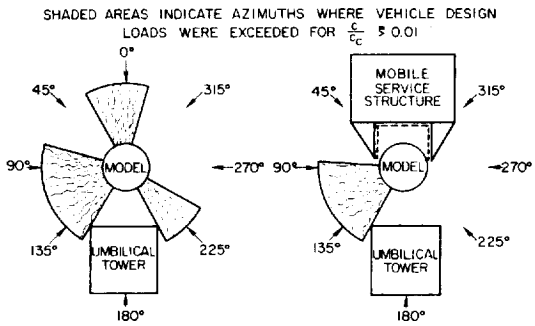

Fig. 21- Effects of nearby structures on the Saturn V vehicle response.

Saturn IB (TDT Tests 65, 71, and 88): Ground-wind loads testing of the Saturn IB launch vehicle began in 1963. A 5.5 percent aeroelastic model of the vehicle was designed for tests at the TDT along with geometrically scaled models of both Launch Complex 34 and 37B umbilical towers. There were three distinct payloads which included standard Apollo command and service module, and space station proposed as part of the Apollo Orbital Workshop program, and a generalized payload shroud as flown on AS-203. The Apollo spacecraft and space station payload testing took place during TDT tests 65 and 71 and are illustrated in Figs. 22 and 23. During Saturn IB ground-wind loads testing of the space station payload (test 71), wind-induced oscillations were severe enough to "send it down the tunnel" and thereby destroying the Saturn IB model. A second model was fabricated and testing continued in March of 1965 with the Apollo spacecraft and a generalized payload shroud as shown in Figs. 24 and 25.

All model hardware was mounted to the TDT ground-wind loads turntable and tests were conducted in R-12 heavy gas as a test medium. Because of the model's size and compressibility limitations, Reynolds number had a scale factor of only 0.85. The vehicle was tested in the unfueled and fueled configurations up to full-scale wind speeds of 46 knots. If the model azimuth angle is held constant and the velocity varied, the vehicle responds typically as shown in Fig. 26. In this figure, base bending-moment data measured on the Saturn IB model at the wind direction shown are used to present each component that contributes to the maximum resultant ground-wind load on the vehicle. As in the Saturn V tests, it was found that the critical configuration was for the unfueled vehicle. Figure 19 illustrates this critical ground-wind loads condition for the unfueled Saturn IB vehicle in which undefined peaks at 39 mph (34.3 knots) exceed the design bending moment of the base of the S-IB first stage structure. The design bending moment was only exceeded when the vehicle was tested in the presence of the LC-37B umbilical tower. Base bending moments were not exceeded with the LC-34 umbilical tower in place, nor were they exceeded with the vehicle in the fueled configuration.

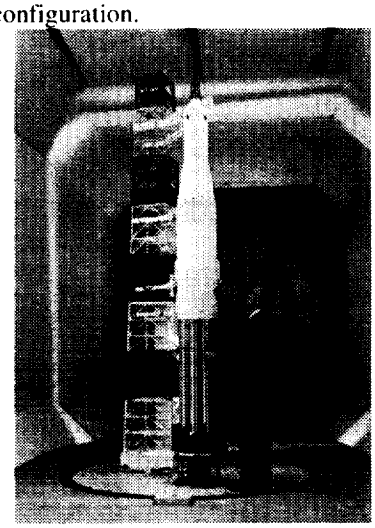

Fig. 22- 5.5 percent scale Saturn IB model with Apollo spacecraft and Launch Complex 37B umbilical tower.

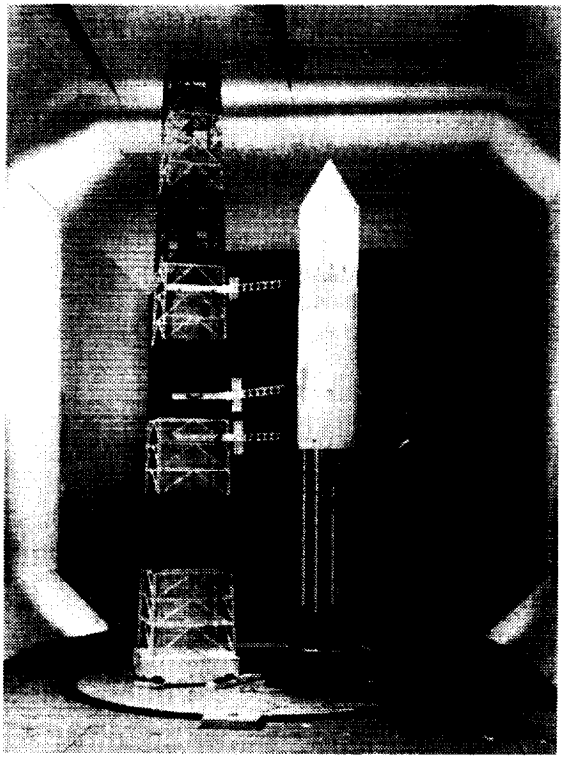

Fig. 23- 5.5 percent Saturn IB model with space station payload and Launch Complex 37B umbilical tower.

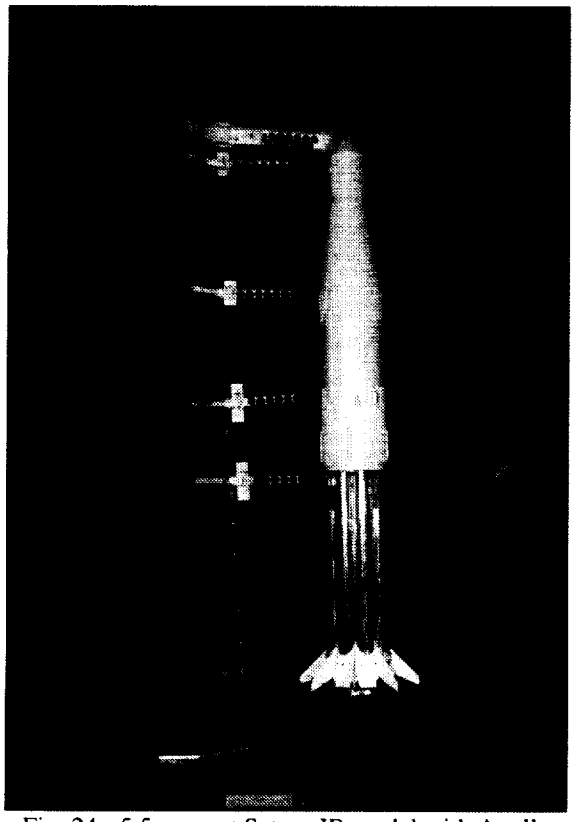

Fig. 24- 5.5 percent Saturn IB model with Apollo spacecraft and Launch Complex 34 umbilical tower.

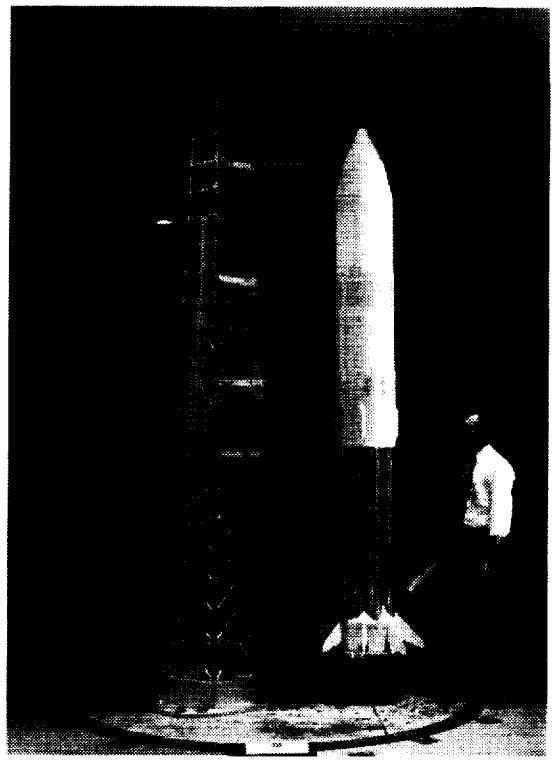

Fig. 25- 5.5 percent Saturn IB model with generalized payload shroud and Launch Complex 34 umbilical tower.

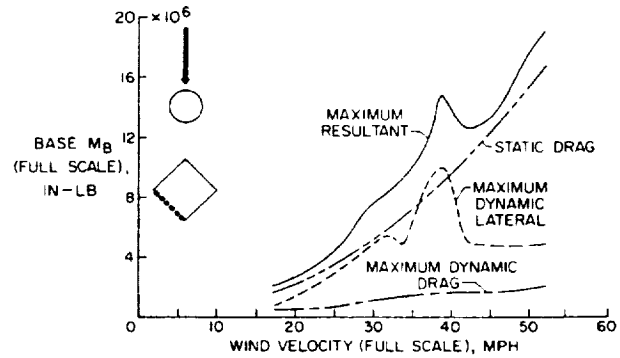

Fig. 26- Typical load variation with wind velocity for the Saturn IB vehicle.

Gemini-Titan (TDT Test 72): A joint test program was organized by NASA Langley researchers at the TDT and with engineers from the Martin Company to study the ground-wind loads response of the Gemini-Titan vehicle and its erector tower. A 7.5 percent, aeroelastically scaled model of the Gemini-Titan launch vehicle was fabricated for testing in the TDT at full-scale Reynolds numbers and up to full-scale wind speeds of 47.5 mph or 42 knots. In addition to the scaled launch vehicle, a dynamically scaled model of the erector tower was designed based on measured full-scale frequencies. Inclusion of the dynamically scaled erector tower was important due to the limited clearance separating the vehicle from the erector

as it is raised or lowered. The full-scale structural damping of the vehicle was duplicated in the model with the aid of the viscous damper discussed in earlier sections. Figures 27 and 28 shows the Gemini-Titan vehicle and erector as tested in the TDT.

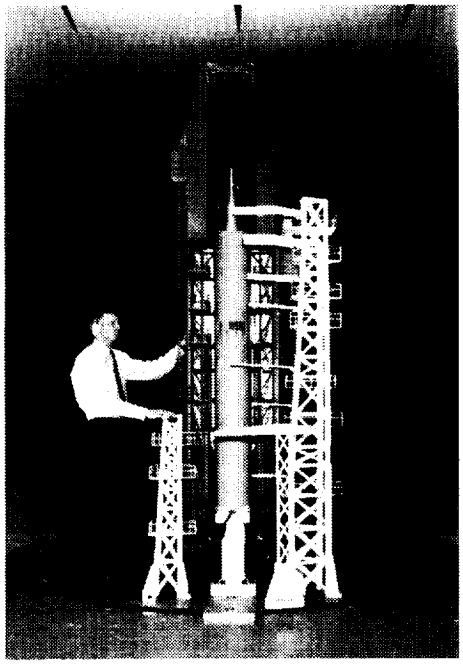

Fig. 27- 7.5 percent Gemini-Titan launch vehicle with erector in the fully-raised position.

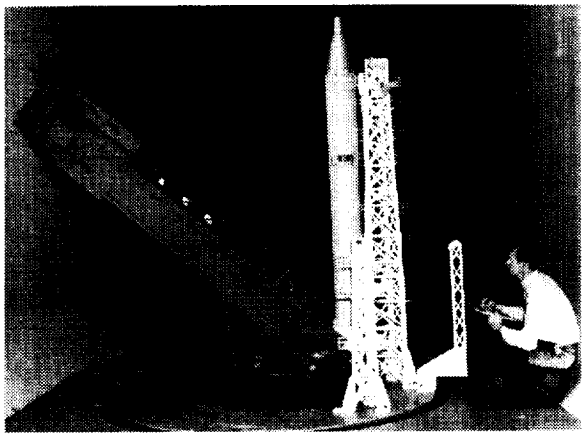

Fig. 28- 7.5 percent Gemini-Titan launch vehicle with erector lowered.

Test configurations included the launch vehicle without the erector (simulating pre-launch condition), the vertical and fully curtained erector, and the launch vehicle in the presence of the erector positioned at angles of 6, 33, and 50 degrees from the vertical. The TDT ground-wind loads turntable was used to position the model azimuth with respect to wind direction.

The maximum base bending moment on the Gemini-Titan vehicle occurred when it was in the wake of the erector (which was 33 degrees from vertical). This condition caused the vehicle to experience very little static load. The large dynamic load was apparently induced by a field of unsteady forces in which the body was immersed due to the presence of the erector.

As in the case of the launch vehicle, maximum dynamic responses of the erector were found to exist when it was in the wake of the air vehicle, although all dynamic responses were relatively low. Maximum total loads of the erector model were invariable static in nature, generally by large margins.

In addition to wind-tunnel tests, full-scale ground-wind load measurements were made on the Gemini-Titan vehicle and its erector tower as part of a complete ground-wind loads program. Figure 29 shows full-scale data together with wind-tunnel test results and theoretical predictions of response due to turbulence.

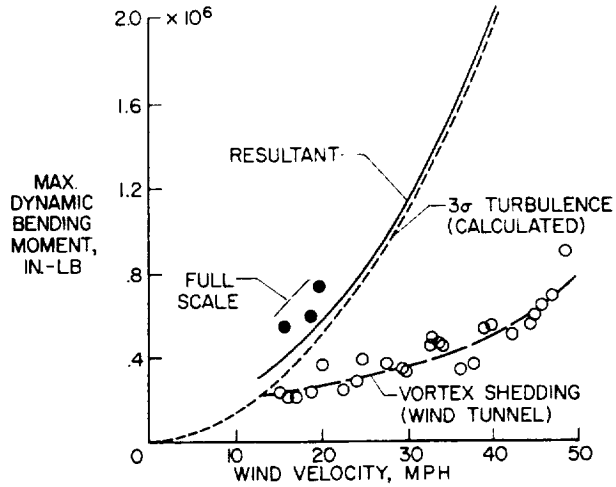

Fig. 29- Response of Gemini-Titan to ground-wind loads.

Two-dimensional cylinder forced oscillation model (TDT Test 94): Most of the launch vehicle ground-wind loads studies conducted at the TDT involved vehicles small enough that full-scale Reynolds number conditions could be duplicated at model scale. However, vehicles in the Saturn V class operated at Reynolds numbers well beyond the capabilities of the TDT, or any wind-tunnel for that matter, as pointed out earlier in this paper. Furthermore, a growing body of evidence indicated that vortex-shedding effects at Reynolds numbers of the order of 10^7 are not necessarily reproduced at supercritical Reynolds numbers of the order of 10^6. This concern led to many discussions with design engineers from Marshall Space Flight Center (the chief TDT customer for design-type ground-wind load studies) regarding ways and means of providing fundamental information about vortex shedding effects at high Reynolds numbers. These discussions culminated in a joint NASA-Martin Company research program to study vortex shedding on a two-dimensional cylinder in the TDT at Reynolds numbers up

to those typical of Saturn V type vehicles. This research program contributed a major extension to the existing fundamental knowledge in this field as indicated in Fig. 30. Also shown is the typical full-scale Reynolds number condition for the Saturn V vehicle immersed in a 60-knot wind. This research would therefore help bridge the gap between model-scale testing of the Saturn V at sub-critical Reynolds numbers and full-scale ground-wind load characteristics of the Saturn V.

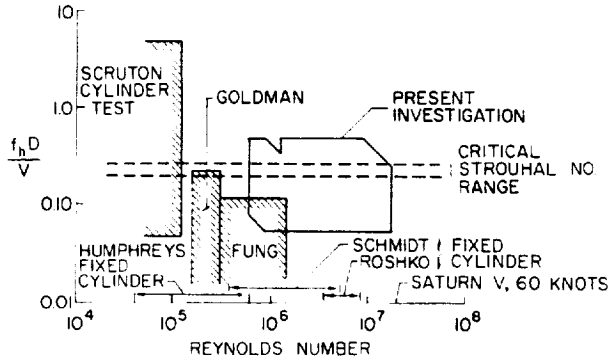

Fig. 30- Previous investigations of two-dimensional wind-induced oscillation effects on cylinders.

The wind-tunnel investigation at the TDT was conducted on a large circular cylinder that vertically spanned the TDT test section in a two-dimensional flow at Reynolds numbers from 0.36 million to 18.7 million. Figure 31 shows the model as tested in the TDT. The cylinder was instrumented to read directly the mean-drag and unsteady lift forces. In addition to the being fixed, the cylinder could be laterally oscillated over a range of frequencies and amplitudes. This oscillation capability was used to investigate the effects of cylinder motion on the aerodynamic forces generated.

The results of this study indicated the following conclusions:

(1) The mean-drag coefficient on the stationary cylinder, at Mach numbers less than 0.2, follows the trends established by previous investigations and has an approximately constant value of 0.54 for Reynolds numbers between 4 million and 10 million.

(2) The frequency content of the unsteady lift force on the stationary cylinder can be categorized into three regimes dependant upon Reynolds number as follows: wide-band random (1.4 million < Rn < 3.5 million), narrow-band random (3.5 million < Rn < 6 million), and quasi-periodic (Rn > 6 million).

(3) The Strouhal number of the unsteady lift on the stationary cylinder in terms of the center frequency of a Strouhal bandwidth follows the trends established by previous investigations at Reynolds numbers from 1.4 million to 8 million. At previously unexplored Reynolds numbers from 8 million to 17 million, the Strouhal number is nearly constant at about 0.3.

(4) At Mach numbers less than 0.3, the root-mean-square unsteady lift coefficient on the stationary cylinder fluctuates at Reynolds numbers from 1.5 million to 8 million, then the range narrows into a single function which decreases slowly with higher Reynolds numbers.

(5) A lift force due to cylinder oscillation exists when the cylinder is oscillated at or near the aerodynamic Strouhal frequency of the stationary cylinder. This lift force increases with increase in amplitude of motion, building up to several times the lift on the stationary cylinder. When the cylinder is oscillated at frequencies far removed from the aerodynamic Strouhal frequency of the stationary cylinder, there is no significant lift due to motion.

(6) The unsteady lift due to motion was found to have a destabilizing aerodynamic damping component for cylinder motion at frequencies below the stationary cylinder vortex-shedding frequency. This component shifts abruptly to a stabilizing damping force at frequencies above the vortex-shedding frequency.[11,12]

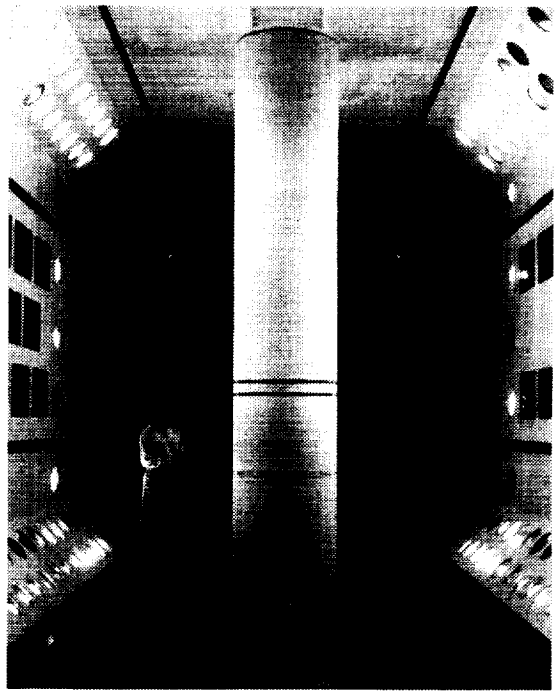

Fig. 31- Two-dimensional wind-induced loads model as tested in the TDT.

Titan III Phase II (TDT Test 95): The Air Force Titan IIIC launch vehicle was designed to be transferred from the assembly areas to the launch pad at Cape Kennedy by the Integrated-Transfer-Launch (ITL) transporter. On four occasions during the fall of 1964, the empty transporter was observed to oscillate in both moderate and high winds. In two instances the structure was damaged.

Concern over hazards resulting from wind induced oscillations forced the Air Force to reduce the placard wind speed for operation of the Titan IIIC transporter from 40 knots (46 mph) to 22 knots (25 mph).

The Martin Company of Denver (Titan IIIC contractor) proposed a joint TDT wind-tunnel test program with NASA Langley that utilized a dynamically-scaled ITL transporter together with components of an existing 7.5 percent scale Titan III model used in an earlier program. Dynamic characteristics of the full-scale ITL transporter were measured by the Martin Company and were used to properly scale the 7.5 percent transporter model. Testing was conducted in R-12 heavy gas at 45 percent of the full-scale Reynolds number. The wind-tunnel test was conducted to (1) reproduce the observed transporter phenomena, (2) define the problem, and (3) determine suitable fixes to eliminate the transporter problem without inducing any oscillation problems with the launch vehicle. Also, it was desired that the mast fix would eliminate the resonant forced oscillations of a vehicle with a bulbous payload fairing when mounted on the transporter. Proposed aerodynamic fixes included ITL transporter spoilers, an open lattice configuration, and a modified cross section configuration. Figures 32-36 show the various transporter fixes and the transporter with the Titan III vehicle with bulbous payload fairing in the TDT test section.

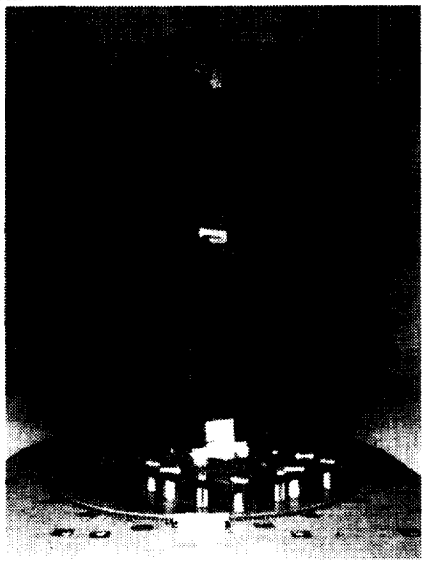

Fig. 32- Basic configuration of the Titan III ITL transporter.

The low speed wind induced oscillations of the full-scale ITL transporter mast were successfully reproduced in the wind-tunnel tests at the TDT. The nature of the problem was explicitly defined as a forced response due to periodic vortex shedding and this confirmed pretest predictions. Full-scale oscillations observed at 53 knots (60 mph) were probably the torsion mode of the transporter that was reproduced in the wind-tunnel tests. Several of the aerodynamic modifications to the ITL transporter were found to be satisfactory and performed as predicted. Figure 37 illustrates the effects of each aerodynamic fix on the resultant bending moment at the base of the leeward transporter pylon at the critical wind direction. The open lattice fix was selected as the most desirable because it eliminated the wind induced oscillation problem of the bulbous payload vehicle on the transporter.[13]

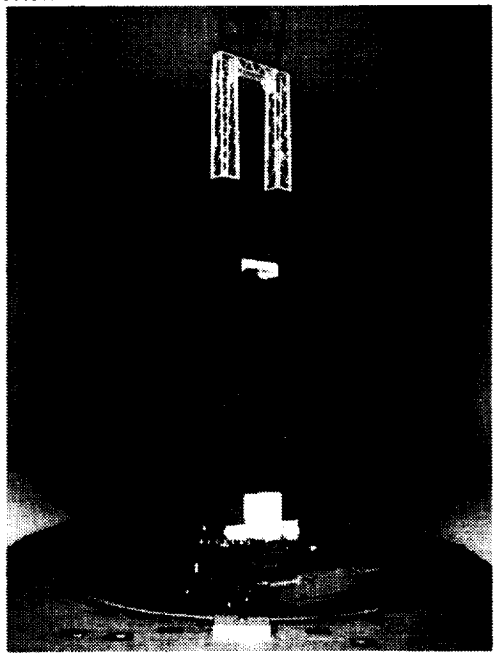

Fig. 33- Open lattice configuration of the Titan III ITL transporter.

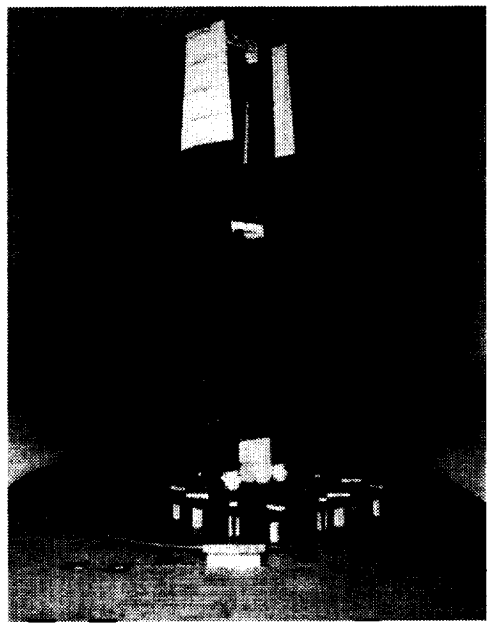

Fig. 34- Spoiler configuration of the Titan III ITL transporter.

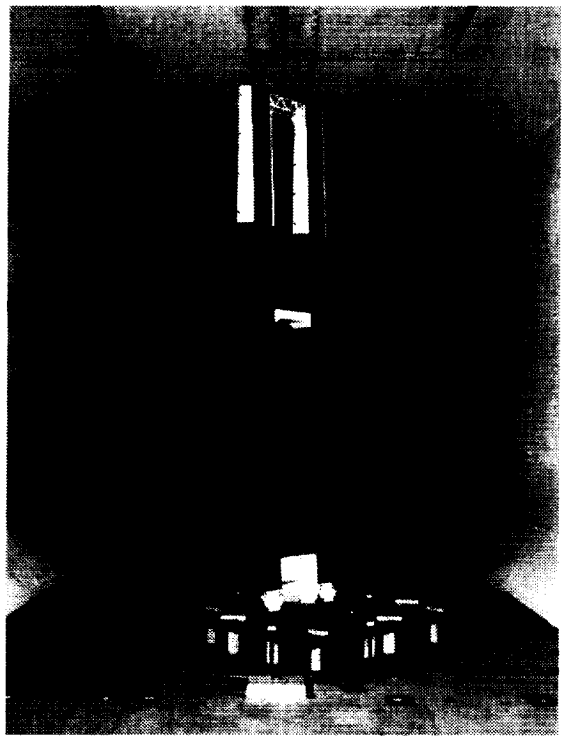

Fig. 35- Modified cross-section configuration of the Titan III ITL transporter.

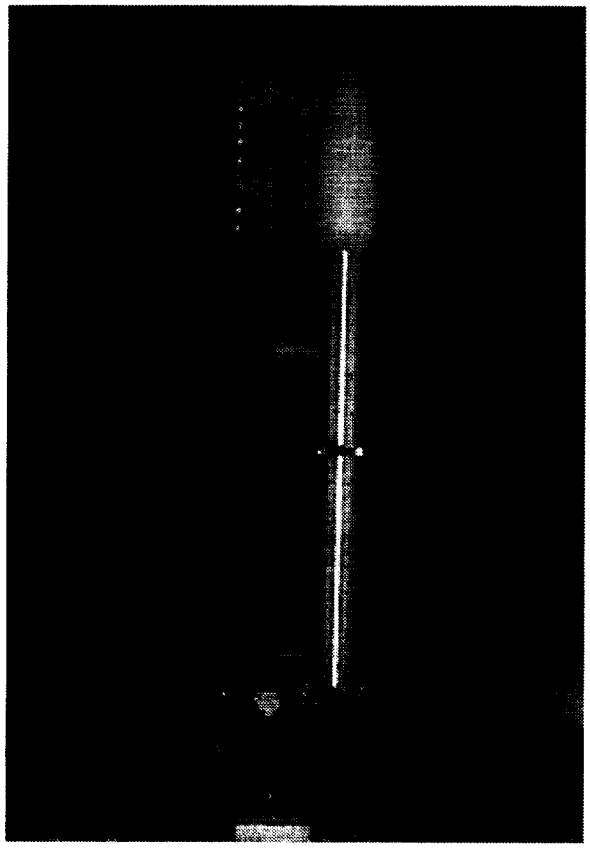

Fig. 36- Titan III with bulbous payload fairing and ITL transporter in TDT.

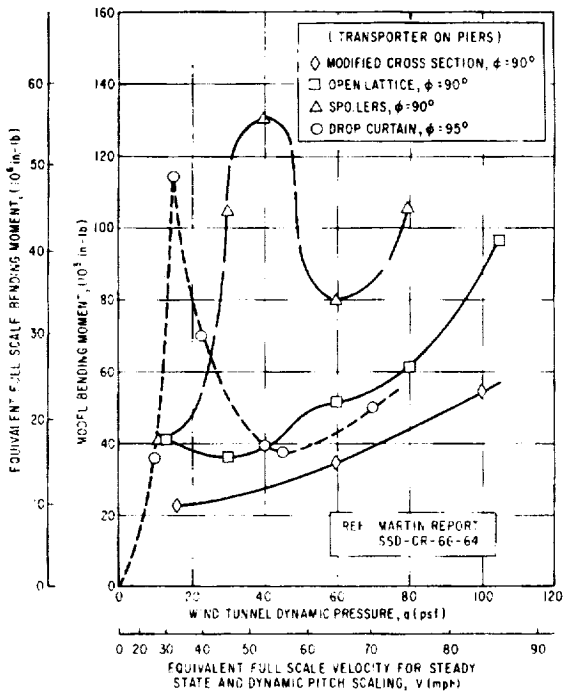

Fig. 37- Resultant bending moment versus wind speed for the isolated ITL transporter at the critical wind direction.

Skylab Launch Vehicles (TDT Tests 182 and 200): Early on in the development of Apollo-Saturn hardware, NASA began to look toward a follow on program to Apollo moon missions that would utilize flight hardware for missions other than to the moon. This culminated in the first U.S. manned space station as a part of the Skylab program. The Skylab was essentially an S-IVB third stage outfitted by McDonnell-Douglas as a living and research quarters for astronauts to work in a shirtsleeve environment. Skylab was boosted into orbit by the first two stages of a Saturn V launch vehicle and manned Apollo missions to Skylab were orbited by Saturn IB launch vehicles. Both launches were from Launch Complex 39B. Because of geometric and dynamic differences of the Saturn V with the Skylab payload and geometric differences of the Skylab Saturn IB launch complex configuration from past Saturn IB launches, a ground-wind loads program was sought to clear the vehicles of any possible wind-induced oscillation and load problems.

In a cooperative program with the Marshall Space Flight Center, approximately 600 hours of wind-tunnel testing at the TDT were involved in establishing the ground wind load environments for the Skylab launch vehicles. Tests were conducted on a modified 3 percent-scale Saturn V aeroelastic model with complex 39B and of a 5.5 percent-scale Saturn IB with the upper part of complex 39B. In both cases, the 39B umbilical tower was a geometrically-scaled model. Figures 38 and 39 show the Skylab launch vehicles as tested in the TDT.

Figure 40 shows results for the Saturn IB Skylab tests which indicate that the critical wind azimuth is 120° and that the addition of structural damping can effectively reduce the maximum resultant base bending moment from near the critical design value to one much more manageable.

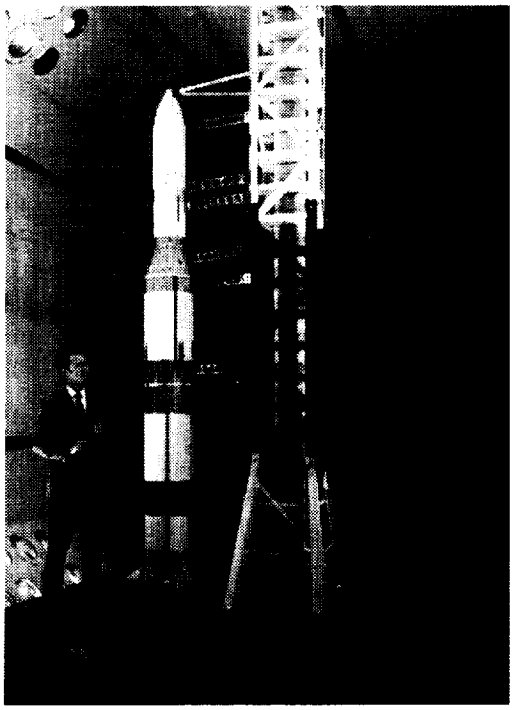

Fig. 38- Saturn V with Skylab payload in TDT test section.

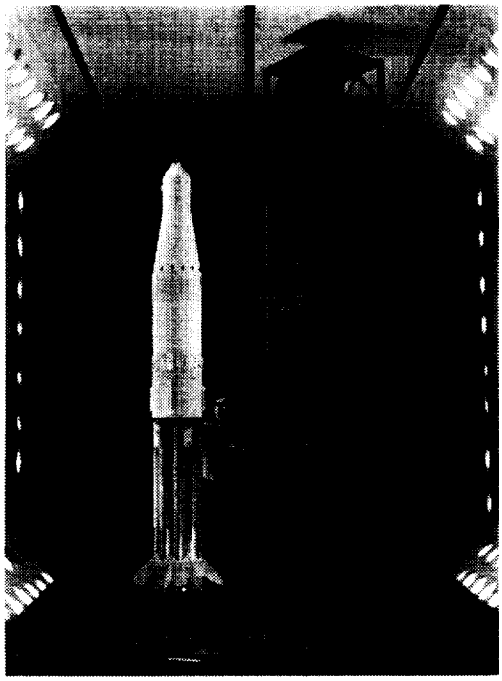

Fig. 39- Skylab Saturn IB with Launch Complex 39B.

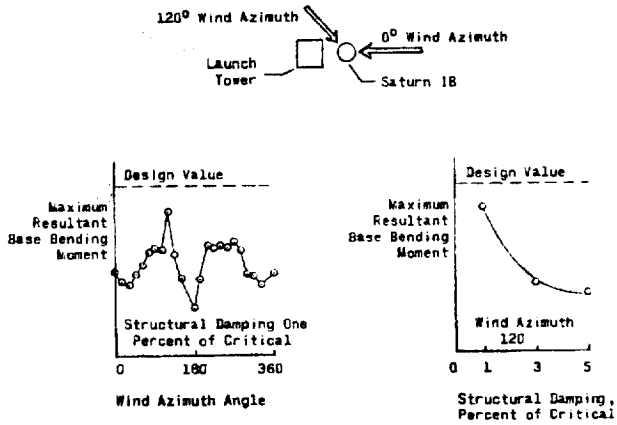

Fig. 40- Saturn IB Skylab vehicle ground-wind loads.

This cooperative program resulted in the verification of the Skylab vehicles ground-wind loads design criteria, confirmed the fact that the external damper system for suppressing dynamic response was satisfactory, and provided the necessary information to define the operational wind constraints.

Space Shuttle (TDT Tests 210 and 306): Early in the development of the NASA Space Shuttle, researchers at the TDT realized that the winged orbiter and booster configuration presented many rather unique problems associated with ground-wind loads. While the Shuttle is erected on the launch pad, it may be exposed to occasional high-wind conditions. In the case of the final Shuttle design, the criterion for peak winds of 81 knots corresponds to a one percent risk of exceeding that velocity during a two-week exposure at the windiest time of year. This ground-wind environment creates a wide range of potential problems that include fatigue damage due to long wind-exposure times accumulated during the Shuttle's expected 100 mission service life.

Because space shuttle vehicles possess configuration features that are unlike those of any previous launch vehicle, it is not surprising to find new problems related to ground-wind loads. For example, associated with the Shuttle's noncircular bluff body shape is a potential for aerodynamic galloping instability, and associated with the large planform lifting surfaces is a potential for "stop-sign" flutter- a stall flutter phenomenon involving torsional oscillations about the longitudinal body axis.[14]

In order to address these newfound problems associated with wind-induced loads of space shuttle vehicles, a 3 percent scale aeroelastic model of a preliminary Space Shuttle design was tested in the TDT in October of 1972. Figure 41 shows the model mounted on the ground-wind loads turntable in the TDT test section. This wind-tunnel study was designed to provide an early indication of the severity of ground-wind loads for shuttle-type vehicles as a function of wind velocity, wind azimuth angle, and structural damping; to assess the

effects of variations of stiffness of vehicle tie-down restraints and orbiter-to-booster links; and to evaluate the types of modal response to the simulated ground winds. Figure 42 shows results from this test for the no fuel, 73 knot design wind condition and illustrates the effect of launch towers on the vehicle static overturning moment coefficient. This coefficient is defined as the measured static moment normalized by the product of dynamic pressure, planform area, and vehicle height and is shown as a function of wind azimuth angle.

Fig. 41- Three percent aeroelastic model of early Space Shuttle design.

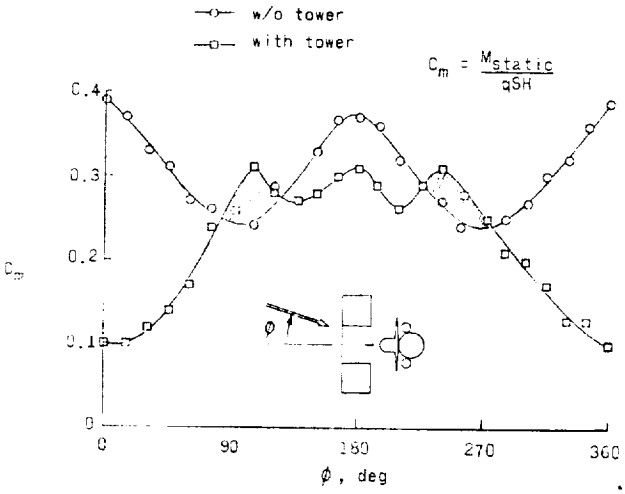

Fig. 42- Effect of launch tower on Shuttle static hold-down moments for 3 percent aeroelastic model of early Space Shuttle design.

After the Shuttle design fully matured, a cooperative wind-tunnel test with Rockwell International Space Systems Group was conducted in the TDT in July of 1978 of a 4.6 percent aeroelastic model of the final Shuttle configuration with and without geometrically-scaled service structures. Figures 43 and 44 shows this model mounted on the TDT ground-wind loads turntable. The 4.6 percent scale orbiter model was the same used for earlier flutter/buffet tests of the 747 and orbiter piggy-back configuration. Testing was conducted using R-12 gas as the test medium, which resulted in full-scale wind conditions and subcritical Reynolds numbers on the order of 0.3 scale factor. Model instrumentation included a pedestal mount to which the orbiter was attached that was instrumented with an array of strain gages calibrated to yield the pitch, roll, and yaw bending moments. Attachment struts with the least margin of safety were instrumented with strain gages. These struts included the forward orbiter-to-external-tank strut, the orbiter-to-external-tank vertical strut, and the aft external-tank-to solid-rocket-booster diagonal strut. Accelerometers (11 total) were distributed within the external tank, solid rocket boosters, and orbiter such that the expected low frequency modes of the vehicle could be detected if the vehicle responded at those frequencies.

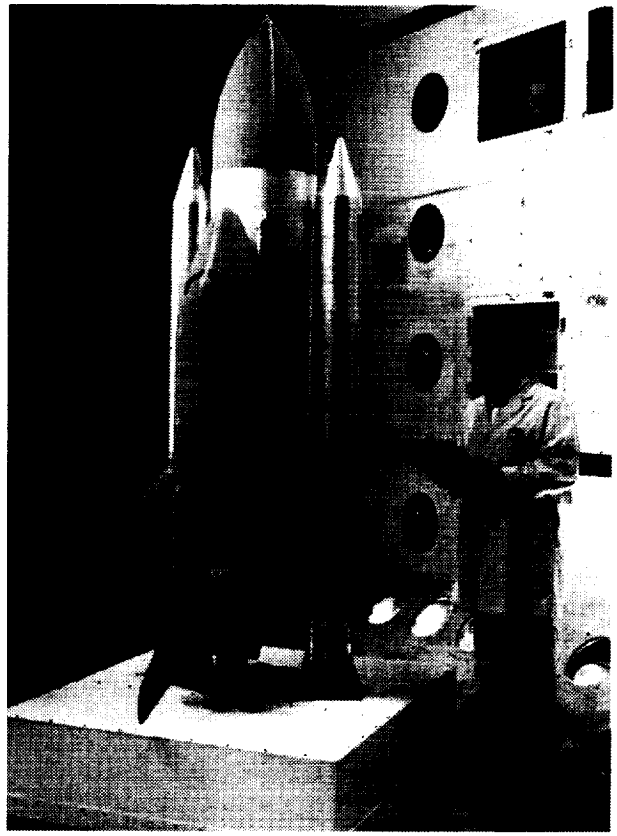

Fig. 43- 4.6 percent aeroelastic model of the final Space Shuttle configuration.

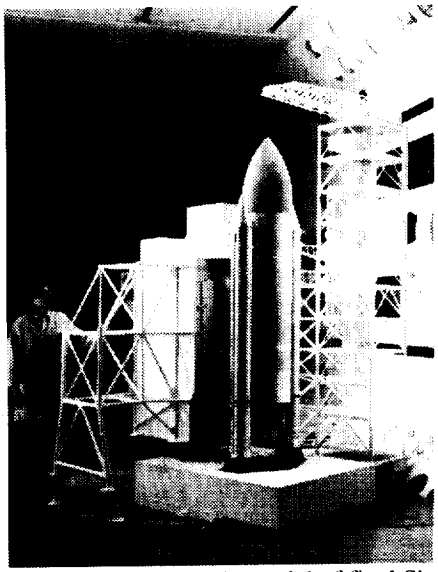

Fig. 44- 4.6-% aeroelastic model of final Shuttle configuration (geometrically-scaled service structures).

Results from this study are presented in Fig. 45 which shows the variation of the base bending moment as a function of wind azimuth angle for a scaled wind velocity that corresponds to a statistically-derived one percent risk of exceeding 72 knots. The measured resultant bending moment (static plus dynamic loads) is normalized by the design value. The data for the launch vehicle alone (as when being transported to the launch complex) indicate the design moment is not reached regardless of wind direction. For the case where the launch vehicle is on the pad surrounded by the service structures, data were obtained only at wind azimuth angles from 0° to 120° due to a static load failure of the structures representing the service tower, rotary bridge, and payload change-out room. However, design moments were not exceeded over the range tested as shown in Fig. 45. It was later decided by Rockwell not to test with a new service structure at a later date because they felt that the data could be obtained using analytical techniques. During testing, no torsional or "stop-sign" flutter was observed at any azimuth angle in spite of the fact that the torsional stiffness was less than full-scale requirement.[15]

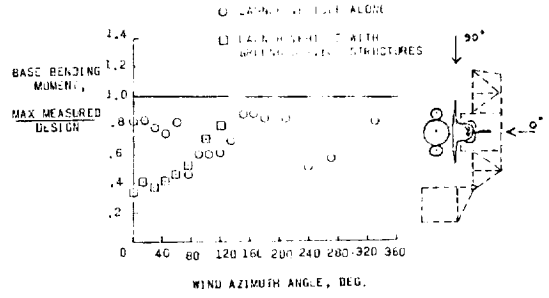

Fig. 45- Normalized base bending moment of 4.6 percent scale model of final Shuttle configuration.

Atlas II (TDT Test 443): The most recent ground-wind loads test at the TDT took place in June of 1989 and involved an Atlas II launch vehicle built at the time by General Dynamics Space Systems Division. The model consisted of an 8.6 percent aeroelastically-scaled model of the Atlas II vehicle and a rigid, geometrically-scaled umbilical tower model. The model design included a scaled ground-winds damper connected to both the vehicle and tower to allow for qualification of the damper to reduce ground-wind loads and vibration. Test objectives included: (1) define steady state lift and drag coefficients for vehicle responses as a function of wind speed and direction and (2) define vortex shedding lift and drag coefficients for vehicle responses as a function of wind speed and direction. Design wind speed for the Atlas II was 30 knots. Tests were performed using R-12 heavy gas as a test medium to match full-scale Reynolds number and Strouhal number and the model was configured in both the fueled and unfueled configurations. Figure 46 shows the Atlas II model and umbilical tower mounted to the TDT ground-wind loads turntable.

Figure 47 shows the results for the Atlas II in the unfueled condition. The total resultant base bending moment is shown versus wind speed for a critical wind azimuth angle. With the damper installed, the resultant bending moment is almost entirely due to the steady bending moment and at 30 knots it is less than the critical limit. Without the damper, it is shown that the design bending moment is exceeded at approximately 23 knots. Ground-wind loads testing of the Alas II at the TDT showed that it would be free of wind-induced load problems during fueling and launch preparations prior to launch.

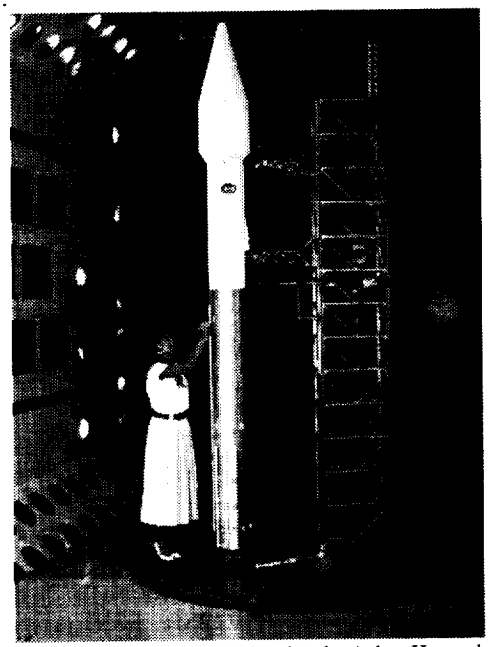

Fig. 46- 8.6 percent scale aeroelastic Atlas II model and umbilical tower.

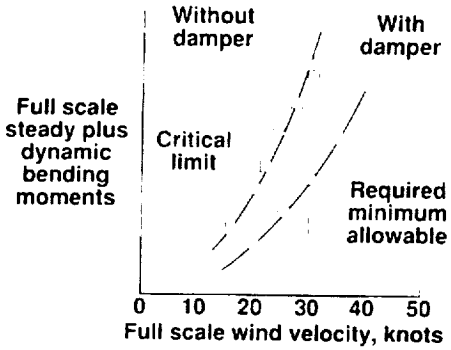

Fig. 47- Full-scale resultant bending moment of Atlas II vehicle versus wind velocity.

LAUNCH VEHICLE DYNAMICS

The TDT has supported a number of launch vehicle dynamics measurement tests over the facility's history. This section of the paper deals with some of the basic launch vehicle configurations and measurements that were most pertinent to the in-flight atmospheric transition of launch vehicles. TDT testing of a less conventional launch system, the Space Shuttle, will be included in a later section of this paper.

Most of the TDT launch vehicle tests centered on Saturn-Apollo manned space flight vehicles. All of these tests occurred in the first decade of testing in the TDT (through 1969). Aside from Space Shuttle testing, no additional testing of launch vehicles occurred until 1988. Since 1988, three basic launch vehicle configurations have been tested. All known TDT tests associated with the flight of launch vehicles are covered in this section of the paper. Not all of these tests would be described as typical TDT tests. Based on the limited amount of information that could be found on some of these tests from many decades ago, it is possible that a few of them did not entail dynamics testing.

Precursory manned launch vehicle (TDT Tests 24 and 31): A TDT wind-tunnel investigation was completed in the early 1960's to research buffet characteristics of representative launch vehicle for the manned lunar mission. The basic model design was quite similar to the eventual Saturn-Apollo vehicle. The investigation primarily involved the testing of two different scale rigid models of the same vehicle to assess scaling effects on buffet measurements. However, there was also an approximately two-percent aeroelastically scaled model of the same vehicle. A limited number of response measurements were made using this aeroelastically scaled model. The primary purposes of these tests were to define any buffet problem areas on the manned launch vehicle configuration and to study whether buffet pressure characteristics measured on models could be scaled with confidence to full-size vehicles using normal scaling relationships.

The two rigid models were 8-percent and 1.6-percent scaled models of the planned manned launch vehicle. The basic 8-percent wind-tunnel model is shown sting-mounted in the TDT test section in Fig. 48. Figure 49 shows both of the rigid models together. For both of these rigid models, four different escape-tower configurations were available for testing. These models were instrumented with six unsteady pressure measuring transducers for measuring buffet response. The 8-percent scale model had one additional unsteady transducer located on the forward cone-cylinder shoulder. Additionally, the 8-percent model had 22 steady pressure measurement devices to give a steady pressure distribution over the same streamwise length of model that was covered by the unsteady pressure measurement transducers.

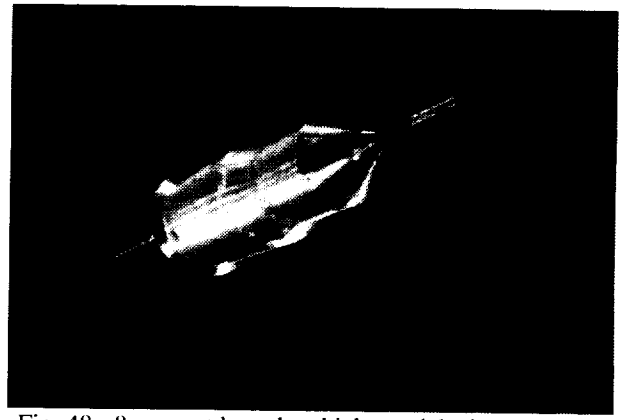

Fig. 48- 8-percent launch vehicle model sting-mounted in the TDT.

Fig. 49- The 8-percent and the 1.6-percent rigid launch vehicle models.

The two-percent aeroelastically scaled model was a previously existing model with similar geometry to the manned vehicle. This model was modified with a removable sleeve to simulate the proper shape of the

forward portion of the manned launch vehicle configuration. With this sleeve attached, the aeroelastic model became a 1.427-percent model of the full-scale vehicle, with the model downstream of this sleeve oversized compared to this scale factor. The model scaled the first free-free bending rigid-body pitching frequencies to within about 20 percent of the frequencies for the full-size vehicle. The aeroelastically scaled model without the removable sleeve is shown in Fig. 50. The purpose of this aeroelastically scaled model was to determine if model flexibility would significantly increase buffet loads. Although the aeroelastic model was not an exact replica of the flight vehicle, it was felt that this model would indicate any substantial increases in buffet response. It was found that buffet response was not significantly affected by the flexibility for this configuration.

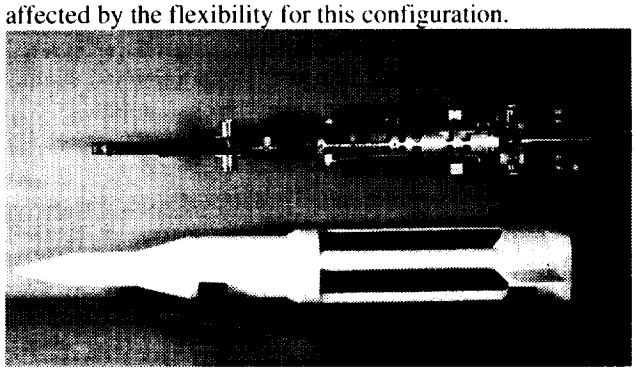

Fig. 50- Photograph of the 2-percent aeroelastically scaled model without the removable skirt installed.

The major conclusions from this test program were drawn from the two rigid model tests. The first conclusion was that the wake off of the escape tower for the vehicle, under certain conditions, produces relatively high noise levels (about 168 decibels) on the nose and cone-to-cylinder shoulders of the upper stages of the vehicle. Certain tower rocket configurations produced more noise than others did. Secondly, it was concluded that regardless of the presence or absence of the escape tower, large pressure fluctuations occurred on the vehicle just aft of the cone-to-cylinder shoulders in a narrow band of Mach number just below 1.0. It was noted that these fluctuating pressures could cause a problem in venting unpressurized portions of the vehicle; however, the fluctuating pressures were not anticipated to cause any structural response problem. This lack of impact on the structural response was inferred from the tests with the 1.427-percent aeroelastically scaled model. The final conclusion drawn from this work was that an evaluation of buffet scaling relationships derived from simply dimensional considerations for these tests provides evidence that properly scaled models of launch vehicles can be used to determine buffet pressure characteristics. Reference 16 provides a more complete summary of these wind-tunnel models, the data obtained from the TDT tests, and discussion of the test results.

Project FIRE Buffet and Air Loads (TDT Test # 38): Project FIRE (Flight Investigation Reentry Environment) was a flight reentry program conducted by NASA to study total heat transfer and related phenomena of atmospheric reentry. The Project FIRE vehicle consisted of a blunt shaped reentry package and rocket motor (velocity package) mounted to an Atlas D launch vehicle.[17-19]

The relatively blunt nose of the Project FIRE space vehicle nose suggested the possibility of buffeting problems in the transonic and supersonic portion of the launch ascent. Consequently, a test program was conducted in the TDT to determine if buffeting problems existed and to investigate configuration variations that would alleviate any buffeting problems that might occur. The test also provided detailed static pressure distributions required for loads and stability calculations on the vehicle (A. Gerald Raney, 1662- internal memorandum available from the NASA Langley Aeroelasticity Branch).

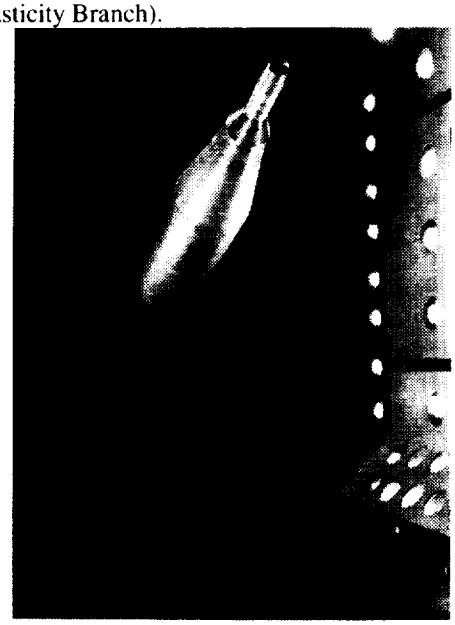

Fig. 51- 1/6-scale rigid Project FIRE buffet model.

The model was 1/6-scale, rigid, and included the reentry vehicle, velocity package and three diameters of the Atlas rocket. Model instrumentation included 10 high-frequency unsteady pressure transducers at locations selected as likely for unsteady flow conditions and 69 static pressure orifices spaced along 21 longitudinal stations. Four configurations were tested; a baseline configuration, shown in Figs. 51 and 52 and three modified configurations which added combinations of wooden pods which simulated explosive bolts and a "doughnut" shaped fairing that would house four spin

rocket motors at the base of the velocity package. The test was conducted using R-12 as the test medium over a Mach number range of approximately 0.40 to 1.15, at angles-of-attack from –8° to 8°, and at Reynolds numbers up to 1.5 x 10^6 based on the velocity package diameter of 0.418 feet.

Test results indicated that typical values of pressure fluctuations were approximately 8 percent of the dynamic pressure. The maximum pressure fluctuations occurred in the high subsonic/transonic region with values as high as 20 percent of dynamic pressure. A description of the model, test procedures, and results are presented in an internal memorandum (Brydsong and Foughner, 1962) available from the NASA Langley Aeroelasticity Branch.

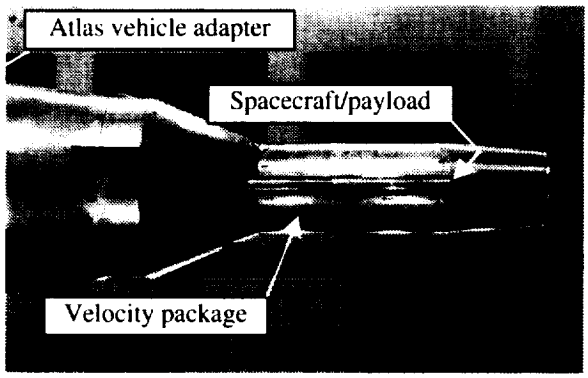

Fig. 52- Project FIRE model: forward section details, baseline configuration.

Saturn I booster aeroelastically scaled model (TDT Tests 48 and 60): At the time of the development of the Saturn I-Apollo launch-vehicle system, it was recognized that while buffet response could be reasonably assessed based rigid-model measurements, aerodynamic damping estimates were much more difficult to obtain. In order to address this concern for the Saturn I configuration, NASA began a program to develop analytical means of predicting full-scale vehicle dynamics, and to experimentally measure aerodynamic damping using scaled wind-tunnel models. The analytical work was conducted by Lockheed Missiles and Space Company and is summarized, along with some of the experimental results, in Ref. 20. Experimental studies were conducted at the NASA Ames and Langley Research Centers. The Langley tests were conducted in the TDT in 1962 and 1963 and are summarized in Ref. 21. The basic objectives of the TDT tests were to measure the aerodynamic damping and the buffet response for use in assessing the full-scale flight vehicle.

The Langley model of the Saturn I-Apollo launch vehicle was an 8-percent aeroelastically scaled model that was build by North American Aviation, Inc. The model was a very complicated system for that time and cost over one million dollars to design and fabricate. The wind-tunnel model was about 14.5 ft. long, weighed 786 lbs., and was sting mounted in the TDT test section. The basic structure consisted of a central aluminum tube that gave the model the proper scaled-stiffness distribution while providing the strength need to conduct the dynamic wind-tunnel test. The mass distribution of the model was scaled to match the flight vehicle for the Mach number = 1.0 condition. This model had a fairly unique capability of exciting dynamic response for measuring aerodynamic damping because it had an electromagnetic shaker built into the model structure. The moving coils of the shaker were attached directly to the inside of the model. The fixed-field coils of the shaker were mounted on the sting that supported the model. In addition to the flexibility of the model structure itself, the model was mounted to the sting by a system of leaf-springs, cables and torsion bars to provide the proper pitch stiffness of the model and to assist in supporting the weight of the model. The resulting support system provided simulation of the full-scale rigid body pitch frequency with a minimum of restraint imposed on the elastic deformations of the model.

The basic wind-tunnel model configuration consisted of the Saturn booster, the Apollo spacecraft (command module), and the launch escape system attached to the command module. In addition to the basic configuration, several modifications were tested in the TDT. The modifications included the addition of a flow-separator disk to the escape system rocket, removal of the first stage fins, removal of the launch escape system for the command module, substitution of a Jupiter nose cone for the Apollo-spacecraft-and-escape system, and the substitution of some modified thin fins for the relatively thick wedge airfoil fins of the basic configuration. A drawing of the basic configuration is show in Fig. 53 with the removable flow-separator disk attached above the launch escape system tower. The figure also shows a drawing of the Jupiter nose cone that could be substituted for the Apollo command module and the escape rocket system. Fig. 54 is a photograph of the model sting-mounted in the TDT test section.

The test in the TDT was conducted using the heavy gas test medium for which the model was scaled. The model was tested throughout the transonic range at conditions up to a Mach number approaching 1.2. The model was also tested for angles of attack up to six degrees.

The results of these Langley TDT tests are discussed in Ref. 21. Aerodynamic damping and buffet response measurements were made for the basic launch vehicle configuration with an Apollo spacecraft payload. Six additional modified configurations were also studied. Figure 55 shows an example of measured aerodynamic damping valves as compared to analysis predictions. This data figure is taken from Ref. 22. These data are described as typical of data obtained during the test. It shows that the basic damping with Mach number was

nearly opposite in trend for the no-disk versus flow-separation-disk configurations. The analysis is based on a quasi-steady technique developed by Lockheed Missiles and Space Company as discussed in more detail in Ref. 21. Reference 22 states that the correlation between the analysis and the measurements is good. This statement is based on two considerations. First, the qualitative agreement between analysis and experiment in predicting the reversal in the basic Mach number trend between the two configurations. Secondly, the quantitative correlation is considered good in light of the fact that: 1) obtaining experimental values of damping for launch vehicles is difficult because of the low values of damping involved, and 2) the aerodynamic complexity of the configuration is difficult to capture given the analytical technique. The data from these TDT tests was later evaluated again in Ref. 23 with respect to aeroelastically destabilizing effects on slender payload bodies at high subsonic speeds. Reference 23 discusses two types of destabilizing effects predicted by analysis and speculates that some of the data from these TDT experimental tests may represent an experimental occurrence of one of these types of destabilizing effects.

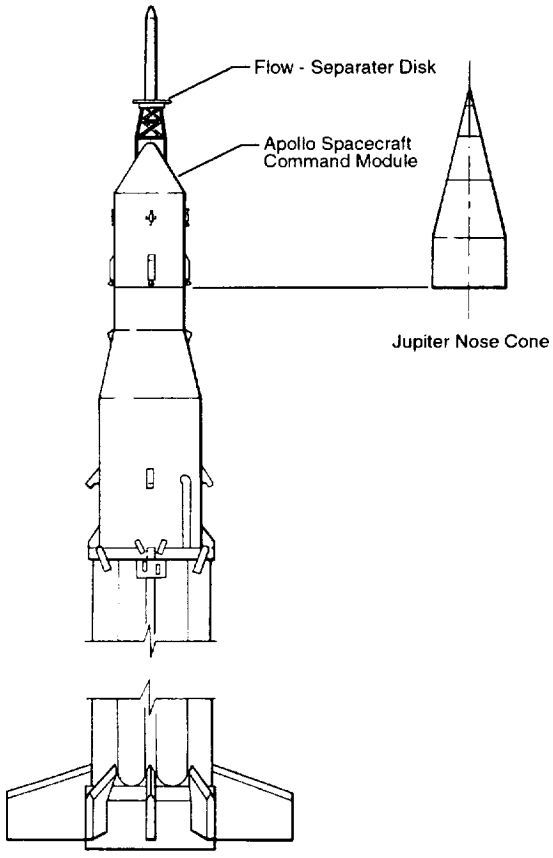

Fig. 53- Drawing of the Saturn I launch vehicle model showing nose cone configuration variables.

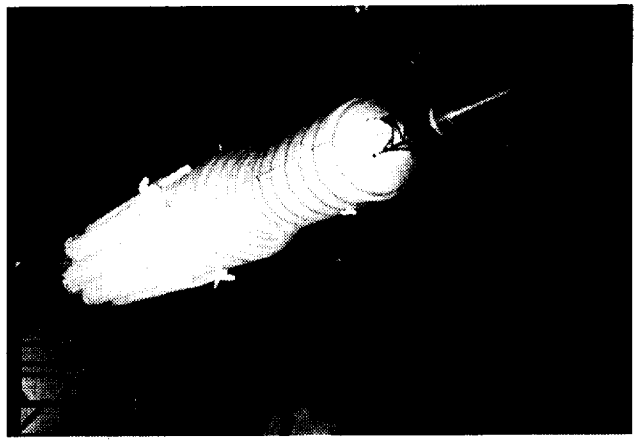

Fig. 54- Photograph of the Saturn I launch vehicle mounted in the TDT.

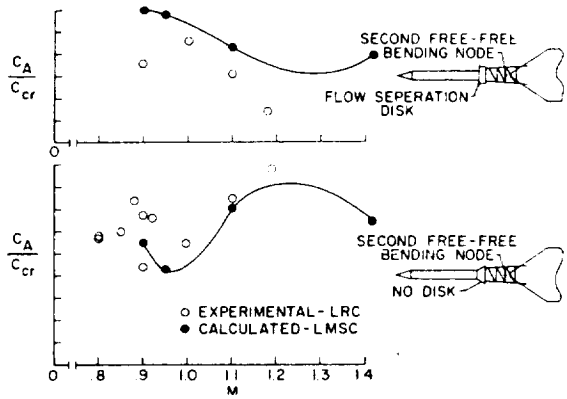

Fig. 55- Comparison of experimental and calculated aerodynamic damping for the basic Saturn-Apollo second bending mode with and without the flow-separation disk.

Launch Escape Canard Model- (TDT Test 66): A key capability of the Apollo spaceflight vehicles was the ability to return the crew to the Earth's surface in the event of a malfunction during the atmospheric ascent phase of the launch. This was done via a portion of the overall Saturn Apollo launch vehicle known as the launch escape vehicle (LEV). The LEV actually consists of the crew-containing command module and a rocket that is used to pull the command module away from the launch booster should a problem develop. This rocket was attached above the command module by a tower structure. At the nose of the rocket on the LEV, there was a set of canard surfaces that could be deployed during a launch abort. Figure 56, from Ref. 24, shows the deployed canard configuration. In the normal, undeployed flight configuration, these canards were actually external skin components of the LEV rocket nose.

The idea behind the LEV was that if a flight malfunction occurred, the LEV rocket would quickly transport the command module forward of the launch booster. Once the command module was safely removed

away from the Saturn booster, it was necessary to rotate the LEV until the command module heat shield was facing forward in flight to ensure the survivability of the returning command module. This phase of the escape sequence involved deploying the rocket-nose canards after escape rocket motor burnout to destabilize the LEV, causing it to rotate into a heat-shield-forward position. The canard surfaces also provided aerodynamic damping after the vehicle had attained the desired flight attitude. This damping reduced or eliminated the oscillations that result from the rotating maneuver.

A number of wind-tunnel tests in many facilities were conducted for this LEV canard configuration. Most of these wind-tunnel tests were intended to determine static and dynamic stability characteristics of the LEV with the canard surfaces in the deployed (open) position. Refs. 24 and 25 summarize many of these tests.

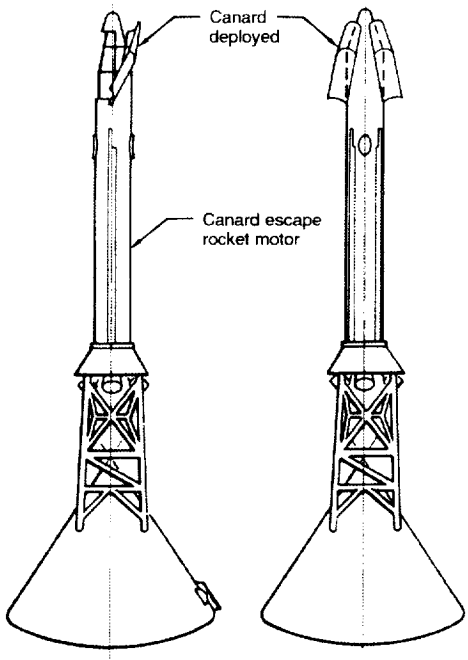

Fig. 56- Drawing of the LEV with the canard surfaces deployed for launch-abort escape.

A single test of the LEV canard configuration was conducted in the TDT in late 1963. This test is not covered in the previously mentioned references and no other documentation has been found regarding this test. However, photographs and films are available that shed some light on the test and its objectives. The TDT model (Fig. 57) was sting mounted and apparently was an actual flight-vehicle article or a full-scale model. The model only represented the most forward portion of the LEV escape rocket, to just beyond the rocket nose cone. Films show that the TDT test involved the actual deployment of the canard surfaces from their stowed, "rocket-nose-cone-skin" position, until their fully opened, deployed configuration. The TDT was probably used for these tests because of its relatively large size, accommodating the full-scale model, and because the TDT was suitable for testing the dynamics involved in the deployment motions and possible model failures. The test may have simulated flight dynamic pressures to help ensure that the opening canards were strong enough for actual flight deployments. However, from what is known about this test, it is believed that these tests were conducted in the air test medium at atmospheric pressures. One interesting aspect of the deployment sequence in the TDT, based on film clips of the test, is that these operational checks of the canards probably began by detonating small pyrotechnic charges that released the canard surfaces and initiated their opening into the launch-abort escape attitude.

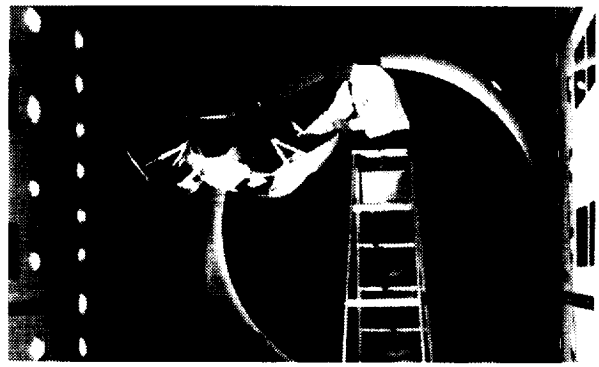

Fig. 57- Photograph of the LEV forebody model, with the canards deployed, sting-mount in the TDT.

PSTL1 Saturn Apollo Model (TDT Test 102): Reference 24 discusses the need to define transient, fluctuating pressure levels during launch trajectory for structural design of the Saturn Apollo vehicle. The reference mentions two models, identified as PSTL-1 and PSTL-2 that were built for the purpose of determining transient, fluctuating pressures of the Saturn Apollo vehicle. The acronym PSTL stands for "pressure, static, transient, launch". Data from these models were also useful in determining buffet response of the launch vehicle. These models were supposedly built to be as large as reasonably possible given facility limitations. Reference 24, published in December 1966, covers models tested through October of 1964. The report discusses three facilities in which the PSTL-1 and PSTL-2 models were tested; the North American Aviation Trisonic Wind Tunnel, the Ames 14-ft Transonic Wind Tunnels, and the Ames Unitary Plan Wind Tunnel. The TDT is not mentioned with regard to unsteady pressure measurement models because of the time period covered. However, records indicate that a test of the PSTL-1 model was conducted in the TDT in February and March of 1966. No documentation of this TDT wind-tunnel test has been found other than photographs. Figure 58 is a photograph of the PSTL-1 model sting-mounted in the

TDT. Although no information is available about this test, it would be reasonable to speculate that this additional test was conducted because of the availability of the PSTL-1 model and the interest at that time in experimentally researching launch vehicle dynamics in the TDT. Furthermore, there may have been a desire to correlate test data for the model from the larger TDT facility with the results from the original three facilities used for PSTL model testing. The cross-sectional area of the TDT is approximately 40-percent larger than the largest of the other three tunnels.

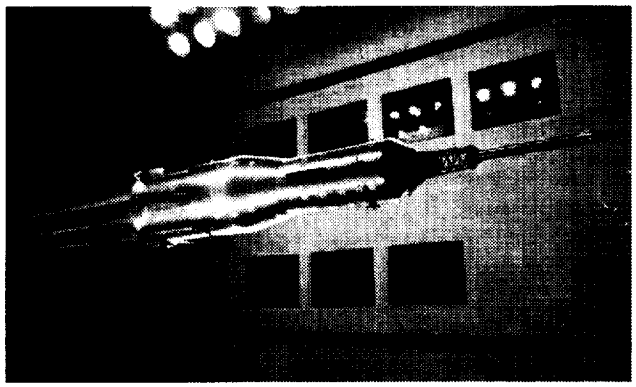

Fig. 58- Photograph of the PSTL1 model sting-mounted in the TDT.

Bulbous shaped payloads (TDT Test 58): TDT operational logs indicate that two bulbous payload launch vehicle models were tested beginning in late December 1967. One was described as a large bulbous payload and the second was described as a small bulbous payload. Other than this operational log evidence that the testing occurred, no other documentation of the test has been found. Some evidence of the planning process that was taking place at NASA Langley regarding launch vehicle research during this time period is available in the form of internal Langley correspondence memorandums (memos). These memos may shed some light on what took place in the TDT wind-tunnel test. Therefore, in an attempt to more fully complete the summary of TDT space-related contributions, the content of some of these memorandums will be discussed here.

The first memo that was found is dated July 1965. It describes a research proposal to test a series of bulbous payload models to measure static pressures. The memo describes the lack of information that was available at that time for bulbous payload shapes. The research project was envisioned to provide a database that would allow empirical estimation of airload distribution on launch vehicles with bulbous-shaped payloads. The basis for needing this data was that ever increasing demands to enlarge payload volumes containing less-dense packages was resulting in larger fairings to encompass the payload. The larger payload fairing resulted in a necked-down shape upstream of the primary booster stage. This type of configuration came to be described as a bulbous payload vehicle. Analysis of this type of configuration for the purpose of predicting airloads, particularly transonically, was considered very difficult during this time period. The proposed project called for about a dozen different bulbous payload configurations to be tested to gather the empirical database. The model variations were anticipated to include different nose cone angles, fairing boat-tail angles, booster flare angles, fairing cylinder length-to-diameter ratios, and various ratios of forward cylinder diameter to downstream cylinder diameter. The tests were planned to cover a Mach number range from about 0.7 to 5.0 and an angle-of-attack range from 0 to 8 degrees. The planned Mach number range means that some facilities other than the TDT would have to be used to meet the Mach number requirements. In fact, the memorandum does not actually mention any particular test facility. However, an engineer in the Aeroelasticity Branch associated with the TDT wrote the memo.

A later memo, dated September 1965, shows that the test program had evolved into a proposal to contract the work for the government. The idea was for a contracted staff to design the models, pursue their fabrication, and then gather the test data for NASA. NASA research engineers would then utilize the data to develop the empirical methods of predicting airloads. This memo states two targeted wind-tunnel facilities for conducting this work, the Ames Unitary Plan 9-ft tunnel and the Langley 16-ft transonic tunnel.

It is unclear if this program was ever really accepted within NASA. A memo dated June 1966 indicated that the work loads of some of the larger wind tunnels was such that it precluded the testing of these proposed bulbous payload models in the foreseeable future. This 1966 memo proposed that two pressure models, differing in size by a factor of six, be tested instead as a first step. The larger model tests were to be conducted in the Ames 11-ft by 11-ft tunnel and in the Langley TDT. This may have been to acquire data for two Reynolds numbers, with the Ames tunnel providing a Reynolds number nearly twice the value of the TDT-test Reynolds number according to the memo. The smaller model would be tested in the Ames 2-ft by 2-ft transonic tunnel. The memo goes on to state that if the data correlated well between these different facilities for the two models, then the original proposal to test many configurations would continue to be pursued. However, the memo further states that if the data did not correlate well between these facilities for the similar, but different geometric scale models, that the larger test program would have to be reevaluated.

No other information regarding the development of this proposed bulbous payload launch vehicle test program has been located to explain events leading up to

the subject TDT test. As previously stated, the authors of this paper have not been able to locate any specific information on the TDT test except that a large and a small bulbous payload model were tested. It is also not known if any testing from this proposed program actually occurred in other facilities. It may be possible that the two different-size models proposed in the June 1966 memo were the models that were tested in the TDT, and that they were simply described as large and small bulbous payload models. What little evidence exists seems to indicate that the TDT test was for static pressure measurements. This in itself would have been unusual for the TDT, which concentrates on dynamic, aeroelastic testing. However, as previously discussed, the unavailability of other facilities may have contributed to the use of the TDT, perhaps in an attempt to provide evidence that would help force the initiation of the full-scope program.

An additional, undated memo was found in some facility records from the March 1968 time period summarizing once again a proposed research study of twelve bulbous payload models. This may be an indication that some NASA engineers continued to pursue this research program after the completion of the one test in the TDT in early 1968. A drawing showing the basic bulbous payload models that were targeted for this long pursued research program is shown in Fig. 59.

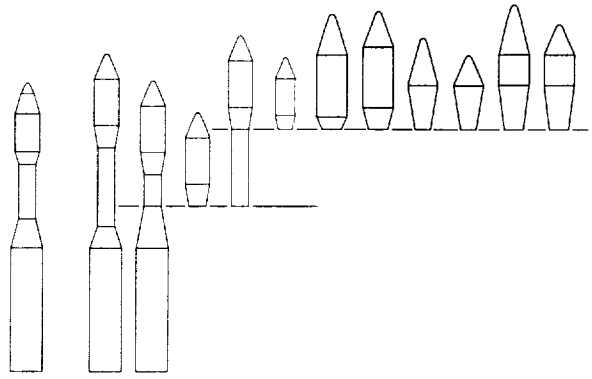

Fig. 59- The bulbous payload model series proposed as a NASA research program in the late 1960's.

Saturn-Apollo Command Module Blast Wave Study (TDT Test 148): During the development of the Saturn Apollo vehicle for the lunar landing flights, there was concern about pressure effects on the Apollo command module spacecraft of the shock front produced by the detonation of launch vehicle propellants in the event of an aborted launch. The escape tower with a solid rocket motor was provided to remove the Apollo command module (capsule) from the overall vehicle, but a detonation blast wave could potentially interact with the capsule. In order to evaluate this transient loading, a model of the Apollo capsule with the escape tower was floor mounted in the TDT and a series of TNT charges were detonated from a tower behind the capsule. This test took place in 1969. A photograph of the test setup is illustrated in Fig. 60. A close-up photograph of the command module model is shown in Fig. 61. Unsteady pressures were measured to evaluate the blast wave effects. Visual observations may have contributed qualitative information regarding the effects of such explosions. Some photographs, not included here, show dark spots (possibly material pitting) on the downstream side of the command module, which faced the explosive blasts. Safety problems with such a test were of considerable concern, and consequently the amount of TNT was limited to 0.1 pound per blast. Pre-test correspondence indicates that there was also a requirement to build the detonation primer caps and explosive container out of a non-metallic material to prevent shrapnel damage to windows in the TDT test section adjacent to the control room. The test results were provided to the project personnel and no additional documentation has been found.

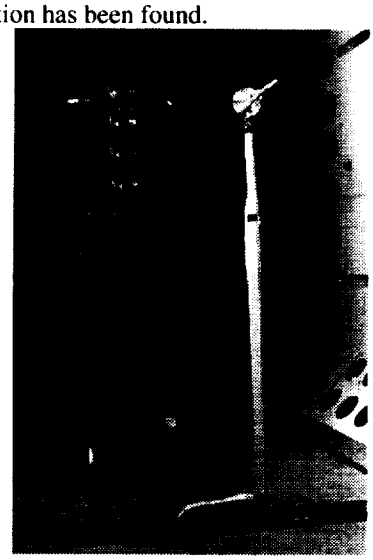

Fig. 60- Setup in TDT for measuring blast loads on Apollo Command Module.

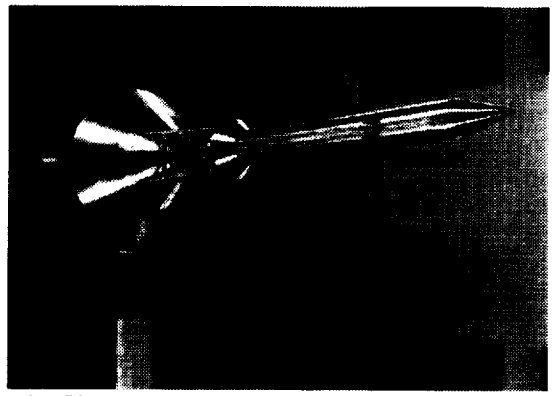

Fig. 61- Photograph of the command module for the TDT blast wave study test.

Atlas-I Large Payload Fairing (TDT Test 423): A wind-tunnel test of a 1/10th-scale Atlas-Centaur I Large Payload Fairing launch vehicle model was conducted in the TDT in 1988. This was the first flight dynamic response test of a basic launch vehicle in the TDT since 1968. Ever increasing sizes and weights of launch vehicle payloads had resulted in an effort to provide a larger payload capability for the Atlas-Centaur launch vehicle. The original Atlas-Centaur payload bay external diameter was the same as the propulsion stages of the launch vehicle. The new design, known as the Atlas-Centaur I Large Payload Fairing configuration (hereafter referred to as the Atlas-I LPF), had a 37.5 percent larger external diameter payload fairing. This new "hammerhead" payload fairing raised questions as to the unsteady aerodynamic loadings which might develop in flight. The NASA space vehicle design criteria specified in Ref. 26 would classify the Atlas-I LPF configuration as "buffet prone" compared to the baseline Atlas-Centaur that would be classified as a "clean body of revolution". Furthermore, wind-tunnel test results documented in Ref. 27 indicated a relationship between payload fairing cylinder length-to-diameter (L/D) ratios and vehicle stability. A Titan III hammerhead configuration with an L/D=0.4 was shown to be unstable during that test. In order to correct this instability, the model L/D was increased to 1.1. The Atlas-I LPF configuration does not have the flow complexities associated with the large solid rocket motors of the Titan III configuration; however, the L/D ratio of the large payload fairing is 1.0. While the previous wind-tunnel test results did not provide sufficient data to define stability criteria for $0.4<L/D<1.1$, they did indicate potential stability problems for configurations in this range. These launch vehicle stability and buffet response phenomena are not easily predictable by analysis. Due to concerns about these phenomena, a wind-tunnel test was performed to determine such effects on the overall vehicle response of the Atlas-I LPF.

An aeroelastically-scaled model of the Atlas-I LPF vehicle was constructed for wind-tunnel testing in the TDT. The model was scaled for heavy gas testing in the TDT. The primary features of the TDT that were important for the Atlas-I LPF were the facilities relatively large size, the heavy gas testing capability and the transonic speed capability. The primary objectives of the wind-tunnel test were to verify that the Atlas-I LPF configuration was aeroelastically stable and to determine the overall vehicle bending moments due to buffet expected during transonic flight. A secondary objective was to conduct a parametric study to determine the effect of various hammerhead fairing configurations (in addition to the nominal design) on model response.

The wind-tunnel model was an aeroelastically-scaled version of the flight vehicle and was capable of simulating either of the first two bending vibration modes of the full-scale vehicle by a partial mode technique. A photograph of the wind-tunnel model for the nominal flight configuration is shown in Fig. 62. Figure 63 is a drawing of the wind-tunnel model showing its basic dimensions. The primary purpose of the test was to gather data concerning buffet response, which could be used to clear the vehicle for flight. Additionally, angle-of-attack studies were conducted and several payload fairing configurations were tested to assess the buffet response and dynamic stability of off-design flight conditions and geometric parameters. No dynamic instabilities were found for any of the configurations tested. The buffet response data for the nominal flight configuration indicate that the unsteady buffet loads represent 5-10 percent of the total design load and, therefore, the buffet loads are not a large factor affecting the overall vehicle design. Payload fairing length-to-diameter ratio variations were found to have small effects on the buffet response of the model, except in the case of the smallest length-to-diameter ratio in the second bending mode configuration. The various payload fairing shapes that were tested are shown in Fig. 64. This configuration experienced much greater transonic buffeting relative to the other length-to-diameter models for the second bending mode simulation. The effects of angle-of-attack on buffet response were found to be small. The model was more sensitive to Mach number changes than to angle-of-attack. Reference 28 contains a more thorough summary of this wind-tunnel test program.

The wind-tunnel model configurations were dynamically scaled to simulate either the first or second vehicle bending modes during transonic flight with a partial mode technique. This testing technique[29] was developed at the NASA Ames Research Center and was used in the Ames 14-ft Transonic Wind Tunnel. The primary assumptions for this simulation are that, for a typical launch vehicle, the mode shape forward of the first node point can be considered linear and that the majority of the unsteady aerodynamic forces are introduced through the forward portion of the vehicle. Thus, a forebody model can be used to simulate the important structural dynamic properties and the majority of the unsteady aerodynamics of the entire launch vehicle. Figure 65 shows calculated mode shapes for a forward portion of the full-scale Atlas-I LPF vehicle for the first two modes. The mode shapes forward of the first node point are seen to be nearly linear. The Atlas-I LPF model geometrically modeled the forward portion of the flight vehicle with a single pivot point (see Fig. 66) about which to simulate the structural dynamics of a given vibration mode forward of the first node point. The wind-tunnel model design mode shapes for the first two modes are also indicated on Fig. 65. The wind-tunnel models represent the linear (rigid) portion of the mode shapes forward of the first node point. Based on the assumptions used in the partial mode testing technique concerning the

unsteady aerodynamic loading, the generalized mass of the wind-tunnel model is scaled from the generalized mass of the entire flight vehicle. Provisions were made to allow the model to be moved relative to the dynamic pivot point (see Fig. 67) and to redistribute the internal weight so that the frequencies and generalized mass of the first or second bending mode could be appropriately simulated.

Some of the wind-tunnel results from this Atlas-I LPF test were actually compared with flight data. The first flight of the Atlas-Centaur I vehicle successfully occurred on July 25, 1990. Some strain gauge data were acquired from this initial flight which were compared with results from the wind-tunnel test. This comparison is shown in Fig. 68. The wind-tunnel results are for the L/D=1.0, first bending mode simulation configuration. This configuration is considered to be the best available simulation of the flight vehicle. The bending moment coefficient, C_{σ}, shown for the wind-tunnel model in Fig. 68 has been scaled to full-scale flight data and adjusted to represent the same body station as that measured in flight. Since the majority (greater than 95 percent) of the flight bending moment response at this station was found to be attributed to the first vehicle bending mode, it can be directly compared to the narrow-band response of the wind-tunnel model in the first bending mode configuration. Assuming that the flight data approximates a normal random process, then it can be said that the flight data is well below the 3σ level determined by the wind-tunnel model, as would be expected. Although no proper conclusion can be drawn from this observation, it is interesting to note that the peak response flight data generally occurred near the 1σ level of the wind-tunnel model. The flight data indicates a slight peak in the buffet response at approximately M=0.73. The wind-tunnel data peaked at a higher Mach number condition, approximately M=0.85. The wind-tunnel model response is shown to continue to increase beyond M=1.0, possibly due to the influence of wind-tunnel facility mechanical vibration. In comparison, the flight data tends to consistently decrease beyond M=1.0 as was expected based on past experiences with launch vehicles.

The results of this test have prompted a few additional comments in the literature. Reference 30 discusses buffet loads of launch vehicles during atmospheric flight, and notes that the Atlas-I LPF 1σ wind-tunnel data matches flight data rather well. Perhaps more significantly, Ref. 31 evaluated the Atlas-I LPF results for small payload fairing length-to-diameter ratios, compared this with additional data available in the literature, and concluded that existing NASA design criteria guidelines regarding the aeroelastic stability of launch vehicles needs to be updated.

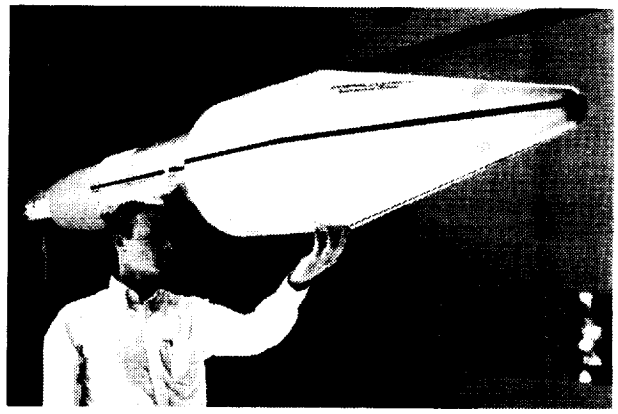

Fig. 62- Photograph of the Atlas-I LPF model sting-mounted in the TDT.

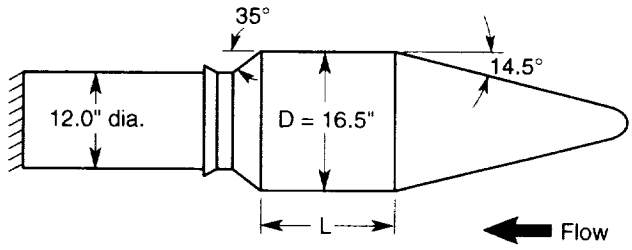

Fig. 63- Drawing of model showing fairing dimensions.

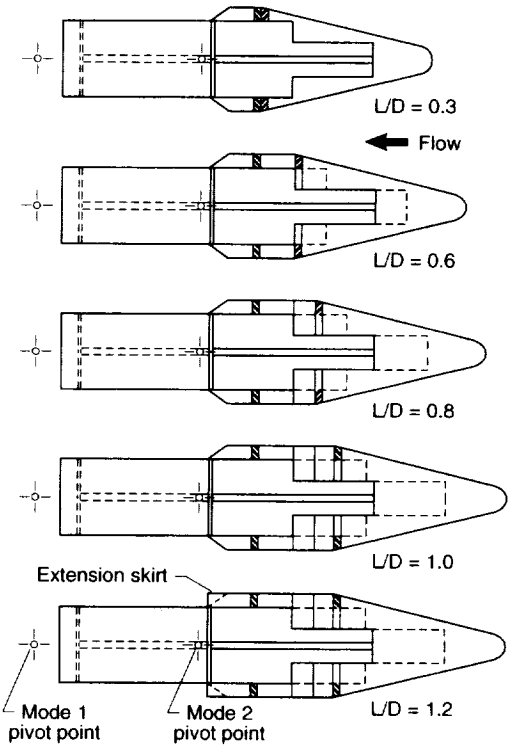

Fig. 64- Payload fairing configurations.

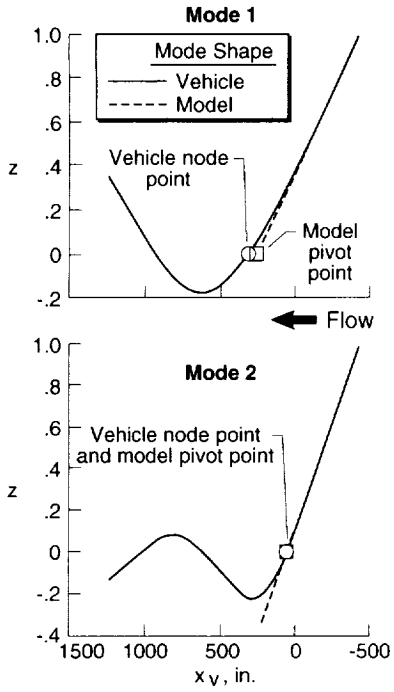

Fig. 65- Vehicle and linearized-model mode shapes (scaled to flight) utilized for partial mode simulation.

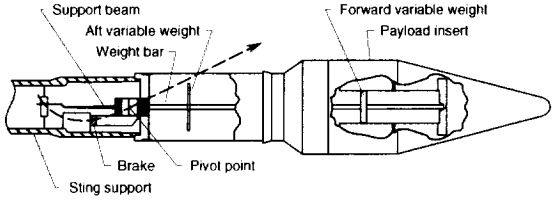

Fig. 66- Drawing showing model details.

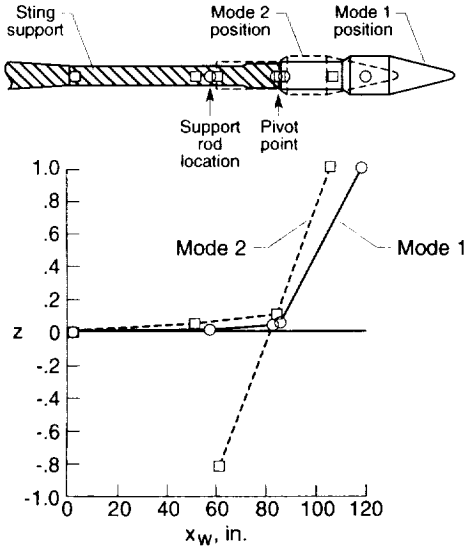

Fig. 67- Normalized mode shapes (with stiffening rods installed) and a drawing indicating position of payload fairing relative to pivot point for both mode simulations.

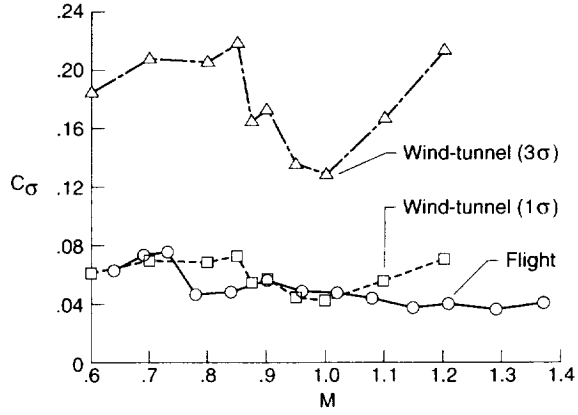

Fig. 68- Comparison of flight measurements with scaled wind-tunnel test measurements. (L/D=1.0, first bending mode configuration with vertical stiffening rods installed.)

Delta II and III launch vehicles- (TDT Tests 510 and 519): In order to extend the viable market for the Delta II launch vehicle series, a new payload fairing was developed to allow for a larger payload capacity. Two versions of the payload fairing were developed for mission specific operations, referred to as the baseline and stretched configurations. The new fairings were unique in that they incorporate a modified Haack nose instead of the classical cone/cylinder construction. The new fairing boattail was at a much shallower angle than had been used in the past. According to NASA space vehicle design criteria,[26] the new configurations are considered "stable buffet-prone" bodies of revolution. Because of the significant fairing configuration changes, it was decided to experimentally determine the unsteady pressure environment during transonic flight. A test of these Delta II configurations was conducted in the TDT in 1995. Figure 69 is a photograph of the Delta II model sting-mounted in the TDT. The objective of the test was to measure the fluctuating pressure distribution along the fairing configurations to later be used in the development of forcing functions that are required in the performance of spacecraft/launch vehicle coupled loads analyses.

The models were designed as rigid geometric representations of the forward portions of the full-scale vehicles. The models do not represent any dynamic properties of the full-scale vehicles. It was assumed that the buffet excitation forces would not significantly amplify vehicle motion. The noses for both models consisted of three-arc approximations of Haack configurations. The nose on the baseline configuration had a length-to-diameter ratio of 1.0 while the stretched configuration had a slightly blunter nose with a length-to-diameter ratio of 0.8. The length-to-diameter ratios for the cylindrical section of the fairings were approximately 1.2 and 1.5 for the baseline and stretched configurations.

Both configurations included a 9.75° boattail. The boattail included two separation bolt covers because they were considered significant protuberances. The bolt covers were located at the base of the boattail 180° apart. Sketches of the two test configurations are presented in Fig. 70. The two model configurations were designed to share as much hardware and instrumentation as possible.

Instrumentation included 78 dynamic pressure transducers, 49 static pressure ports, a 6-component balance, and 5 accelerometers. The dynamic pressure transducers were located at six azimuth positions around the body at 13 stations on the model. The stations were selected to provide good coverage of the model, concentrating on areas of transition where the highest pressures were expected. The transducers were mounted flush to the model surface. The static pressure ports provided a finer distribution along the top of the model, this data was used to give a more detailed definition of the shock locations. The balance was located within the model, aft of the model center of gravity. The five accelerometers were distributed on either side of the center of gravity. Two accelerometers forward and two aft measured pitch and yaw accelerations. An addition accelerometer was used to measure axial acceleration. Data was collected at Mach numbers ranging from 0.6 to 1.2 and angles of attack of 0, 3, and 5 degrees. Data included fluctuating pressures, static pressures, accelerations, and balance force and moment measurements.

In 1996, a similar test was conducted for a Delta III configuration. A photograph of the Delta III sting-mounted model is shown in Fig. 71.

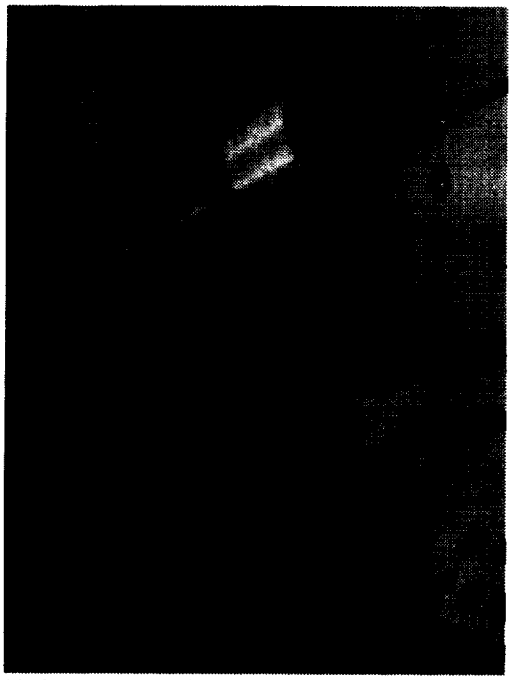

Fig. 69- Photograph of the Delta II launch vehicle model.

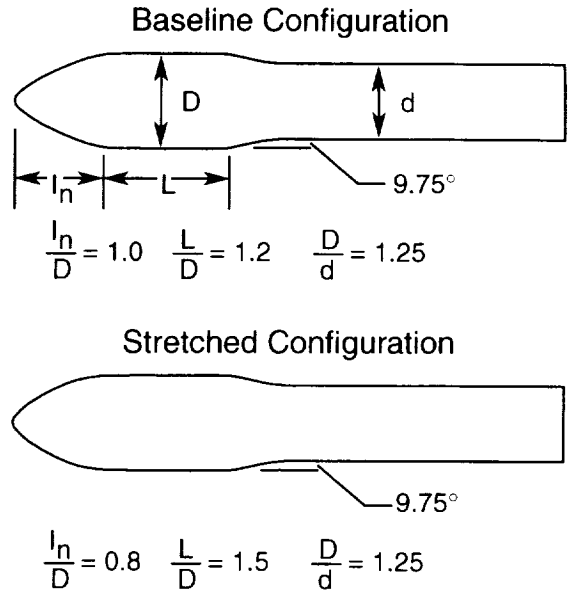

Fig. 70- Delta II test configurations .

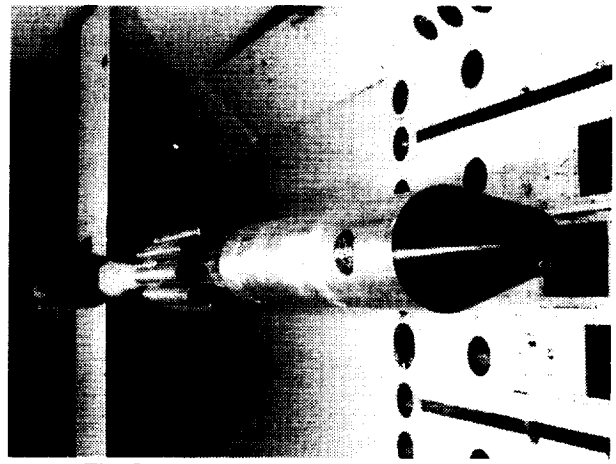

Fig. 71- Photograph of the Delta III launch vehicle model.

ATMOSPHERIC FLIGHT OF SPACE VEHICLES

Aeroelastic problems, when encountered by high speed aircraft and other flight vehicles, most often occur in the transonic region of flight. For a space vehicle, this flight regime is generally encountered soon after launch or during the latter phase of reentry just prior to landing. Unfortunately, this is also the flight regime where analytical methods used to predict aeroelastic phenomena are the least developed due to the extremely challenging nature of transonic steady and unsteady aerodynamics. In addition, spacecraft configurations can be significantly different than those of typical aircraft and therefore analytical and experimental results for aircraft may not be

applicable to predicting aeroelastic and aerodynamic phenomena for spacecraft configurations. As a result, the TDT has been employed to provide the critical wind-tunnel test data for the development and successful operation of space vehicles that will experience subsonic and transonic flight conditions.

Aeroelastic and aerodynamic testing of space vehicles in the TDT, however, has been very similar to those conducted to investigate the phenomena that are the same or very similar to those experienced by aircraft. These have included flutter, buffet, control surface buzz, and divergence along with performance testing where loads have been acquired using a strain gauge balance. Vehicles as diverse as the Space Shuttle, National Aerospace Plane (NASP), and Mars Airplane concepts have been tested in the TDT because of the same properties and capabilities that make it so well suited for testing aircraft and similar research configurations. The large test section, various mount systems available, variable pressure capability, use of air or heavy gas as the test medium, high-speed data acquisition system, and a staff experienced in transonic aeroelastic and aerodynamic testing make it the logical facility to test space vehicles for aeroelastic and aerodynamic phenomena at speeds up to Mach numbers of 1.20.

The following sections describe and provide an extensive list of references for the model tests performed in the TDT of space vehicles where the goal was to simulate flight through earth or planetary atmospheres, up to Mach numbers of 1.20. For Space Shuttle wing concepts through NASP and more recently the Mars Airplane program, the TDT has provided a significant impact on these programs by employing the unique features of the TDT and its staff to determine the aeroelastic and aerodynamic properties of space vehicles.

Reentry Vehicle – Surface Roughness Effects on Aerodynamics (TDT Test 150): The success and knowledge gained during the lifting body program of the 1960's and 1970's led directly to the capability of the Space Shuttle to reenter the atmosphere and land without propulsive power. A critical factor in lifting reentry is the ability to maintain stability and the required L/D through to landing on a runway. Thermal protection is required for reentry from space and may suffer significant degradation from the heating, cooling and aerodynamic forces experienced during reentry. A USAF investigation into the possible effects of ablation roughness on the aerodynamics of a lifting body vehicle indicated that the adverse effects could be very significant.[32] In addition, NASA and USAF personnel agreed that the present state of knowledge on the effects of ablation roughness on subsonic aerodynamic characteristics was inadequate (internal NASA Langley aeroelasticity branch memorandum). As a result, a cooperative NASA/USAF research program was initiated to investigate these aerodynamic effects of ablation roughness to provide a database for use in predicting how an affected full-scale manned reentry vehicle would fly after experiencing reentry.

The vehicle selected for the investigation was the Martin SV-5D/FV-3 PRIME (Precision Recovery Including Maneuvering Reentry) vehicle which was a 0.28-scale model of the X-24A manned low-speed flight research vehicle. This SV-5D had been flown on a suborbital flight and then restored and modified to allow for aerodynamic performance testing in the TDT. The rough surface caused by reentry remained although there was concern that results for the SV-5D would not be directly applicable to a manned vehicle since the roughness scale may not be appropriate. This issue was never fully resolved. A nearly identical second model was constructed with the only significant difference being that it had a smooth surface. Both models were sting mounted in the TDT and loads and moment data acquired using an internal balance. The models are presented in Figs. 72 and 73. The tests were conducted at Mach numbers from 0.30 to 1.00 at angles-of-attack of -3° to 20° at a sideslip angle of 0°. Limited testing was also performed at a constant angle-of-attack of 5° while sideslip angle was varied from -7° to 10°. Testing was also conducted at low (2.5×10^6 to 4.5×10^6) and high (4.5×10^6 to 12.5×10^6) Reynolds number conditions to determine its effect on performance for each of the models. Both models had provisions for varying upper and lower surface flap angles.[33]

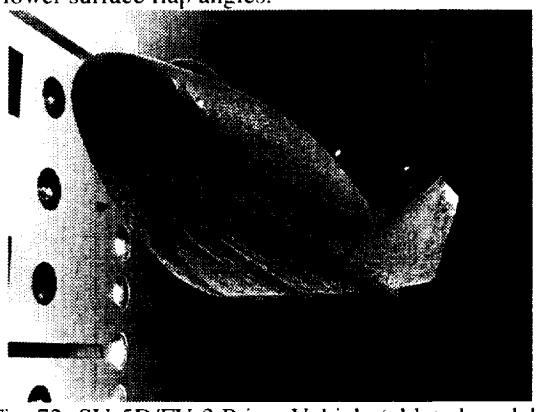

Fig. 72- SV-5D/FV-3 Prime Vehicle (ablated model).

Results from the testing indicated that static longitudinal stability of the ablated model (SV-5D) decreased significantly for Mach numbers below M=0.7 when compared to the smooth model and became unstable for Mach numbers above M=0.70. Ablation roughness was also found to cause pitch up, significant loss of lift at moderate angles-of-attack, and a substantial increase in minimum drag, especially at lower subsonic speeds. This is shown in the data presented in Fig. 74. Finally, ablation roughness was found to improve directional stability at low subsonic Mach numbers but decreased

directional stability at higher Mach numbers. This test in the TDT clearly demonstrated the need to consider the roughness and durability of thermal protection systems in the design of lifting reentry vehicles and was a significant factor in selection of the ceramic tiles used as part of the thermal protection system selected for use on the Space Shuttle.

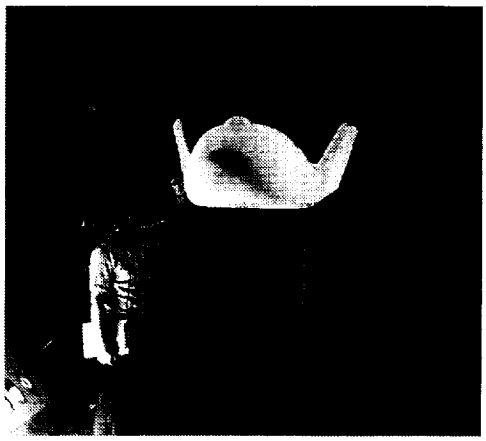

Fig. 73- Smooth replica of ablated model.

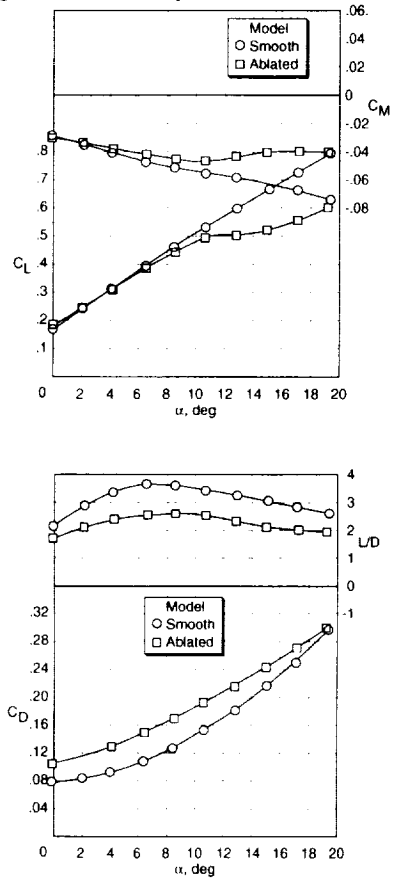

Fig. 74- Longitudinal aerodynamic characteristics of smooth replica and ablated model with lower flap angle of 0° and upper flap angle of –15°, Mach number = 0.40.

Space Shuttle Wing Concepts Buffet and Stall Flutter (TDT Test 157, 158 and 186): Several space shuttle vehicle concepts proposed in the early 1970's had the shuttle reenter at very high angles of attack (α_{max}=60°), and remain at these high angles until they had decelerated to moderate subsonic Mach numbers. The proposed operation of a shuttle vehicle at these high angles of attack and over an extensive speed range raised concerns that stall flutter and/or significant buffeting would be encountered. A significant amount of data existed for stall flutter and buffeting for normal aircraft operations but the unusual requirements for the proposed space shuttle concepts required additional studies of wings at very high angles of attack at high Mach numbers. In addition, no analytical tools existed that would allow accurate prediction of these phenomena at those flight conditions. As a result, a two part exploratory experimental investigation was conducted at the TDT to provide stall flutter and buffet data for three simple semispan wing models that were representative of proposed shuttle wing designs.[34]

The first two wind-tunnel tests used two semispan wing models shown in Figs. 75 and 76. The straight wing concept model had an aspect ratio of 7.36, a taper ration of 0.42, and a NACA 0012-64 airfoil. The clipped delta wing concept model had a 50° swept leading edge, unswept trailing edge, aspect ratio of 2.66, and symmetric 3% t/c circular-arc airfoil. Both models were constructed from tailored aluminum alloy plates covered with a balsa wood airfoil. The models were mounted cantilevered to the tunnel sidewall turntable with the root clamping block covered by a simulated half-fuselage fairing that projected through the tunnel wall boundary layer. During testing, test section speed was established at a selected Mach number and dynamic pressure. Model angle-of-attack was then increased from 0° to 90° and then decreased back to 0° at a nominal rate of 0.6°/sec. Strain gauge outputs were recorded and regions of buffet and stall flutter determined for Mach number range of 0.20 to 1.10 in both air and R-12.

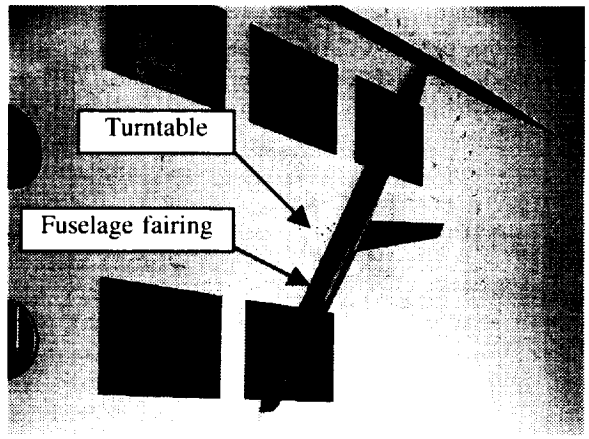

Fig. 75- Shuttle straight wing concept model at high angle-of-attack.

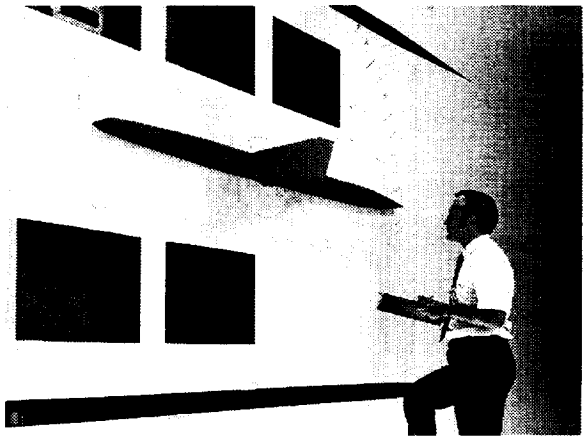

Fig. 76- Shuttle clipped delta wing concept model at zero angle-of-attack.

Results from testing of these two models indicated that stall-flutter criteria developed previous to these tests for thin wings seemed to be applicable for thicker wings at higher speeds. No stall flutter was encountered for the clipped delta concept wing model although both models experienced buffet over a wide range of angles and Mach number as shown in Fig. 77.

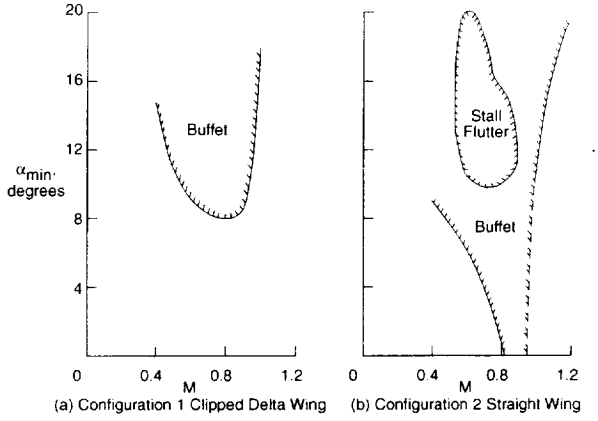

Fig. 77- Stall flutter and buffet boundaries for space shuttle wing concept models.

The third wind-tunnel test was conducted to determine the effects of a large tip fin on the stall flutter and buffet characteristics of a 0.05-scale shuttle booster wing concept model. The model was mounted on the TDT sidewall turntable in the same manner as the previous two models as is shown in Fig. 78. As in the earlier tests, this model was rotated through an angle attack range of 0° to 90° to obtain stall flutter and buffet boundaries.

No stall flutter was encountered for this model over the test Mach number range of 0.50 to 1.10; however, significant buffet was encountered similar to the earlier clipped delta wing concept model with maximum buffet response occurring between 26° and 30° angle-of-attack over the Mach number range tested.[35]

The results from the TDT tests of the three models provided an important database for stall flutter and buffet at high angles-of-attack for transonic speeds. The data was available for evaluation of preliminary space shuttle designs and analytical methods, as well as providing insight into potential stall flutter and buffet phenomena.

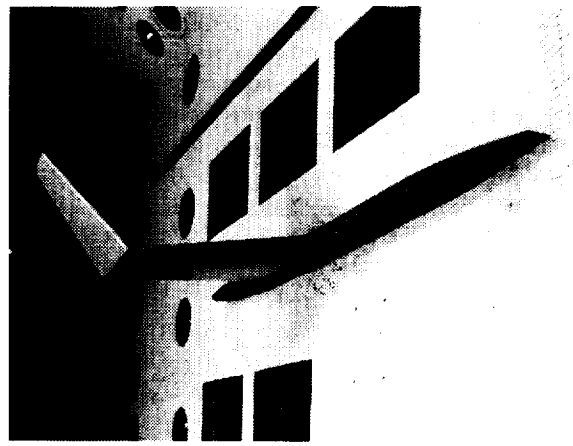

Fig. 78- Shuttle booster wing concept model with tip fin.

Space Shuttle Vertical Tail Buffet/Flutter/Buzz (TDT Tests 246, 258, and 321): During development and design of the Space Shuttle, there was concern that the vertical tail could experience aeroelastic problems such as flutter, buffet, and buzz (rudder) during ascent and reentry. As was typical for the 1970's, the analytical tools available at that time to predict these aeroelastic phenomena were not considered adequate and therefore a wind-tunnel test of an aeroelastic model of the vertical tail was required. In addition, due to the shuttle's complex aerodynamics and structural interactions, a reasonably detailed model of the vertical tail and related structures and aerodynamics surfaces were needed to conduct the required experimental investigation.

The TDT wind-tunnel test program involved three separate tests using a 0.14-scale dynamically scaled vertical tail mounted on a rigid model of a segment of the orbiter upper aft fuselage. This rigid portion of the model was attached to the sidewall turntable to allow variation of sideslip angle. The objectives of the first test in the TDT were to determine the flutter characteristics of the then current vertical tail design as well as investigate vertical tail buffet and rudder buzz. The model had a control surface rudder with actuator stiffness modeled by steel flexural pivots. Different flexures were tested to simulate nominal, 75% of nominal and 50% of nominal actuator stiffness. The fuselage fairing was size scaled to simulate proper local flow characteristics but was not dynamically scaled. The model was also equipped with its own internal shaker and control surface deflector/release mechanism to allow for subcritical damping

measurements.[36] This initial vertical tail model is shown in Fig. 79.

Results from this test indicated no flutter for any of the configurations tested. Regions of buffet were encountered with onset around a Mach number of 0.90 for the nominal- and 75-percent actuator-stiffness configurations. The lower actuator stiffness configurations experienced rudder buzz at a Mach number of 0.80. These results are shown in Fig. 80.

The two follow-on wind-tunnel tests in the TDT concentrated on determining more accurate buffet bending moments on the vertical tail, especially those in the fore-and-aft direction generated by actuation of the speed brake used during shuttle reentry and landing. The first test employed a wedge to simulate a deployed speed brake as shown in Fig. 81 while the second test employed a more realistic split rudder speed brake as shown in Fig. 82. In addition, the structural properties of the fuselage fairing in the region of the vertical tail were modified slightly for the latter two tests to more closely represent those of the shuttle. Maximum opening angle for the deployed speed brake in the final test was 87.2° which was then the maximum scheduled angle for Mach numbers less than 0.90.

Results from the last test showed that the static fore-and-aft bending moment exceeded the limit load at Mach numbers above 0.70. When measured 3-sigma buffet moments were added, the combined buffet and static moments exceeded the limit moments throughout the Mach number range tested. These results are presented in Fig. 83 as full-scale vertical tail bending moment in the fore-and-aft direction as a function of Mach number for the maximum permissible orbiter dynamic pressure. This finding confirmed results of the first vertical tail test and indicated a more restrictive schedule of speed brake openings and/or a vertical tail redesign might be necessary.

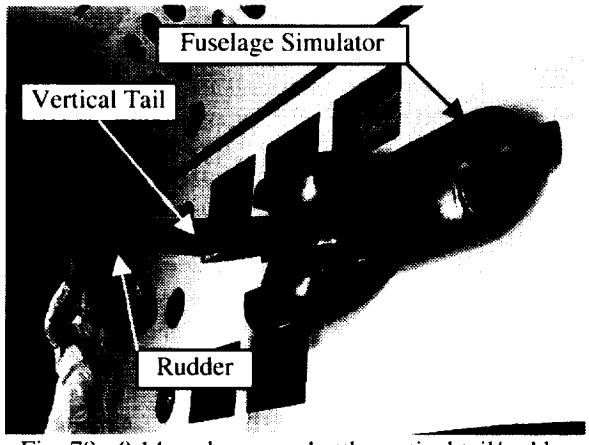

Fig. 79- 0.14-scale space shuttle vertical tail/rudder model mounted on TDT sidewall turntable.

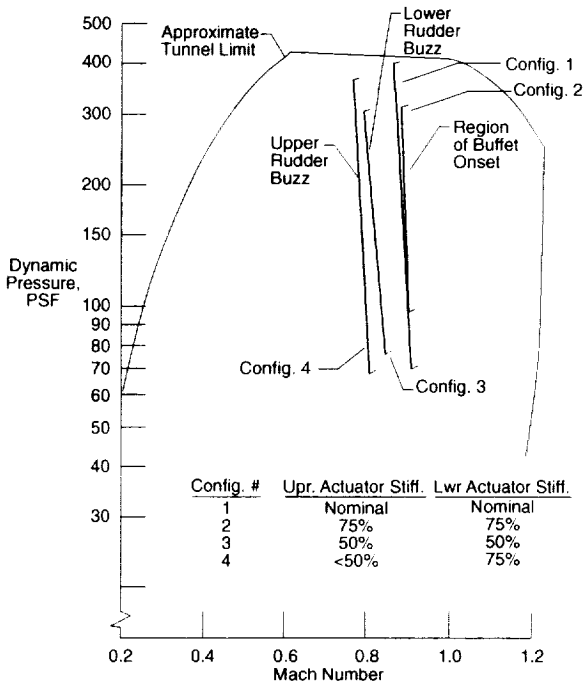

Fig. 80- Results for first shuttle vertical tail model test in TDT.

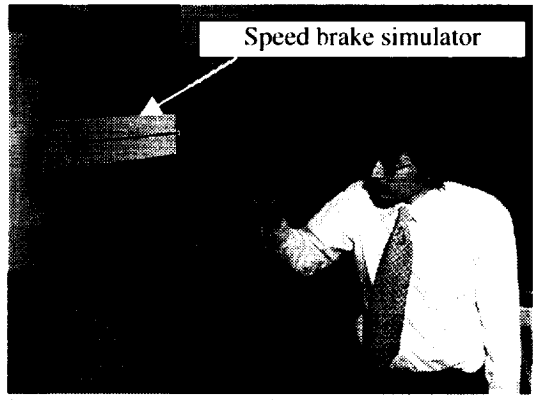

Fig. 81- Shuttle vertical tail buffet model with speed brake simulated by wedge.

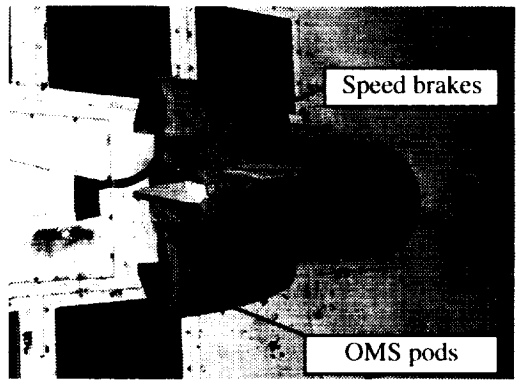

Fig. 82- Shuttle vertical tail buffet model with speed brakes deployed to 87.2° (maximum opening).

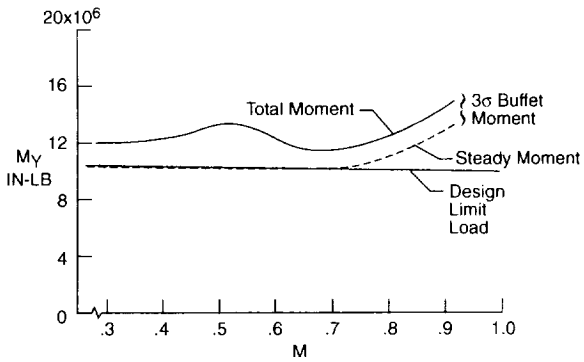

Fig. 83- Vertical tail fore-aft root bending moment loads due to buffet. Full-scale values for q=375 psf. Speed brakes deployed at 87.2°.

Space Shuttle Wing/Elevon Flutter/Buzz (TDT Test 246): During development and design of the Space Shuttle, there was concern that the orbiter wing could experience aeroelastic problems such as flutter, and buzz (elevon) during ascent and reentry. As was typical for the 1970's, the analytical tools available at that time to predict these aeroelastic phenomena were not considered adequate and therefore a wind-tunnel test of an aeroelastic model of the wing was required. In addition, due to the shuttle's complex aerodynamics and structural interactions, a reasonably detailed wind-tunnel model of the wing and related structures and aerodynamics surfaces were needed to conduct the required experimental investigation.

The TDT wind-tunnel test program involved using a 0.14-scale dynamically scaled wing mounted on a rigid model of a segment of the orbiter starboard fuselage. This rigid portion of the model was attached to the sidewall turntable to allow variation of angle-of-attack. The objectives of the test were to determine the flutter characteristics of the then current wing design as well as investigate elevon buzz. The model had a control surface with actuator stiffness modeled by steel flexural pivots. Different flexures were tested to simulate nominal, 75% of nominal and 50% of nominal actuator stiffness. The fuselage fairing was size scaled to simulate proper local flow characteristics but was not dynamically scaled. The model was also equipped with its own internal shaker and control surface deflector/release mechanism to allow for subcritical damping measurements.[37] The shuttle wing/elevon model is shown in Fig. 84.

Results from this test indicated no flutter for the nominal configuration at Mach numbers up to 1.10. The 75% actuator stiffness configuration also was found to be flutter free up to a Mach number of 0.95 although a region of low damping was encountered around a Mach number of 0.70. The 50% actuator stiffness configurations experienced flutter at a Mach number of 0.65 that caused loss of the outboard portion of the elevon. Data and visual observation determined that the flutter mechanism involved outboard elevon rotation and wing first bending modes. The test showed that the then current space shuttle wing design would be free from aeroelastic instabilities within the planned flight envelope for Mach numbers up to 1.10. In addition, the test provided a database for evaluating analytical tools used in the design of the Space Shuttle.

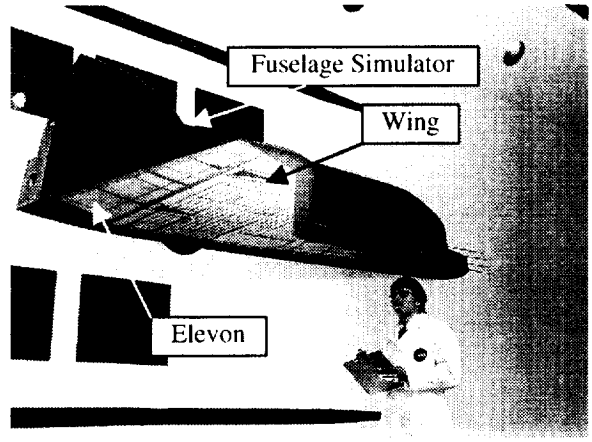

Fig. 84- 0.14-scale space shuttle wing/elevon model mounted on TDT sidewall turntable.

Space Shuttle Full-span Testing The final verification of acceptable aeroelastic characteristics for an aircraft prior to operational use is generally obtained during a flight test program. The Space Shuttle program, however, did not include any actual flight tests except for air drops from a 747 carrier aircraft. These only represented a small portion of the flight regime encountered during orbital launch and reentry. This placed increased importance on wind-tunnel tests of scaled dynamic models of the entire Shuttle orbiter (reentry) as well as the complete launch configuration (orbiter with external fuel tank and SRB's). As a result, an extensive wind-tunnel test program was conducted in the TDT between October 1975 and October 1978 to demonstrate the Space Shuttle had adequate safety margin with regard to flutter and vehicle buffet loads in the transonic and subsonic regions of flight.

Shuttle Rigid Model on TDT Cable-Mount System (TDT Test 266): The first wind-tunnel test of the complete Shuttle orbiter involved the use of a 0.055-scale "rigid" stability model. This model represented the Space Shuttle orbiter with a 65,000 lb. payload. Only geometry and total mass properties were scaled.[38] The primary objective of the test was to demonstrate acceptable flying qualities of the model on the TDT cable-mount system over the operating range of the TDT in preparation for the orbiter aeroelastic model test, which followed. In addition, the use of upper and lower lift cables provided the capability to position the model at high angle-of-

attack which was used to define the wing buffet onset boundary. Finally, although not in direct support of the Space Shuttle program, the stability model was used as part of an effort to demonstrate the ability to extract free-flying stability derivatives using system identification techniques and a cable-mount model. This model installed in the TDT is shown in Fig. 85.

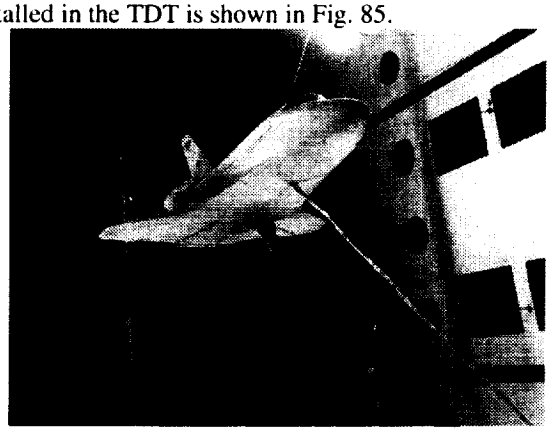

Fig. 85- 0.055-scale Space Shuttle rigid stability model on cable-mount system.

The orbiter model was found to have acceptable flying qualities up to a Mach number of 1.20, which allowed later testing of the more critical flutter model to the desired test conditions. The active capability (no longer available) of the TDT cable-mount system and the snubber cables suppressed a limit amplitude short period mode (pitch) instability that was present during most of the test. Buffet onset was determined using wing root bending moment strain gage output. At each test point, model angle-of-attack was increased and static and dynamic moment plotted versus angle-of-attack. A discontinuity in the dynamic bending moment indicated the angle for wing buffet onset for that Mach number. The buffet onset boundary is presented in figure 86.

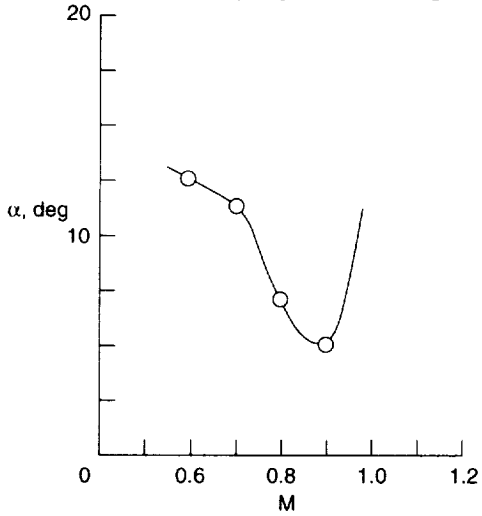

Fig. 86- Space Shuttle wing buffet onset boundary – stability ("rigid") model on cable-mount system.

The final portion of this test was to investigate the concept of extracting stability derivatives using a cable-mount model. The test procedure, results, and data reduction methods are described in Refs. 39 and 40. These results are not known to have influenced the Shuttle orbiter approach and landing test (ALT) program but TDT results did seem to agree reasonably well with values obtained from the ALT program as presented in Ref. 41. Therefore, this portion of the Shuttle stability model test in the TDT was important in proving a concept, which could be, employed in future reentry vehicle test programs.

Shuttle Dynamic Model on TDT Cable-Mount System (TDT Test 300): Testing of a 0.055-scale dynamically scaled Space Shuttle orbiter model was conducted in the TDT to accomplish two primary objectives. First, the test was required to demonstrate that the orbiter had adequate flutter margins of safety up to a tunnel dynamic pressure of 180 psf in the transonic speed range. This corresponded to a full scale dynamic pressure of 552 psf, which was approximately 50% greater than the structural design reentry trajectory value. The required margin was 32% on dynamic pressure. The second objective was to obtain wing and vertical tail buffet response data in the transonic speed range at incremental angles of attack for each of four speed brake positions (0°, 25°, 55°, and fully opened at 87.2°). This data would be used to establish full-scale buffet loads for the orbiter. For this objective, this full-span orbiter model was mounted on the TDT cable-mount system with a remote-controlled pull-down cable attached to the aft fuselage. This allowed the model to be rotated to any nose-up angle-of-attack. The model installed in the TDT is shown in Fig. 87. Model details, test procedures, and results are described in Ref. 38.

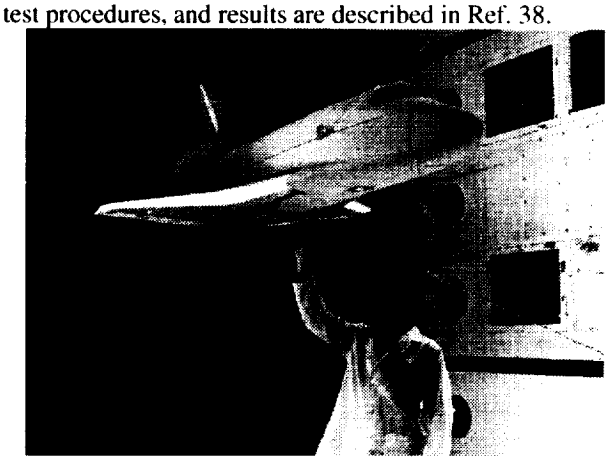

Fig. 87- 0.055-scale Space Shuttle dynamically scaled model on cable-mount system.

Test data did not indicate wing or vertical tail flutter or single degree of freedom instabilities on any of the control surfaces over a Mach number of 0.78 to 1.10 for the required dynamic pressure margin of 32%. Buffet

data obtained over a Mach number range of 0.50 to 1.15 and at angles-of-attack up to 15° indicated peak buffet response at approximately 8°-10° angle-of attack for the vertical tail fore-aft bending and the rudder hinge moments. No peaks were noted for elevon buffet response. The test of this orbiter therefore accomplished its primary objectives by demonstrating that the orbiter would be free of aeroelastic problems during reentry and providing the required buffet data to evaluate buffet characteristics for the full-scale orbiter.

Integrated Space Shuttle Dynamic Model on TDT Sting Support System (TDT Test 308): During the first few minutes following launch, the Space Shuttle orbiter, external fuel tank and SRB's reach supersonic speeds and comprise a very complex structural and aerodynamic system. Since analytical capabilities for predicting transonic flutter and buffet loads during the late 1970's were considered inadequate, a 0.055-scale dynamically scaled launch configuration Space Shuttle model was constructed and tested in the TDT.

This integrated Space Shuttle dynamic model was tested in the TDT with the objectives of demonstrating the required 32% flutter margin based on the Shuttle ascent trajectory and to obtain buffet response data throughout the angle-of-attack range anticipated for transonic speeds during ascent. The model consisted of the previously tested (TDT test 300) orbiter model mated with dynamically scaled models of the external tank and two solid rocket boosters (SRB's). The model was mounted on the TDT sting support system, as shown in Figs. 88 and 89, using a pair of air springs mounted in tandem between the external tank spar and a sting adapter. Since the model was too heavy to be tested on the TDT cable-mount system, this unique air suspension system was used to decouple, as much as practical, the model from the sting support system. Air spring stiffness could be regulated remotely to control support system elastic axis and frequencies. Model details, test procedures, and results are described in Ref. 42.

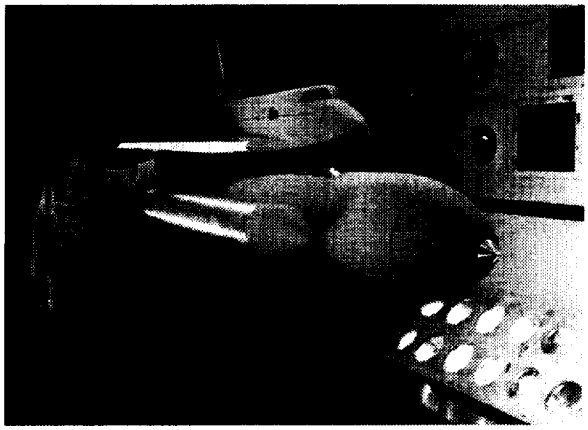

Fig. 88- 0.055-scale Integrated Space Shuttle dynamic model.

Results from the flutter testing portion of the test indicated no flutter of the wing or vertical tail and no single degree-of-freedom instabilities for any of the control surfaces within and even beyond the 32% required margin for dynamic pressure over a Mach number range of 0.50 to 1.10. These results were equivalent to full-scale dynamic pressures of 1006 psf and 905 psf for Mach numbers of 0.60 and 1.13, respectively. Buffet test results indicated minimal response except for Mach numbers between 0.85 and 0.95 where, as expected, there was somewhat significant buffet response. This data was used to evaluate buffet characteristics for the full-scale Space Shuttle launch configuration.

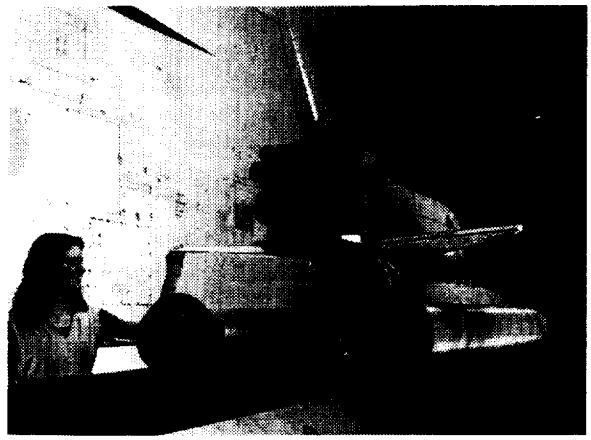

Fig. 89- Integrated Space Shuttle dynamic model – aft view.

National Aerospace Plane- During the 1980's, an effort was underway to demonstrate single-stage-to-orbit flight using a vehicle known as the National Aerospace Plane (NASP), or X-30. Aeroelasticity research was conducted by NASA and by the Air Force Wright Laboratory in support of the NASP design effort. The research included development of computational codes for the prediction of unsteady aerodynamics, aerodynamic heating effects on vehicle aeroelasticity, and fuselage flexibility effects on vehicle flight stability. In addition to these computational studies, research also included some experimental studies aimed at helping to assess the aeroelastic characteristics of the NASP vehicle and to provide a data base from which computational tools could be validated for a NASP-like configuration. Reference 43 is a summary of early thought regarding potential experimental NASP studies, with recommendations of suitable facilities. Many of the preliminary experimental studies that developed were conducted in the TDT. References 44-46 summarize some of the early progress on the NASP program including discussions of some of the initial NASP-related TDT testing. Several of the scaled-model tests completed later in the NASA program were also

conducted in the TDT. Reference 47 is a summary of the NASP aeroelasticity program at a point late in the research program. This section of the report summarizes the experimental studies that were conducted in the TDT in support of the NASP program.

Delta wing models- (TDT Tests 407, 410, 420, 424, 425, and 432): Early in the NASP program, six TDT tests entries were conducted for relatively simple semispan delta-shaped and clipped-delta-shaped wing models. These tests were primarily aimed at providing low-speed and transonic flutter characteristics for planform shapes that were similar to the wing and tail surfaces anticipated for the eventual NASP flight vehicle design. A large range of wing parameters was researched in these early tests. Wing tip shapes included fully triangular delta shapes and delta shapes with the wing-tip region clipped off parallel to the cantilevered root (essentially the fuselage centerline). While the trailing edge of these delta-planform wings were always perpendicular to the freestream flow, a large range of leading edge sweeps, from 30° to 72°, were tested. In one portion of these tests, a series of four models with constant planform and leading edge sweeps of 30°, 45°, 60°, and 72° were tested. Another test series examined wing-root-clamping effects. For a model with 45° leading edge sweep, the amount of the wing root that was cantilever-mounted was varied from 21- to 100-percent of the wing root. Linear method flutter calculations were made for all of the tested configurations. Nonlinear small disturbance code calculations were also made for some of the configurations. The results of these flutter tests and the correlative analyses are documented in Refs. 48-50. Figure 90 shows some flutter results from these tests along with some analysis predictions. Figure 91 shows a typical delta-wing model sidewall mounted in the TDT. Some additional tests were conducted in the TDT for a delta-wing model mounted on a flexible-mount system to simulate vehicle pitch and plunge motions more realistically. These tests are not well documented. Reference 51 mentions these models and includes a representative drawing of the mount system.

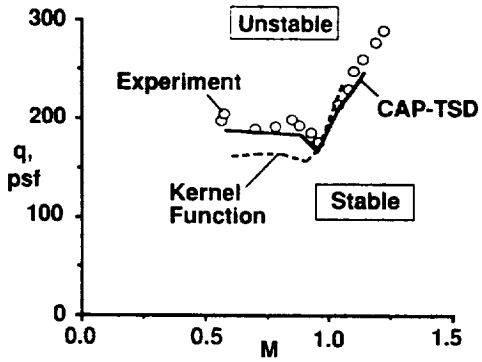

Fig. 90- Analytical and experimental flutter results for some preliminary NASP-related delta-wing models.

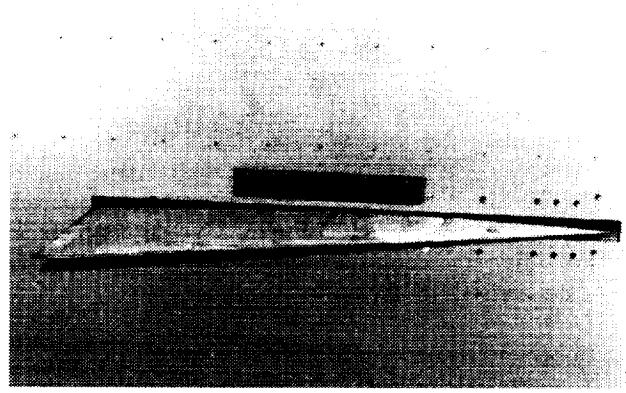

Fig. 91- Photograph of a typical NASP-related delta-wing model.

Aileron buzz studies (TDT Tests 431, 446, 448, 454, 460, and 464): Another series of tests that were conducted in support of early work in the NASP program consisted of wing models with trailing edge control surfaces. The general shape of the wings and control surfaces were built based on candidate NASP vehicle wing designs at the time of these experimental studies. Figure 92 shows a typical aileron buzz study model mounted in the TDT. Figure 93 shows some experimental buzz results obtained during the testing. Buzz characteristics were obtained for several highly-swept, clipped-delta-wing models that had full-span, trailing-edge control surfaces. Single degree-of-freedom "buzz" oscillations were obtained in the transonic speed regime for all configurations tested. For certain of the configurations tested, flutter was obtained at low transonic speeds that changed to a pure buzz instability as the speed was increased to near sonic flow conditions. Linear flutter analysis calculations were made for these cases and correlated well with the measured flutter boundaries. References 52 and 53 summarize these aileron-buzz studies.

Fig. 92- Photograph of a NASP aileron-buzz study model mounted in the TDT.

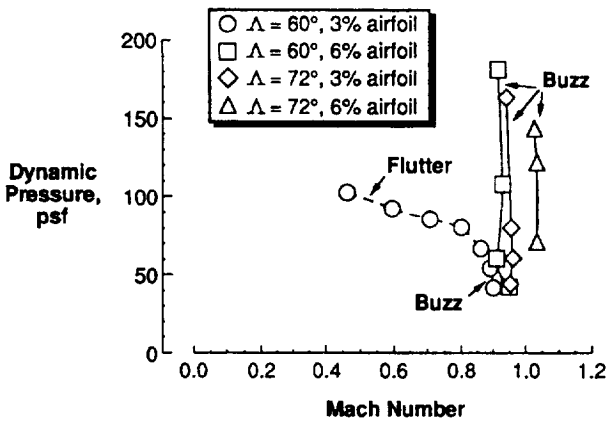

Fig. 93- Experimental buzz-study results from the TDT generic NASP model tests.

Panel flutter tests (TDT Tests 449, 458, and 466): A number of experimental panel flutter tests were conducted in the TDT, some in conjunction with the McDonnell-Douglas company, in an attempt to simulate and gain understanding of possible panel flutter conditions for the NASP vehicle. Even prior to this series of tests, it was anticipated that slightly higher Mach number conditions than available at the TDT might be required in order to achieve panel flutter. This possibility was verified in that no panel flutter conditions were obtained during this TDT testing. However, a more formal panel flutter testing activity was planned under the NASP program that would be carried out in the Langley Unitary Plan Wind Tunnel (UPWT) facility. Lessons learned from the TDT panel flutter test efforts contributed to the success of the UPWT tests. Primarily, the TDT tests identified the extreme importance of balancing the pressure in the support system cavity behind the test panel in order to prevent pressure-stiffening effects on the panel that might prevent, or modify, the onset of panel flutter. As a result of this finding, a pressure control system was built into the UPWT panel flutter model support apparatus. Also, the UPWT panel flutter support apparatus had the additional remote capability of temporarily loosening the boundary constraint on the test panel to allow stress relief from temperature or pressure changes. The boundary was then constrained immediately prior to panel flutter testing to ensure the panel was relatively free of temperature-induced-inplane-stress stiffening or pressure-induced stiffening. No formal documentation exists for the TDT panel flutter tests. However, Ref. 54 summarizes some of the findings from the UPWT tests.

Engine inlet tests (TDT Tests 471 and 495): Two wind-tunnel tests were conducted in the TDT dealing with divergence concerns for the engine inlet apparatus. One of these tests was of a simple model to obtain some experience in testing this type of model and to provide some data for correlation with analysis. The second test used a more complex model that was scaled to the anticipated engine configuration of the NASP vehicle design. These tests have not been formally documented. Furthermore, security classification of these types of results for the scaled engine model currently prevents public dissemination of these test data.

Full-span NASP model (TDT Test 476): One of the most elaborate NASP models that was tested in the TDT was a full-span, floor-pedestal-mounted model of the complete NASP vehicle design configuration. The purpose of this model was to study the aeroelastic behavior of a wind-tunnel model that was based on an unclassified demonstrator version of the NASP vehicle. Parametric variations of the baseline model were tested to examine the effects of all-moveable-wing actuator stiffness, the location of the pivot along the wind root chord, and the thickness of the fuselage. A secondary objective was to determine how effective an existing linear aerodynamics flutter analysis code performed in predicting flutter conditions for the model. Figure 94 is a drawing of the wind-tunnel model on the floor pedestal support. The pedestal support stand was designed to allow some movement of the overall model in the pitch and plunge directions. Figure 95 is a photograph of the model in the wind tunnel. Figure 96 presents the experimental flutter points obtained during the TDT test for several configurations. Figure 97 is one example of the correlation between measured data and analysis. Reference 55 discusses the details of these measured data and summarizes the overall results of this test.

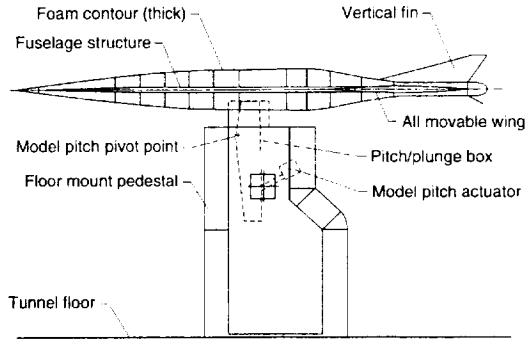

Fig. 94- Full-span TDT NASP model and the floor-pedestal mount system.

Fig. 95- Full-span NASP model in the TDT.

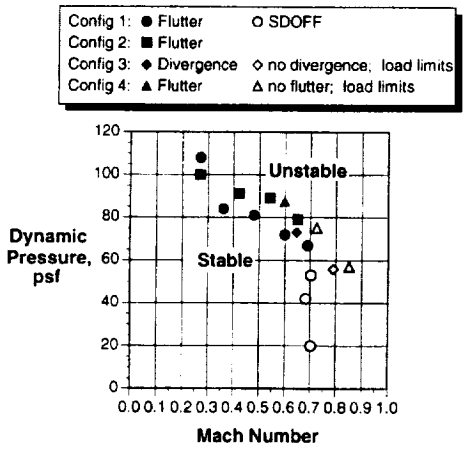

Fig. 96- Experimental flutter points obtained with the full-span TDT NASP model.

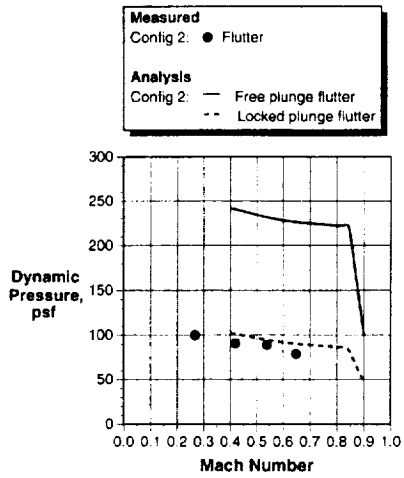

Fig. 97- Comparison of measured and calculated flutter points for the full-span TDT NASP model.

NASP lifting surface tests (TDT Tests 477, 481, and 490): A number of NASP lifting surface aeroelastic tests were conducted in the TDT and in several other facilities. These tests are distinct from the previously discussed delta-wing models in both their complexity and the level of scaling of the flight vehicle. The models used in these lifting surface tests were conducted at a point where a NASP structural and aerodynamic configuration had firmed up to the point that it was reasonable to select a fixed geometry and attempt to scale to a specific structural model. Component lifting surface models were built and tested for both the NASP vehicle wing surface and the vertical tail. The NASP vehicle wing was anticipated to be supported on a pivot-mechanism to operate in an all-moveable fashion. All moveable models were built for testing in three wind-tunnel facilities at Langley: the TDT to cover low-speed and transonic conditions, the UPWT for supersonic flow, and the Hypersonic Helium Tunnel for conditions up to a Mach number of nearly 20. All of these wings had some pivot mechanism for simulating the all-moveable NASP surface. Analysis predicted that this wing pivot arrangement made the NASP flight vehicle design particularly susceptible to body-freedom flutter, which involves substantial coupling of the wing with the actual vehicle fuselage. When such pivot-mounted wings are reduced to semispan wind-tunnel models, absent of the influence of the aerodynamics and the structure of the fuselage, this body-freedom flutter has a tendency to exhibit itself as static divergence. Based on these analytical findings, the TDT wing model and the UPWT wing models were designed to obtain divergence conditions. These divergence conditions could then be correlated against analysis in order to gain confidence in using the analysis techniques in the design of the actual vehicle.

The model design for the TDT wing model is summarized in Ref. 56 and some results of the TDT test are presented in Ref. 57. The results of the test are discussed inn depth in Ref. 58. A photograph of this NASP wing model is shown in Fig. 98. Reference 59 summarizes the lifting surface test that was conducted in the UPWT. This model was also later tested in the TDT to obtain subsonic and transonic divergence conditions to complement the supersonic data obtained in the UPWT. The results of the TDT test of the UPWT model have not been formally documented. A drawing of the UPWT model, showing the pivot mechanism and pitch-spring element, is shown in Fig. 99. A photograph of the model in the TDT is shown in Fig. 100. The high-speed HHT wing models were scaled such that they exhibited a flutter instability instead of divergence. The HHT models were not tested in the TDT. However, for completeness in covering the models of the NASP aeroelasticity program, the test results for the HHT wings are available in Ref. 60.

Finally, one model vehicle was built and tested in the TDT that was scaled to represent the vertical tail surface of the NASP. A photograph of this model is shown in Fig. 101. Reference 61 summarizes the vertical-tail model design and Ref. 58 presents test results for the vertical-tail test.

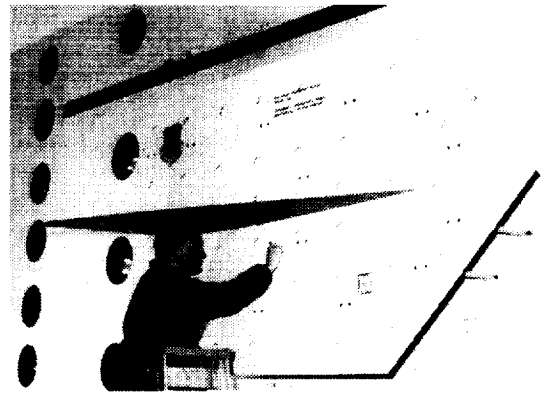

Fig. 98- The NASP wing surface model mounted in the TDT.

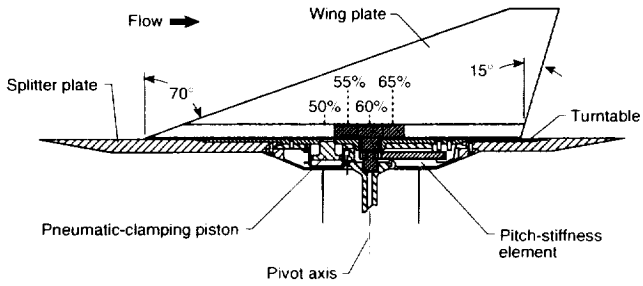

Fig. 99- Drawing showing the support mechanism for the UPWT NASP wing surface.

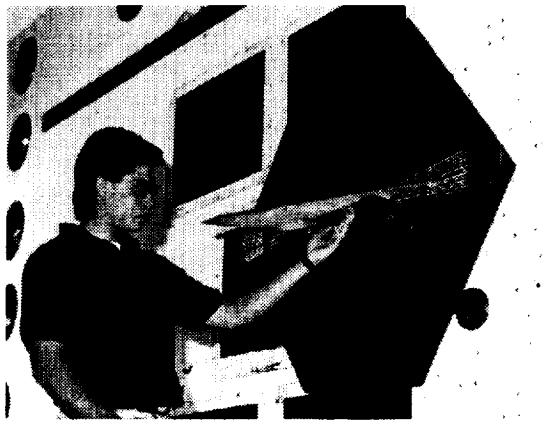

Fig. 100- UPWT NASP wing surface mounted in the TDT to gather subsonic and transonic divergence conditions.

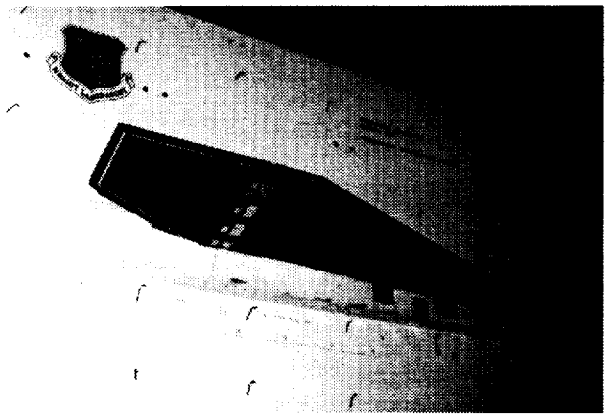

Fig. 101- A photograph of the NASP vertical tail model.

Mars Airplane Concepts Test (TDT Test 540 and 541): The Mars Airplane program (MAP) was initiated in early 1999 with the objective of rapidly developing the technologies required to produce an airplane to fly over the surface of Mars. The airplane was to have been part of a larger Mars science mission with launch from Earth scheduled for late 2002 and flight on Mars to occur in December 2003.[62] The objective of the MAP mission was to determine the feasibility and advantages of planetary exploration by an airplane platform and to provide high resolution imagery of Mars not currently possible using orbiting satellites and/or surface rovers. The program was cancelled in late 1999 due to budget and schedule constraints but not before extensive scale model testing was completed in the TDT.

The flight profile for the MAP included deployment from an aeroshell and execution of a pullout maneuver at transonic speeds as high as M=0.90. Cruise speed after completion of the pull-out maneuver was targeted at M=0.65. Due to the very low atmospheric density on Mars, flight Reynolds numbers (Re) were expected to be between 40,000 and 60,000 with flight dynamic pressures of 1-2 psf. No transonic aerodynamic data was known to exist for these low Re conditions and there was concern that existing low Re CFD methods could not accurately predict airfoil and aircraft performance. Therefore, due to its ability to simulate the required flow conditions, the TDT was selected to test a series of MAP design concept models. The objectives of the tests were to identify the most robust aerodynamic concept(s), provide data for evaluation and calibration of 3-D CFD methods, and to identify and correct any potentially serious aerodynamic problems caused by the low Re transonic flow conditions.

The TDT wind-tunnel tests were conducted using four 1/4-scale full-span sting mounted models that represented four candidate MAP configurations. Models were designated according to their airfoil shape and sweep. A brief description of the models is presented in Table 2. A photograph of model MA-SC-1 is presented in Fig. 102. Parametric variations included tail on/off, tail incidence angle, wing flap angle, and a transition "bump" at x/c=0.15. Model instrumentation consisted of a 6-dof balance, a row of hot-film sensors (flow transition, separation, and reattachment data) on the upper and lower surface of the port wing and a row of static pressure orifices on the upper and lower surface of the starboard wing. Loads, static pressure and hot-film data was acquired for angle-of-attack and sideslip angle polars conducted at Reynolds numbers of 40,000, 60,000 and 100,000 for M=0.65 and 0.80. Data was also acquired at M=0.50, 0.70, 0.85, and 0.90 for Re=40,000. Re effects on wing static pressure distribution and Mach number and Re effects on lift are presented in Figs. 103 and 104, respectively.

Results indicated that acceptable lift characteristics could be achieved at the low Re conditions although many of the configurations were only marginally stable in both the longitudinal and lateral directions. The second TDT test determined an inverted empennage and reduced fuselage fairing thickness would improve stability characteristics for a MAP vehicle. The unique low Re, transonic database acquired will be a valuable resource for any future Mars and/or high altitude earth airplane

program. A formal NASA report documenting both of these tests is to be published in the future.

Table 2- Mars airplane model descriptions.

Model	Airfoil	Sweep, degrees	Trailing edge flap
MA-E387	Eppler 387	0	None
MA-SC-1	Supercritical	0	Starboard only
MA-SF-1	Supercritical	0	Split flap both wings
MA-SC-1t	Supercritical	30	None

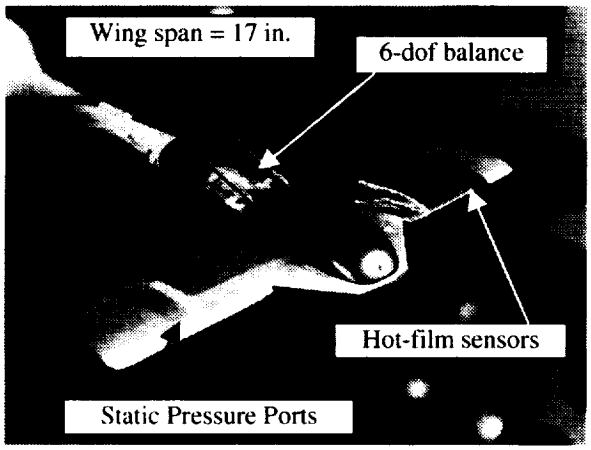

Fig. 102- 1/4-scale Mars Airplane concept model MA-SC-1.

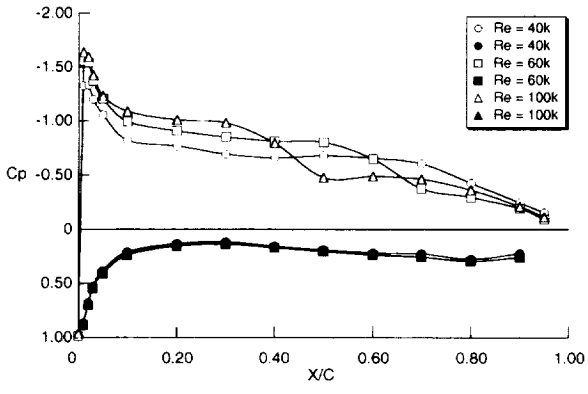

Fig. 103- Effects of Reynolds number and Mach number on wing static pressure coefficient distribution: MA-SC-1, transition bump at x/c=0.15, tail incidence = 0°

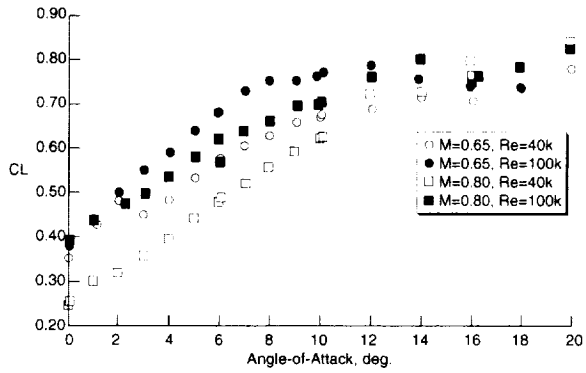

Fig. 104- Effects of Reynolds number and Mach number on lift: MA-SC-1, transition bump at x/c=0.15, tail incidence = 0°

ATMOSPHERIC REENTRY MODEL TESTS

A number of Earth atmospheric reentry concepts have been tested in the TDT. Extensive parawing-type configurations were tested in the early 1960's as possible concepts for returning re-entering space vehicles to Earth's surface. Other reentry concepts such as aerodynamic drag brakes, and deployable lighter-than-air balloons also have been tested in the TDT. Finally, parachute, attached inflatable decelerator, and drag-brake concepts for use with planetary-mission vehicles have been testing in the TDT. All of these atmospheric decelerator concepts will be covered in this section of the paper.

AVCO Rigid Drag Brake (TDT Test 13): Several different concepts for aerodynamic braking were considered for reentry vehicles during the early 1960's. One involved an aeroshell-type decelerator that deployed in an umbrella like manner. The AVCO rigid drag brake test was a pathfinder for a more complex and representative model for the concept that was to be tested shortly after completion of the rigid model test. The rigid model, shown in Fig. 105, of this concept was tested and consisted of a wooden aeroshell type fairing attached to a sting and supported by various cables. The more complex model, shown in Fig. 106, was to have included instrumentation for measuring loads and pressures on the decelerator. This more complex test was not conducted apparently due to cancellation of and/or loss of interest in this AVCO decelerator program. No data or published reports on the test are known to be available.

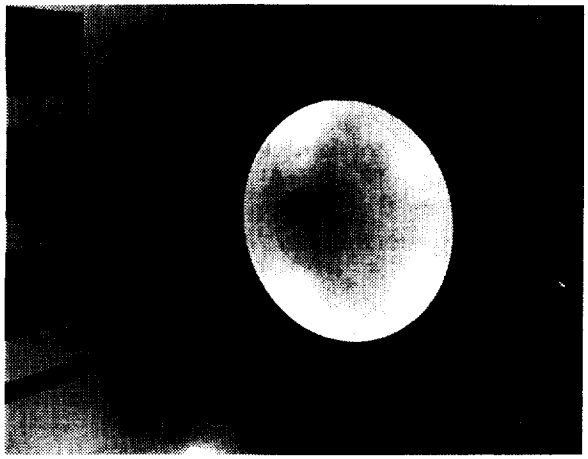

Fig. 105- 1/12-scale rigid AVCO Drag Brake model.

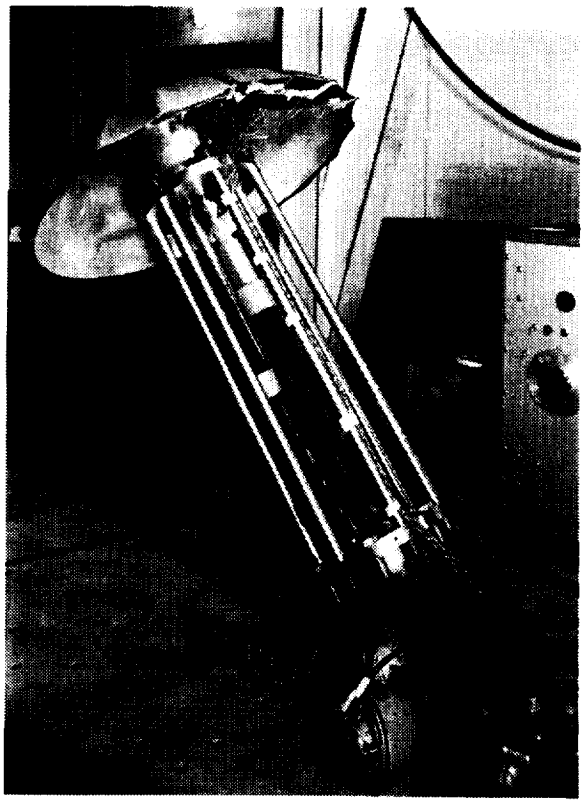

Fig. 106- AVCO Drag Brake model in TDT calibration lab.

Inflatable parawing deployment studies
(TDT Tests 20-22, 46, 67, 73, 74, 82, and 119):
In the early 1960's, a number of spacecraft recovery concepts were being studied to provide for more options in selecting landing sites, particularly by providing flare capability prior to touchdown. One approach to accomplish this was to provide the returning spacecraft with a kite-like gliding device that is deployed during atmospheric reentry for final landing. These recovery concepts are collectively known as parawings. Parawings can include a wide range of configurations from all-flexible sail designs to sails with rigid or semirigid frames. Over a period of several years, NASA conducted free-flight and wind-tunnel studies of one all-flexible parawing concept.

The research program was conducted to determine the deployment characteristics of a 1/8-size dynamically and elastically scaled model of an inflatable parawing suitable for the recovery of an Apollo-type spacecraft. The objectives of the program were: 1) to determine a satisfactory deployment technique, 2) to measure the transient loads associated with deployment, and 3) to determine the applicability of wind-tunnel tests to investigations of this nature. The wind-tunnel tests were conducted in the Langley TDT.

Based on the photographic archives available at the TDT, it appears that an initial, very small scale test of a parawing concept was first tested prior to the start of this 1/8-scale model test program. Nothing further is now known about this initial parawing test. The authors speculate that it served as a learning experience for the series of tests that followed of the 1/8-scale models.

The experimental models were based on a full-scale parawing-spacecraft combination that would have carried a wing loading of 7 lb/ft^2 and a nominal gross weight of 8800 lb. The parawing was similar to a parawing proposed for the Gemini spacecraft, with a conical canopy and equal-length, inflatable structural members. The spacecraft design was dynamically and geometrically similar to the Apollo command module. The parawing attached to the spacecraft by five stainless-steel aircraft cable-suspension lines. The photograph in Fig. 107 shows the parawing-spacecraft model during a successful deployment in the TDT.

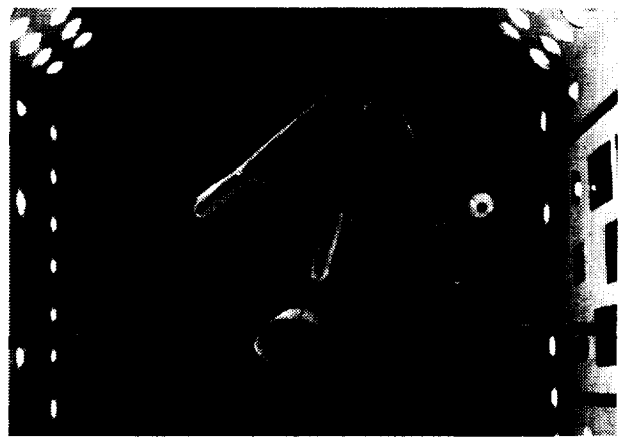

Fig. 107- Photograph of a parawing model configuration showing the spacecraft model, successfully deployed parawing, and the apex drogue parachute.

The deployment technique was developed in an initial series of TDT tests (Ref. 63). These initial tests indicated the need for close control of the various phases of the deployment in order to avoid unstable oscillations and to attenuate dynamic loads. As a result of these initial studies, the deployment sequence used in subsequent flight and wind-tunnel deployments used 1) a three-point aft attachment of the inflatable structural members to improve the stability of the configuration during and immediately after inflation, 2) a small drogue parachute attached to the apex of the parawing to insure clean separation after apex release and to damp the transient motions of the wing after deployment, and 3) a system for controlling the reel-out of the suspension lines in order to attenuate the transient loads. The drogue parachute noted above represents a second parachute used in the deployment sequence. An initial drogue chute was used to remove the cover constraining the parawing against the spacecraft. The drogue parachute and cover would then separate from the parawing-spacecraft combination. The second parachute was introduced, based on test findings, to provide a positive pitching moment to the parawing to ensure clean separation from the spacecraft and to help damp transient motions that immediately followed deployment. However, the attachment position of the apex (second) drogue parachute proved to be critical. This was because all of the parawing configurations tested exhibited roll instability during deployment, which would stabilize as the parawing achieved full inflation and rotated into a flying attitude. An improper attachment point of the apex drogue chute would result in the parachute slipping beneath the parawing, aggravating the roll instability of the parawing and often resulting in termination of a run during the wind-tunnel tests. A drawing showing the general deployment sequence for the parawings is shown in Fig. 108.

Using the equipment and deployment techniques developed in the initial wind-tunnel tests, successful free-flight deployments were accomplished, including the measurement of transient loads during deployments. Subsequent to the initial wind-tunnel tests and the free-flight tests, additional TDT tests were performed to investigate further variations of the deployment sequence. Several of these deployment variations appeared attractive for further study. Reference 64 is a summary report of both the free-flight and the initial and latter wind-tunnel tests. Regarding the final primary objective of these experimental studies, it was found that the deployment technique was not perfected sufficiently to prevent all random motions and loads, with wide variations for even the most similar deployments. On the other hand, the general behavior of the parawing during deployment was similar between wind-tunnel tests and flight tests. Also, the loads measured during wind-tunnel tests were found to be suitable for use as a preliminary indication of those encountered in free-flight. Based on these results, Ref. 64 further concluded that the wind tunnel could serve as a useful tool in the development of an inflatable parawing.

All of the wind-tunnel deployments were made in the air test medium at atmospheric pressure. Deployments were made at three different constant dynamic pressures of 3.5, 7.0, and 10.5 psf. This was intended to simulate three different flight dynamic pressures, starting at the steady-state glide value of 3.5 psf and increasing toward the terminal flight dynamic pressure of 30 psf. The reason for using the TDT for these parawing tests is not specifically stated in any of the available literature that was reviewed. Plausible reasons that the TDT was chosen may be its relatively large size, good low-speed control, acceptance of high-risk dynamic testing, and perhaps the expertise of the aeroelasticians that conducted tests at the TDT.

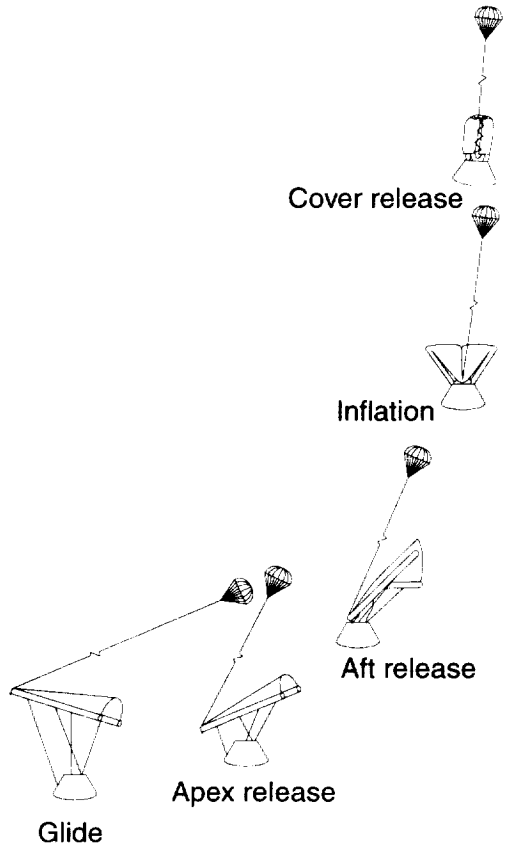

Fig. 108- Parawing deployment sequence.

In addition to developing a satisfactory parawing deployment technique and meeting the other specified objectives, this program provided much useful information regarding the fabrication of dynamically and elastically scaled inflatable structures. These spin-off results are reported in Ref. 65.

Another reentry-type vehicle was tested in the TDT in 1967 that was referred to as "sail plane" parachute. This

model is mentioned here because it is believed by the authors to be a parawing-variety vehicle. An internal memorandum from an engineer in the Langley Aeroelasticity Branch refers to this model as an aerodynamic decelerator device. This wind-tunnel test was in support of a concept being studied by the NASA Manned Spacecraft Center. The letter states that the test "would include deploying a 1/6-scale model of the fabric sailwing in a partially reefed condition" in the TDT. The objectives of the test were stated as being to measure drag and loads introduced at several locations on the model during the deployment event. However, no information can be found on the actual test other than facility operational shift notes that indicate the test occurred.

Apollo Command Module Drogue Parachute Deployment (TDT Test 49): Another aspect of the Saturn Apollo vehicle that was tested in the TDT was the deployment of the drogue parachutes used for landing the returning command module back on Earth. Not too much is now known about the results of this test that was conducted in December 1962. Reference 24 indicates that the model used for this test was a 1/10-scale "dynamically similar" command module. Furthermore, the test was described in a footnote with the words "force, dynamic, parachute". Apparently the test was for the purpose of demonstrating parachute deployment, learning about the dynamics involved in parachute deployment, measuring forces involved in the deployment (and most likely the steady-state deployed-parachute configuration), and to evaluate configuration variables. In particular, it is known that several drogue chute diameters, chute porosities, riser lengths, and elasticity were evaluated in the TDT test. The command module model was gimbal-mounted to a rod support that spanned the test section of the TDT. Figure 109 shows the command module model mounted on the rod support in the TDT. No photographs could be found of the configuration with a drogue chute deployed.

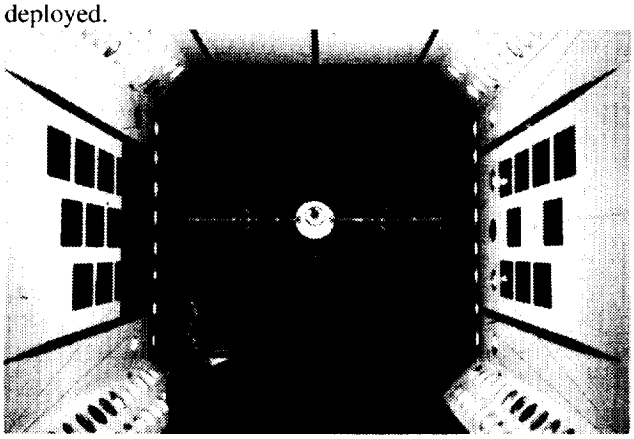

Fig. 109- 1/10-scale model of the Apollo command module used for drogue parachute deployment tests.

Paravulcoon Recovery System (TDT Test 124): Among the many concepts for spacecraft recovery systems in the early 1960's was an idea to use a ram air inflated hot-air balloon that would be deployed during reentry to essentially hover the recovered body for a soft landing. The concept involved pulling a deflated, folded balloon from the aft region of a spacecraft during atmospheric reentry. This concept was known as the Paravulcoon recovery system. During the early 1960's, a series of wind-tunnel and flight tests were conducted to verify this concept. These verification tests used a fairly blunt forebody test vehicle for the demonstration of the balloon deployment. The Paravulcoon concept, flight test results, and results of wind-tunnel tests conducted in the NASA Langley Spin Tunnel and in the Langley Full-Scale Tunnel are summarized in Ref. 66. These wind-tunnel test studies used a scaled-model of the proposed flight test vehicle and balloon system (approximately 1/10 -scale) for the purposes of simulating balloon deployment, inflation, and terminal descent. These wind-tunnel tests provided flight loads information and contributed to the understanding of the dynamic stability of the Paravulcoon during the different flight configurations.

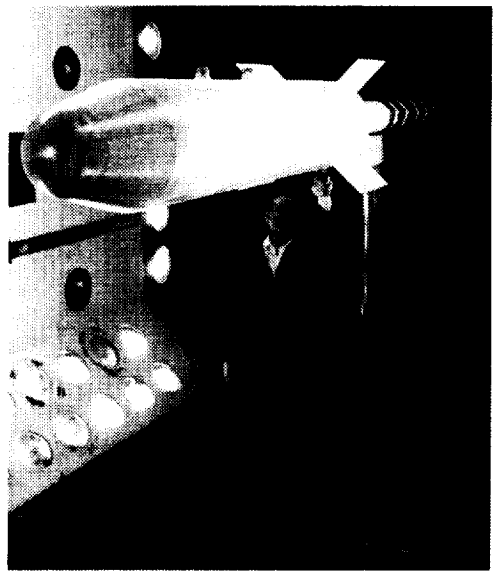

Fig. 110- Paravulcoon forebody model in the TDT.

An additional test of the Paravulcoon concept was conducted in the Langley TDT in 1967. However, the results of the TDT Paravulcoon test are not included in the previously published Ref. 66. Not much is now known about the objectives of this particular test because no other documentation has been found. The wind-tunnel model, shown in Fig. 110, consisted of the balloon-carrying forebody vehicle. Another photograph in the TDT test section (Fig. 111) shows a drogue parachute being extended behind the forebody and hand-held as if

deployed. Reference 66 mentions that some of the other Langley tests used NASA-supplied drogue parachutes to simulate the initial stages of deployment. The first step in deploying the recovery balloon was to use a parachute to detach the lid over the balloon container, and then to pull the balloon out of the vehicle container for inflation. A drawing from Ref. 66 that might assist in visualizing the deployment sequence of the Paravulcoon recovery system is included in this report as Fig. 112. Perhaps the TDT test included an assessment of the dynamics involved in deploying the parachute from the Paravulcoon test body.

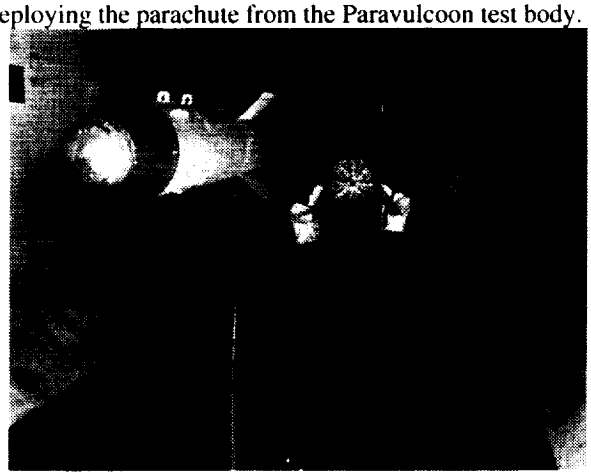

Fig. 111- Paravulcoon forebody model in the TDT with drogue parachute handheld behind the model.

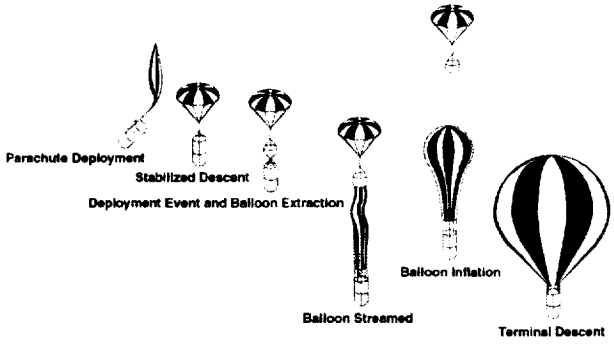

Fig. 112- Deployment sequence of the Paravulcoon vehicle concept.

Space Shuttle SRB Drogue Deployment/Performance (TDT Tests 243 & 275): During development of the Space Shuttle, NASA's Marshall Space Flight Center was responsible for development of the solid rocket booster (SRB) recovery system. The concepts under study utilized parachute systems for deceleration of the SRB's prior to water entry. Several deployment concepts and configurations were under consideration and it was decided that wind-tunnel testing along with drop testing was required to aid in defining the most reliable and cost effective recovery system. Since flight path of the SRB's was anticipated to be nearly vertical at the time of drogue chute deployment, a vertical wind-tunnel facility was considered, but was deemed of minimal importance since accelerations due to aerodynamic forces would be approximately 7 to 10 g's. Testing in the TDT would result in acceptable test section blockage for a reasonable large scale model which would simulate more representative flow conditions as well as allow sufficient room to house a packed parachute and nose cap ejection mechanism. The first test conducted in the TDT was followed by another test two years later due to a change in the baseline configuration and the need for additional parametric testing.

The initial test conducted in the TDT utilized 0.125-scale parachute and SRB forebody models with the primary objective of investigating the dynamic characteristics of four candidate drogue deployment concepts and to perform a parametric steady-state drag investigation of 20° conical ribbon parachutes. Variables included SRB angle-of-attack, nose cap ejection velocity, drogue chute geometric porosity, reefing line length, and dynamic pressure. The correct scaled velocity for the deployment portion of the tests was achieved by testing in air at a nominal Mach number of 0.17. The four deployment concepts tested are described in Ref. 67 and illustrated in Fig. 113. The SRB drogue chute deployment/performance model allowed for deployment and drag measurements to be performed at SRB angles-of-attack from 70° to 130° and is shown in Fig. 114. The SRB forebody for this model represented the forward 40% of a complete SRB. The second SRB forebody model represented a complete SRB and was used for obtaining drogue chute drag force data at an angle-of-attack of 180° (nozzle forward). This model is shown in Fig. 115. Finally, interference free (no SRB forebody) drag forces were measured using the configuration shown in Fig. 116.

Results from the first test in the TDT are presented in Ref. 67. No results for the second test could be located for inclusion in this paper although the second test was similar to the first in that drogue chute deployment and drag tests were conducted using much of the hardware employed during the first test. Results from the first test showed the baseline deployment concept to be promising but concerns were raised regarding possible fouling problems for a full-scale system. The effects of geometric porosity, suspension line length and SRB wake interference on drag are presented in Figs. 117 and 118. These results correlated well with those from earlier full-scale drop tests[68, 69]. Overall, the TDT tests provided valuable data for development of a final SRB drogue chute system. The recovery system currently used on SRB's most closely resembles that shown as method 4 in Fig. 113.

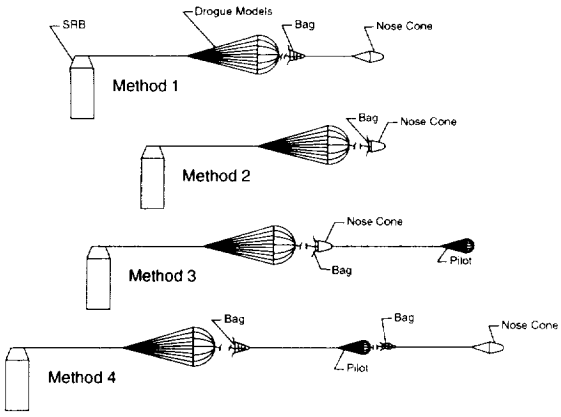

Fig. 113- SRB Drogue chute deployment concepts.

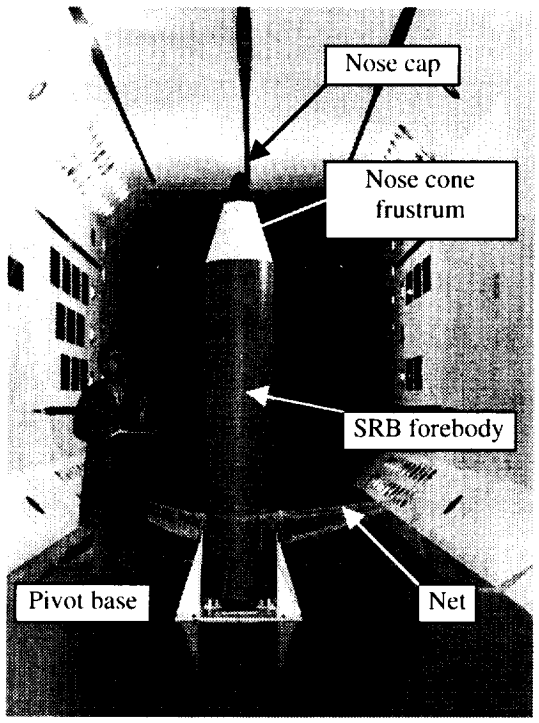

Fig. 114- 0.125-scale Shuttle SRB drogue chute deployment/performance model.

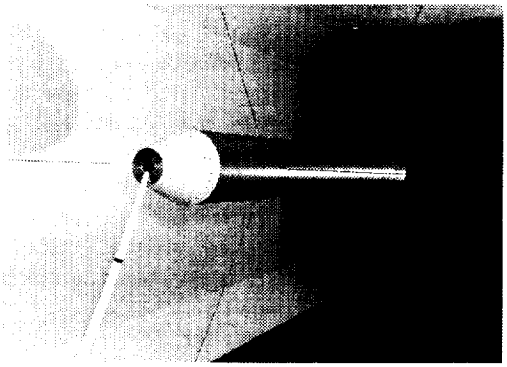

Fig. 115- Shuttle SRB model in horizontal test configuration for drogue chute drogue force testing.

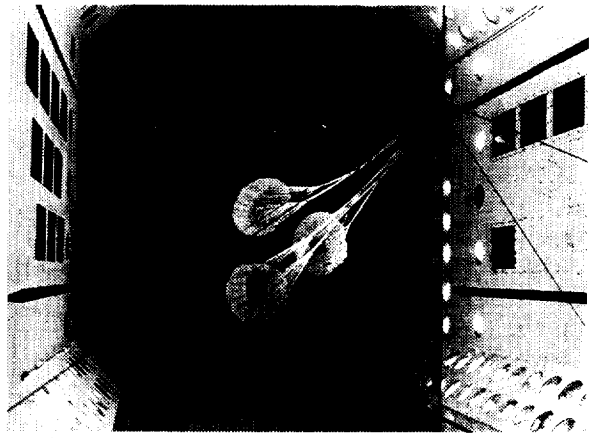

Fig. 116- Shuttle SRB parachutes for determining performance without SRB forebody interference effects.

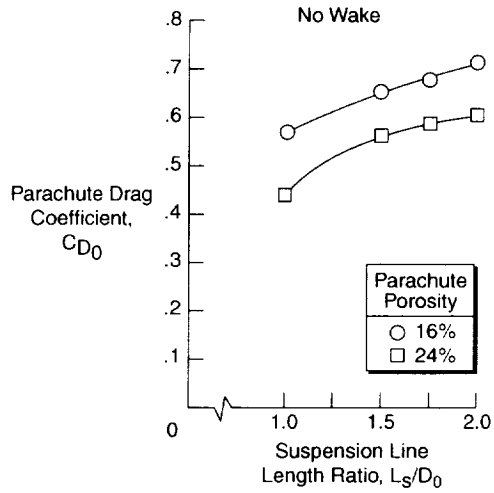

Fig. 117- Effect of suspension line length and chute porosity on SRB drogue chute drag.

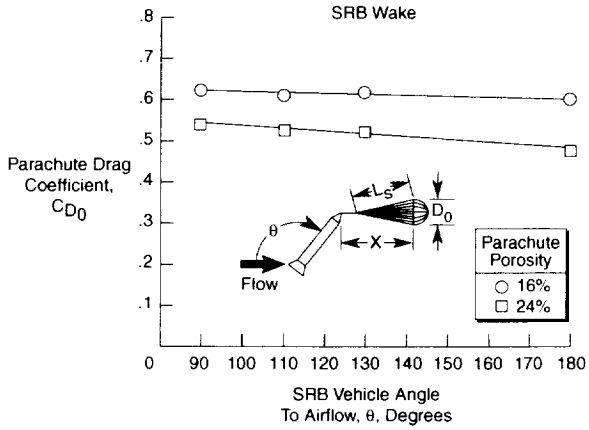

Fig. 118- Effect of chute porosity and SRB forebody angle-of-attack on SRB drogue chute drag.

Attached Inflatable Decelerator (TDT Test 149):
A flight device known as the Attached Inflatable Decelerator (AID) was tested in the TDT in early 1969. NASA extensively researched AID reentry vehicles during the 1960's. Attached Inflatable Decelerators were envisioned to be deployable at supersonic speeds for the purpose of decelerating spacecraft entering a planetary atmosphere. A drawing of a typical AID design is shown in Fig. 119. Ref. 70 indicates that an AID concept was demonstrated to be advantageous for use in planetary entry into the low density atmosphere of Mars. References 71-75 are other documents the authors have found covering some of AID research efforts, including many wind-tunnel tests for AID models. However, no formal documentation of the TDT test has been found.

A letter dated March 1967 from an engineer in the Langley Aeroelasticity Branch indicates an interest in expanding the planned and on-going test efforts for AID devices to include dynamic load testing. This particular letter suggests making dynamic measurements during a planned Langley Full-Scale Tunnel test. So very little is known about the results of the TDT AID models test. A pre-test meeting summary suggests the TDT entry was requested by fellow NASA Langley engineers. The pre-test meeting summary also indicates that the test would be for the purpose of determining static aerodynamic performance and static and dynamic stability of the inflated device. It is known that testing of some of the early tests of AID-type configurations determined that transonic separation was erratically established on the large outer diameter (streamwise) of the inflated decelerator. This resulted in a poorly defined, dynamic line of separation around the decelerator that caused dynamic problems with the downstream skirt region of the inflated decelerator. This situation was improved by the installation of the smaller diameter, inflated "burble fence" shown in Fig. 119. Perhaps the TDT test further examined such dynamic stability issues of AID vehicles. A photograph of one of the TDT AID models, sting-mounted, is shown in Fig. 120. This photograph shows that the TDT models did have burble-fence devices attached to the main decelerator.

Some sparse notes found in operational logs at the TDT state that the model sustained damage on at least two occasions during the two-week entry, requiring that the inflatable model be replaced before testing could continue. However, this statement only attests to the dynamic and high-risk nature of the TDT test and a similar statement could apply to many aeroelastic tests conducted in the TDT. It does not shed any particular light on the success experienced in testing these AID models or of the applicability of such devices in flight.

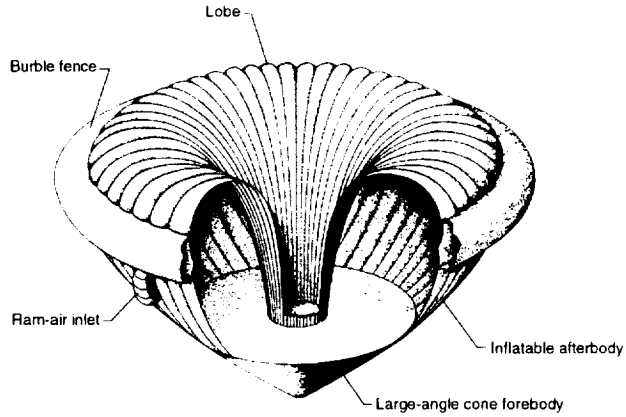

Fig. 119- Drawing of an AID concept reentry vehicle.

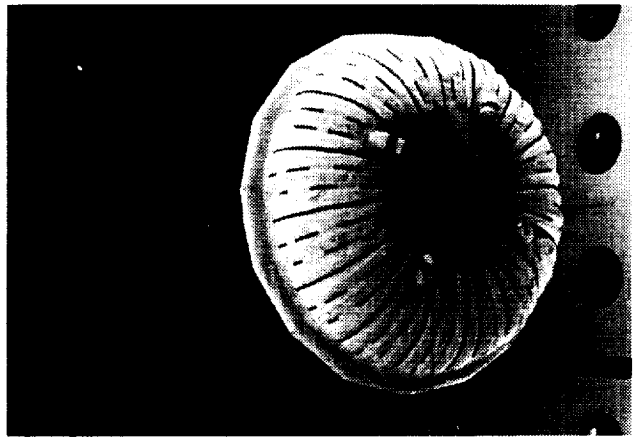

Fig. 120- AID model sting-mounted in the TDT.

Viking - Mars Probe

The goal of the Viking program was to learn more about Mars through direct measurements in its atmosphere and on its surface. The Viking program was initiated in 1969 and culminated in the launching of two spacecraft, each consisting of an orbiter and lander, in 1975 with touchdown on the Martian surface in 1976.[76-78]

Experiments in various wind tunnels were used extensively in support of the Viking mission. Six different experimental investigations were conducted in the TDT during the time period of October 1970 to July 1975.[79] These tests supported elements of the entry and landed phases of the Viking mission and contributed significantly to spacecraft development and ultimately to the success of the program.

Experimental studies in the TDT in support of the entry phase included a determination of parachute environment and performance, aerodynamic

characteristics exhibited by two separating bodies (aeroshell and lander/base-cover), and location and orientation of a stagnation-pressure sensor on the lander. Experimental investigations which supported the landed phase were a convective heat-transfer test related to the lander's radioisotope thermoelectric generators (RTG) and two tests which supported development and calibration of the meteorological science experiment package. The entry aspects of the testing are covered in this section and the landed vehicle tests will be discussed in a later section on planetary-probe testing.

Parachute Environment and Performance (TDT Test 190): An aerodynamic decelerator was required during the Viking entry into the Martian atmosphere and consisted of a main parachute (disk-gap-band canopy) assembly trailing in the entry capsule wake. Initial experimental tests at an AEDC wind-tunnel[80] yielded severe parachute suspension-line vibrations and canopy oscillations, drag-coefficient degradations, and several parachute suspension-line failures. Following suspension-line configuration modifications, transonic testing was begun in the TDT.

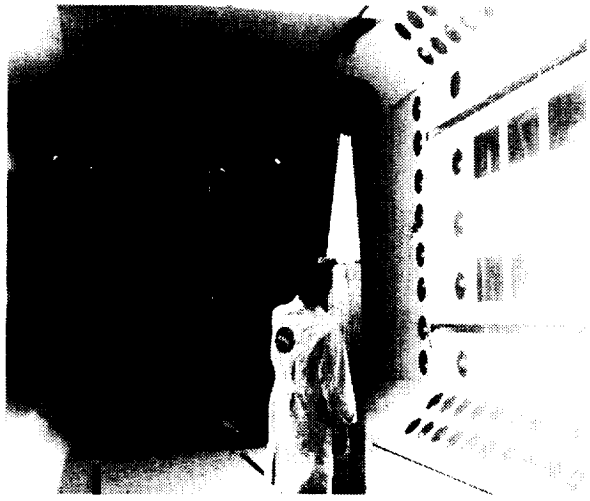

Fig. 121- 10 percent scale parachute model set-up.

The three objectives of the TDT test were to verify AEDC test results, validate parachute design changes, and to obtain additional transonic parachute performance data in the entry capsule wake environment. A photograph of the 10% scale disk-gap-band parachute model is shown in Fig. 121. The objectives of the test were accomplished in that large drag reductions measured for the original configuration tested at AEDC were verified, the design changes produced considerable improvement in system performance, and the new configuration did not suffer any significant failures. Typical results, presented in Fig. 122, show the effect on parachute drag of canopy trailing distance behind the entry capsule. Drag values for the initial-design trailing distance (x/d = 6.12) were much less than the required design values throughout the transonic Mach number range. Based on TDT test results, the Viking parachute subsystem was modified to provide longer suspension lines and thus a greater canopy trailing distance. This provided the desired increase in drag values. This increase in canopy trailing distance also reduced undesirable parachute dynamic motions.

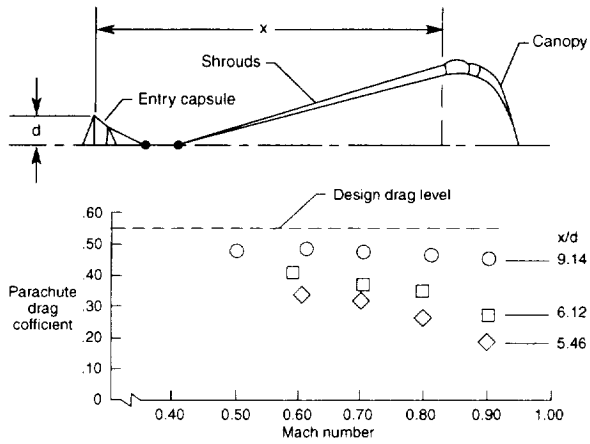

Fig. 122- Viking parachute drag-coefficient variations for several canopy distances behind the entry capsule at q=59.9 psf (initial design x/d=6.12).

Stagnation Pressure sensor Location (TDT Test 193) One of the scientific objectives of the Viking program was to measure the variation of Martian atmospheric ambient pressure with altitude during the parachute phase of the entry. Since the pressure field on and in the vicinity of the descending lander would be affected by its passage through the atmosphere, a test in the TDT was conducted to determine the optimum location and orientation of a sensor to measure stagnation pressure. The ambient pressure was determined from stagnation pressure after corrections for dynamic pressure and temperature effects were applied.[81] The 19%-scale model shown in Fig. 123 was instrumented to measure static, stagnation, and fluctuating pressures at various locations. The model was tested at tunnel conditions simulating the median Reynolds number expected during parachute descent over a Mach number range of 0.20 to 1.10. Parameters varied included model angle-of-attack and roll angle. Stagnation-pressure measurements were made using Kiel probes at various locations on the model. Based on test results and lander geometric constraints and subsystem interference, a probe location and a probe inclination angle of 22.5° (with respect to the bottom surface of the lander) were selected that produced pressure measurements nearly invariant as a function of model angle-of-attack and combined pitch-roll attitude. This Kiel probe was successfully used during the Viking entry to measure pressures during parachute descent and to measure atmospheric pressures after landing on Mars.[81]

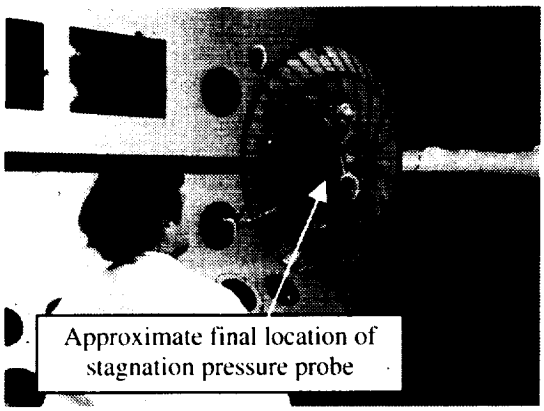

Fig. 123- 19% scale model used in stagnation pressure sensor location test.

Aeroshell-Lander/Base-cover Separation (TDT Test 204): While decelerating from slightly supersonic speeds, the Viking aeroshell was jettisoned from the lander/base-cover. Since forces and moments experienced by the two separating bodies were needed as input to required trajectory analyses, a wind-tunnel test in TDT was conducted. Six component forces and moments were measured on the aeroshell and three components on the lander/base-cover. The 10%-scale wind-tunnel models used are shown in Fig. 124.

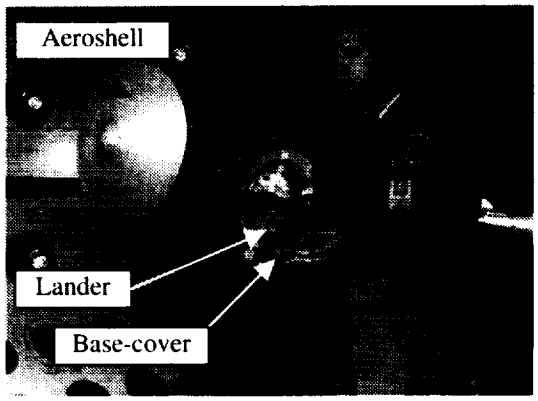

Fig. 124- 10% scale model used in Aeroshell-Lander/Base-cover separation test.

Results from this test are shown in Fig. 125 in the form of drag coefficient as a function of separation distance between the aeroshell and the lander/base-cover. In general, aeroshell drag increased initially, then as the distance between the two bodies was increased, the aeroshell drag gradually approached the values measured under free-flow conditions. The shielding effect of the aeroshell was indicated by the lander/base-cover drag being zero or having a negative value at up to four diameters separation distance, depending on Mach number, and then gradually approaching free-flow values as distance was further increased. The experimental aerodynamic characteristics of aeroshell staging, as measured in the TDT, were incorporated into Viking trajectory analyses and contributed significantly to the design of the successful separation of the aeroshell.

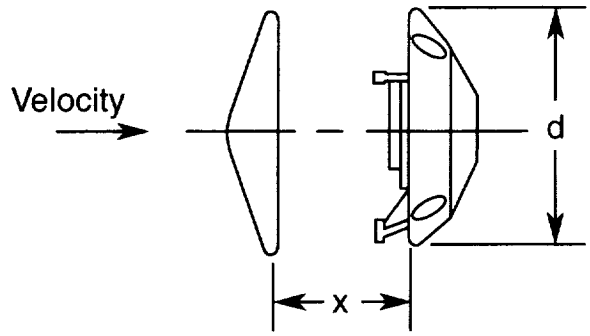

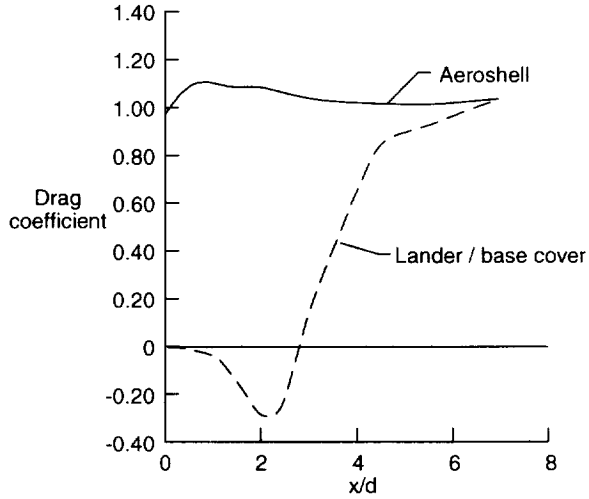

(a) Mach Number = 0.55.

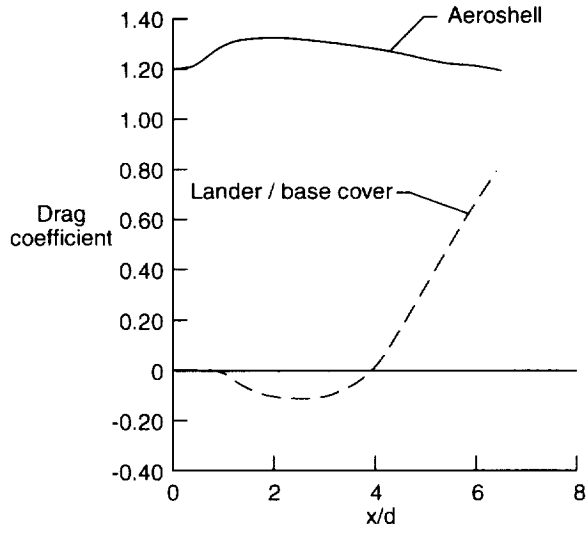

(b) Mach Number = 0.95.

Fig. 125- Effect of separation distance on drag coefficients – Viking aeroshell and lander/base-cover assembly.

Galileo Probe Parachute (TDT Test 383): The objectives of the Galileo mission[82, 83] were to conduct a comprehensive exploration of Jupiter and its satellites by use of an orbiting vehicle and direct measurement of Jovian atmospheric characteristics by an entry probe.[84] The Galileo orbiter with attached probe was launched from Earth on October 18, 1989. The probe entered Jupiter's atmosphere on December 7, 1995 and successfully completed its mission by transmitting data for 57.6 minutes during its descent. The probe entered the atmosphere at high speed and was slowed aerodynamically to transonic speeds by the blunt forebody. A parachute was employed to separate the instrument descent module from the heat shield and then provide drag for a controlled descent through the atmosphere.

The experimental investigation in the TDT[84] was initiated after a balloon drop test of a Galileo probe simulator in 1982 during which the main parachute opened slowly and erratically and the resulting slow separation caused some damage to probe hardware. This result was considered unacceptable since similar performance during the actual mission could result in delay of the initiation of scientific instruments and damage to specific sensors. The primary objectives of the TDT test program were to replicate the drop-test results in a wind-tunnel , perform parametric variations of the parachute system design, and demonstrate acceptable parachute deployment and performance for a revised design.

The TDT wind-tunnel test was conducted at simulated flight conditions using 1/4-scale and 1/2-scale models of the Galileo probe conical ribbon-parachute. The remainder of the test hardware included a forebody, adjustable steel aircraft cable, forward-canted floor-mounted strut, and a winch assembly, located below the tunnel test-section floor, used for controlling parachute position. Model installation details and a photo of the model are shown in Figs. 126 and 127, respectively. Model scale, forebody shape, angle-of-attack, dynamic pressure, Mach number, parachute porosity, and canopy trailing distance were varied to determine their effect on parachute performance. Both steady-state and deployment tests were conducted. Parachute drag was measured and found to degrade severely at canopy trailing distances of 5.5 (drop test distance) and 7 forebody diameters (x/d) as shown in Fig. 128. Performance was shown to be good at trailing distances of 9 and 11 diameters. Improvements in parachute performance were subsequently confirmed in a second probe system drop test[85]. Based on the results of the second drop test and the use of the TDT recommended configuration for the actual probe, the TDT test program of the Galileo probe parachute system contributed significantly to the successful collection of Jovian atmospheric data.[86]

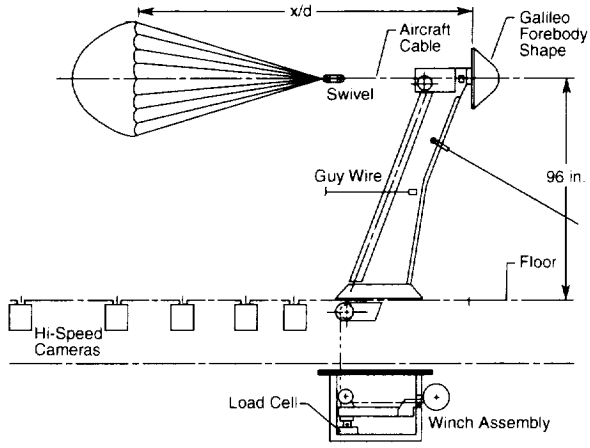

Fig. 126- Galileo probe parachute model installation in TDT.

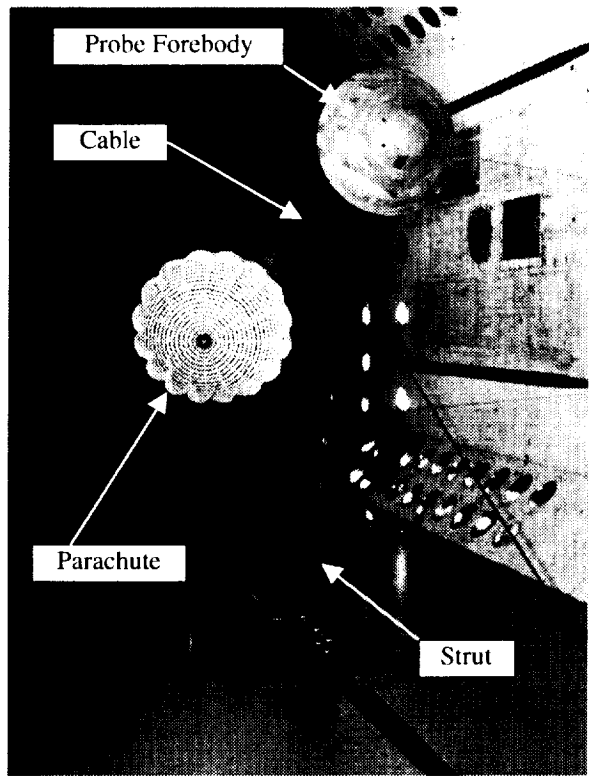

Fig. 127- Galileo probe model with 1/4-scale parachute in TDT.

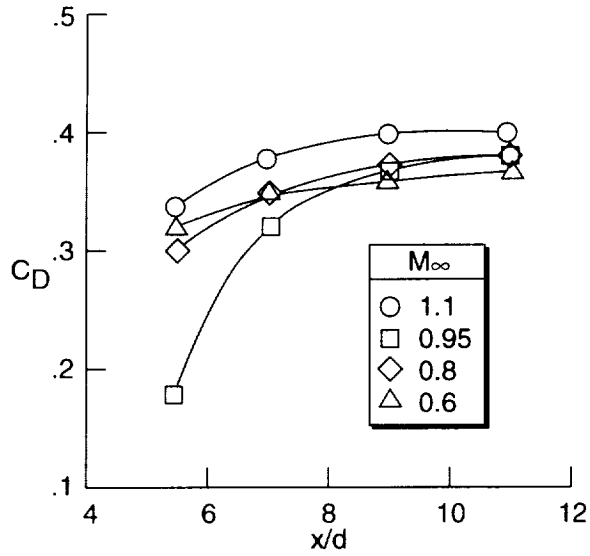

Fig. 128- Galileo probe parachute drag coefficient versus canopy trailing distance: 1/4-scale parachute, forebody AOA=0°, parachute porosity=29%.

PLANETARY-PROBE TESTING

Planetary-probe testing represents a very small portion of all TDT tests. This space-related testing category is distinct from the other four categories in that it does not involve measurements related to any aspect of flight, or to ground-wind loads in the conventional sense. Rather, these tests involved studying the landed-phase of the Mars Viking vehicles to determine the effects of Martian ground winds on instrumentation accuracy and temperature control of instrumentation packages.

Flow Field Measurements around Lander (TDT Test 180): An early concept of the Viking meteorological investigation had wind and temperature measurements made by sensors located at the end of a boom deployed by the lander. The location and length of this boom were dictated by accuracy requirements. The optimum design of this boom required a knowledge of the flow field around the lander. Reynolds number was one of the key parameters for simulating this flow field around the lander. The TDT, with its low density capability and large test section, was well suited to simulate the low Reynolds number conditions expected on Mars with a large-scale geometrically accurate model. A 45%-scale model of a proposed lander was mounted on a turntable in the TDT test section as shown in Fig. 129. This installation permitted the rotation of the model to simulate changes in wind direction. Wind speed, wind direction, and ambient temperature in the flow field around the model were measured using the remotely operated survey device shown in Fig. 129.

Wind-tunnel results[87] showed that the flow field around the lander was relatively insensitive to Reynolds number variation and the influence of the lander on the flow field decreased rapidly with distance from the lander. Hot film anemometers were used on the survey device and were shown to be viable candidates for use on the actual Viking lander. In fact, two hot-film anemometers orthogonally oriented in the horizontal plane were used to determine wind speed and direction on Mars.[88]

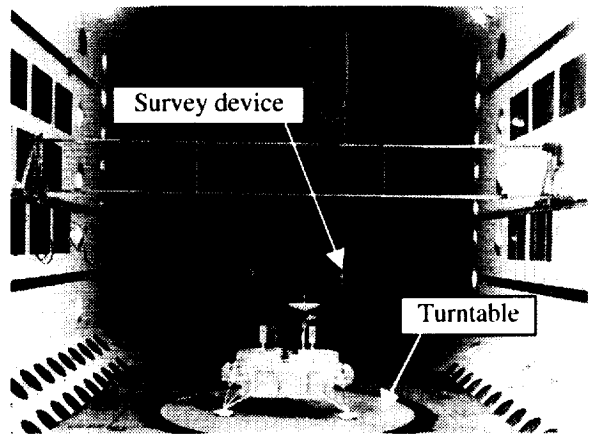

Fig. 129- 45% scale model and remote survey device used in lander flow field measurements.

Heat Shielding for RTG's (TDT Test 181): The purposes of the Viking radioisotope thermoelectric generators (RTG's) were to furnish electrical power to the lander when on the surface of Mars and to provide heat to instrumentation housed inside the lander. One concern was that high-velocity surface winds could result in excessive heat loss by forced convection that could endanger the survival of the lander's systems. Model scale tests were conducted in the TDT to measure the forced-convection heat transfer on simulated RTG's with and without wind shields. Two different wind shields (partially enclosing the RTG's) were tested. The 45%-scale lander model and thermally simulated RTG's are shown in Fig. 130.

Forced-convection heat-transfer coefficients measured in air[87] showed that neither of the two wind-shields provided an acceptable solution to the RTG convective cooling problem. The final solution was to totally enclose each RTG with a wind shield. This insured that excess heat from the RTG's would be available to the scientific instruments and other lander systems and not dissipated uselessly into the Martian environment.

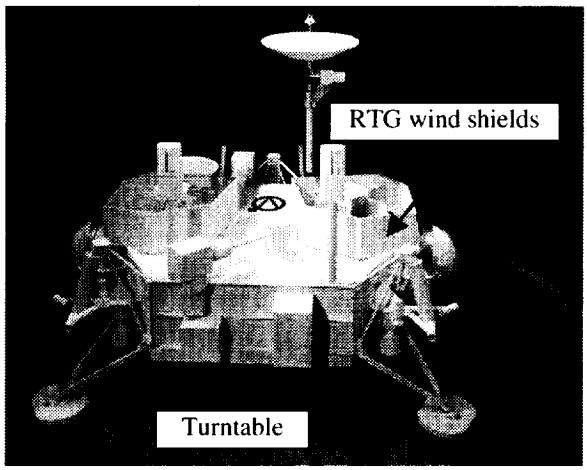

Fig. 130- 45% scale model used to test heat shielding for RTG's.

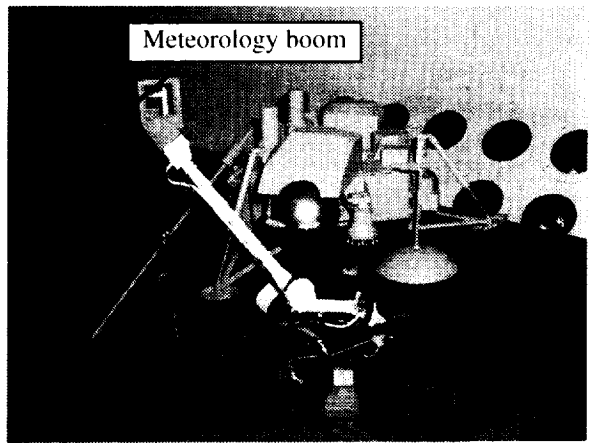

Fig. 131- 37.5% scale lander model with full-scale meteorology boom used in determining lander flow field effects on meteorology instruments.

Lander Flow Field Effects on Meteorology Instruments (TDT Test 263): The objectives of the Viking meteorological experiment were to measure pressure, temperature, wind speed, and wind direction on the Martian surface. The meteorology instrumentation system, including software, was subjected to an extensive test program in TDT.[88]

The configuration for a portion of the test included a full-scale flight sensor and meteorological boom assembly mounted on a turntable in the TDT test section. The data from the TDT test was reduced using flight software and compared with wind-tunnel parameters that were reduced independently. The results of these tests indicated that the instrument system (including software, but not lander flow-field effects) had an accuracy of approximately ±10% for both wind speed and wind direction.

The approximate influence of the lander on local meteorological measurements was determined using a 37.5%-scale model of the final lander configuration in association with the full-scale meteorological boom as shown in Fig. 131. The meteorological boom was positioned on the lander (utilizing data from the 1970 flow-field survey) to minimize the effects of the lander-induced flow field. The boom was deployed 5.25 ft. above the surface and 2.0 ft. from the nearest part of the lander body. Test results showed that the lander effect was about ±10% in both wind speed and direction. Meteorological results obtained on Mars for Viking 1 and 2 are summarized in Ref. 89.

CONCLUDING REMARKS

The NASA Langley Transonic Dynamics Tunnel (TDT) has provided test support for space-related applications throughout its forty year history. Several capabilities of the TDT stand out as being the primary factors as to why the TDT was used for these space-related tests. These factors are the aeroelastic scaling advantage and the relatively high Reynolds number of the heavy gas test medium, the TDT variable pressure capability, and the relatively large test section. Most of these space-related tests have dealt with some aspect of aeroelastic or unsteady response testing, which is the primary objective of the TDT facility. However, some of these tests have utilized the TDT for static, and often unique, wind-tunnel tests because of above stated beneficial characteristics of the TDT. The space-related tests conducted in the TDT have been categorized into five distinct areas. These areas are ground winds loads, launch vehicle dynamics, atmospheric flight of space vehicles, atmospheric reentry, and planetary-probe testing. The TDT still maintains essentially all of the capabilities that contributed to these past space model tests and, therefore, stands poised to continue to support similar space activities in the future.

REFERENCES

1. Cole, Stanley R.; and Garcia, Jerry L.: Past, Present, and Future Capabilities of the Transonic Dynamics Tunnel from an Aeroelasticity Perspective. AIAA-2000-1767, April 2000.

Ground wind loads

2. Reed, Wilmer H. III: Models for Obtaining Effects of Ground Winds on Space Vehicles Erected on the Launch Pad. Presented at the Conference on the Role of Simulation in Space Technology. Virginia Polytechnic Institute, Blacksburg, Virginia, August 17-21, 1964.

3. Hanson, Perry W.; Jones, George W. Jr.: On the Use of Dynamic Models for Studying Launch Vehicle Buffet and Ground-Wind Loads. Presented at the Symposium on Aeroelastic and Dynamic Modeling Technology. Dayton, Ohio, September 23-25, 1963.

4. Farmer, Moses G.; Jones, George Jr.: Summary of Langley Wind-Tunnel Studies of Ground Wind Loads on Launch Vehicles. NASA TM-X-57779, 1966 pp. 2.1-2.25.

5. Bilstein, Roger E: Stages to Saturn: A Technological History of the Apollo/Saturn Launch Vehicles. NASA SP-4206.

6. Runyan, Harry L.; Rainey, A. Gerald: Launch Vehicle Dynamics. Presented at the NASA-Industry Apollo Conference, Washington, D.C., July 18-20, 1961. NASA TM-X-607.

7. Killough, T. L.: Wind-Induced Loads on a Dynamic 1/5 Scale Unfueled SM-78 Jupiter in the Launch Position. Army Ordinance Missile Command Report No. RG-TM-62-65, July 1962.

8. Jones, George W.; Farmer, Moses G.: Wind-Tunnel Studies of Ground-Wind Loads on Saturn Launch Vehicles. AIAA/ASME 7th Structures and Materials Conference, Cocoa Beach, FL, April 18-20, 1966.

9. Hunt, Robert M.: Saturn V Ground Winds Program. NASA TM-X-57779, 1966, pp. 3.1-3.11.

10. (Reference intentionally removed by authors.)

11. Jones, George W.: Unsteady Lift Forces Generated by Vortex Shedding About a Large, Stationary, and Oscillating Cylinder at High Reynolds Numbers. Presented at the ASME Symposium on Unsteady Flow, Philadelphia, Pennsylvania, May 6-9, 1968.

12. Cincotta, Joseph J.; Jones, George W.; and Walker, Robert W.: Experimental Investigation of Wind Induced Oscillation Effects on Cylinders in Two-Dimensional Flow at High Reynolds Numbers. NASA LaRC Meeting on Ground-Wind Loads Problems in Relation to Launch Vehicles, NASA TM-X-57779, pp. 20.1-20.25, June 1966.

13. Lyons, J. M. and Lum, A. J.: Ground Wind Induced Oscillations of the Titan III ITL Transporter. NASA TM-X-57779, 1966, pp. 5.1-5.30.

14. Reed, Wilmer H. III: Wind Effects on Space Shuttle Vehicles Erected on Launch Pad. Presented at the Third International Conference on Wind Effects on Buildings and Structures, Tokyo, Japan, September 6-11, 1971.

15. Flutter and Aeroelasticity Group, Space Division of Rockwell International: Space Shuttle Flutter and Aeroelasticity Data Book, Section XIV - Orbiter Model Flutter Tests. August, 1992.

Launch vehicle dynamics

16. Jones, George W., Jr., and Foughner, Jerome T., Jr.: Investigation of Buffet Pressures on Models of Large Manned Launch Vehicle Configurations. NASA TN D-1633, May 1963.

17. Pearson, Albin O.: Surface Pressure Distributions on 0.0628-Scale Models of Proposed Project FIRE Space Vehicles at Mach Numbers from 0.25 to 4.63. NASA TD D-1961, September 1963.

18. Muraca, Ralph J.: Aerodynamic Load Distributions for the Project FIRE Configurations at Mach Numbers from 0.25 to 4.63. NASA TN D-2604, February 1965.

19. Henderson, William P.: Pressure Distributions over the Forward Portion of the Project FIRE Space-Vehicle Configuration at Mach Numbers from 0.25 to 0.65. NASA TN D-1612, February 1963.

20. Ericson, Lars-Eric, and Reding, J. Peter: Report on Saturn I-Apollo Unsteady Aerodynamics. NASA CR-58375, February 1964.

21. Hanson, Perry W., and Doggett, Robert V., Jr.: Aerodynamic Damping and Buffet Response of an Aeroelastic model of the Saturn I Block II Launch Vehicle. NASA TN D-2713, March 1965.

22. Raney, A. Gerald: Progress of the Launch-Vehicle Buffeting Problem. Presented at the AIAA fifth

annual Structures and Materials Conference, Palm Springs, CA, April 1-3, 1964. Published in the Journal of Spacecraft and Rockets, May-June 1965, pp.289-299.

23. Ericson, Lars-Eric: Aeroelastic Instability Caused by Slender Payloads. Journal of Spacecraft and Rockets. Vol. 4, No. 1, January 1967, pp. 65-73.

24. Moseley, William C., Jr.; and Martino, Joseph C.: Apollo Wind Tunnel Testing Program - Historical Development of General Configurations. NASA TN D-3748, December 1966.

25. Moseley, William C., Jr.; and Redd, Bass: Aerodynamic Stability Characteristics of the Apollo Launch Escape Vehicle (LEV) with Canard Surfaces Deployed. NASA TN D-4280, December 1967.

26. Cole, Henry A., Jr.; Erickson, A. L.; and Rainey, A. G.: Buffeting During Atmospheric Ascent. NASA SP-8001, 1963, Revised November 1970.

27. Bombardier, G. D.: Final Post-Test Report on Seven Percent Transonic Buffet Model for Various Titan III Configurations. Martin Co. Report Number SSD-CR-66-563, January 1967.

28. Cole, Stanley R., and Henning, Thomas L.: Dynamic Response of a Hammerhead Launch Vehicle Wind-Tunnel Model. NASA TM 104050, February 1991.

29. Cole, Henry A., Jr.: Dynamic Response of Hammerhead Launch Vehicles to Transonic Buffeting. NASA TN D-1982, 1963.

30. Ragab, M. M.: Contribution of Buffet to Space Vehicle Loads during Atmospheric Flight. AIAA paper number 92-0716, January 1992.

31. Reding, J. P., and Ericsson, L. E.: Hammerhead Aeroelastic Stability Revisited. AIAA paper number 93-1477, April 1993.

Atmospheric flight of space vehicles

32. Pyle, Jon S.; and Montoya, Lawrence C.: Effect of Roughness of Simulated Ablated Material on Low-Speed Performance Characteristics of a Lifting-Body Vehicle. NASA TM X-1810, 1969.

33. Decker, John P.; and Abel, Irving A.: Some Effects of Ablation Surface Roughness on the Aerodynamic Heating of a Reentry Vehicle at Mach Numbers From 0.30 to 1.00. NASA TM SX-2050, February 1971.

34. Goetz, Robert C.: Exploratory Study of Buffet and Stall Flutter of Space Vehicle Wing Concept. NASA Langley Working Paper 872, May 22, 1970.

35. Goetz, Robert C.: Launch Vehicle Wing with Tip Fin. Presented at the NASA Space Shuttle Technology Conference, March 2-4, 1971. NASA TM X-2274 – Volume III, April 1971.

36. Berthold, C. L.: Results of Flutter Test OS7 Obtained Using the 0.14-Scale Space Shuttle Orbiter Fin/Rudder Model Number 55-0 in the NASA LaRC 16-foot Transonic Dynamics Tunnel. NASA CR-151057, March 1977.

37. Berthold, C. L.: Results of Flutter Test OS6 Obtained Using the 0.14-Scale Wing/Elevon Model (54-0) in the NASA LaRC 16-foot Transonic Dynamics Tunnel. NASA CR-151056, March 1977.

38. Flutter and Aeroelasticity Group, Space Division of Rockwell International: Space Shuttle Flutter and Aeroelasticity Data Book, Section XIV – Orbiter Model Flutter Tests. August, 1992.

39. Bennett, Robert M.; Farmer, Moses G.; Mohr, Richard L.; and Hall, W. Earl, Jr.: Wind-Tunnel Technique for Determining Stability Derivatives from Cable-Mounted Models. Journal of Aircraft, Volume 15, Number5. May 1978, pp. 304-310.

40. Mohr, Richard L.; and Hall, W. Earl, Jr.: Identification of Stability Derivatives from Wind Tunnel Tests of Cable-Mounted Aeroelastic Models. NASA CR-145123, 1977.

41. Freeman, Delma C., Jr.: Dynamic Stability Derivatives of Space Shuttle Orbiter Obtained from Wind-Tunnel and Approach and Landing Flight Tests. NASA TM 1634, April 1980.

42. Flutter and Aeroelasticity Group, Space Division of Rockwell International: Space Shuttle Flutter and Aeroelasticity Data Book, Section XVII – Integrated Shuttle Model Flutter Tests. August, 1992.

43. Reed, Wilmer H. III, Hanson, Perry W., and Alford, W. J.: Assessment of Flutter Model Testing Relating to the National Aero-Space Plane. NASP CR-1002, July 1987.

44. Spain, Charles V., Soistmann, David L., Parker, Ellen C., Gibbons, Michael D., and Gilbert, Michael G.: An Overview of Selected NASP Aeroelastic Studies at the NASA Langley Research Center. Presented at

the AIAA Second International Aerospace Conference, Orlando, FL, October 1990.

45. Noll, T. E., Doggett, Robert V., Jr., Ricketts, Rodney H., and Malone, John B.: Aeroservothermoelasticity - A Review. Paper no. 10, presented at the 10th National Aero-Space Plane Technology Symposium, April 1991.

46. Cazier, F. W., Jr., Doggett, Robert V., Jr., and Ricketts, Rodney H.: Structural Dynamic and Aeroelastic Considerations for Hypersonic Vehicles. NASA TM 104110, June 1991.

47. Ricketts, Rodney H., Noll, Thomas E., Whitlow, Woodrow, Jr., and Huttsell, Lawrence J.: An Overview of Aeroelasticity Studies for the National Aero-Space Plane. AIAA-93-1313-CP, April 1993.

48. Doggett, Robert V., Jr., Soistmann, David L., Spain, Charles V., Parker, Ellen C., and Silva, Walter A.: Experimental Transonic Flutter Characteristics of Two 72°-Sweep Delta-Wing Models. NASA TM 101659, November 1989.

49. Soistmann, David L., and Gibbons, Michael D.: Some Analytical Transonic Flutter Characteristics of a Highly Swept Delta Wing. NASP CR-1084, May 1990.

50. Doggett, Robert V., Jr., and Soistmann, David L.: Low-Speed Flutter Characteristics of Some Simple Low-Aspect-Ratio Delta-Wing Models. Journal of Aircraft, Vol. 29, No. 2, March-April 1992, pp. 273-279.

51. Soistmann, David L., and Gibbons, Michael D.: Some Analytical Transonic Flutter Characteristics of a Highly Swept Delta Wing. Paper no. 63, presented at the 7th National Aero-Space Plane Technology Symposium, NASA Lewis Research Center, Cleveland, OH, October 1989.

52. Parker, Ellen C., Spain, Charles V., and Soistmann, David L.: Experimental Transonic Buzz Characteristics of a Clipped-Delta-Wing Model with a Full-Span Aileron. NASP CR-1083, May 1990.

53. Parker, Ellen C., Spain, Charles V., and Soistmann, David L.: Aileron Buzz Investigated on Several Generic NASP Wing Configurations. AIAA paper no. 91-0936, April 1991.

54. Huttsell, L. J., Sallee, V. J., Bullock, E. P., and Cole, S. R.: Analytical and Experimental Panel Flutter Results. Paper no. 12, NASP Technology Review, Monterey, CA, April 1993.

55. Soistmann, David L.; and Spain, Charles V.: An Experimental and Analytical Study of a Lifting-Body Wind-Tunnel Model Exhibiting Body-Freedom Flutter. AIAA-93-1316, April 1993.

56. Pendleton, Ed: Model Systems Report National Aero-Space Plane Design 201 Horizontal Lifting Surface Model. WL-TM-92-355-FIBR, December 1992.

57. Pendleton, Ed; Harris, Scott; Moster, Greg; Keller, Don; Farmer, Moses; Wasserman, Lee; and Pitman, Wade: A NASP Stabilator Transonic Aeroelastic Model. Paper no. 10, NASP Technology Review, Monterey, CA, April 1993.

58. Pendleton, E.; Moster, G.; and Keller, D.: Transonic Aeroelastic Models of Hypersonic Highly Swept Lifting Surfaces, Journal of Aircraft, Volume 32, Number 6, November-December 1995.

59. Cole, Stanley R.; Florance, James R.; Thomason, Lee B.; Spain, Charles V.; and Bullock, Ellen P.: Supersonic Aeroelasticity Instability Results for a NASP-like Wing Model. NASA TM 107739, April 1993.

60. Spain, Charles V.; Zeiler, Thomas A.; Bullock, Ellen P.; and Hodge, Jeffrey S.: A Flutter Investigation of All-Moveable NASP-like Wings at Hypersonic Speeds. AIAA-93-1315, April 1993.

61. Moster, Gregory E.: National Aero-Space Plane Vertical Lifting Surface Transonic Aeroelastic Model. WL-TM-94-3033-FIBG, March 1994.

62. Parker, Akweli: Langley Takes Lead in NASA Project to Build Mars Airplane. Article in Virginian Pilot Newspaper, June 16, 1999.

Atmospheric reentry

63. Kelly, H. Neale; and McNulty, James F.: Inflatable Parawing Deployment Studies Using a Dynamically and Elastically Scaled Model. Vol. 16, part one of Advances in Astronautical Sciences, Norman V. Petersen, ed., Western Periodicals Co. (N. Hollywood, CA), c.1963, pp.751-758.

64. Ferris, Alice T.; and Kelly, H. Neale: Free-Flight and Wind-Tunnel Studies of Deployment of a Dynamically and Elastically Scaled Inflatable Parawing Model. NASA TN D-4724, Sept. 1968.

65. Raff, Bruce W.: Design and Similitude Testing of Dynamically Scaled Paraglider Model. Vol. 16, part one of Advances in Astronautical Sciences, Norman V. Petersen, ed., Western Periodicals Co. (N. Hollywood, CA), c.1963, pp.731-750.

66. Oberg, A. J.: An Engineering Design Study and Test Program for the Paravulcoon Recovery System. NASA CR62008, prepared for NASA LaRC by Honeywell Systems and Research Div., February 1965.

67. Bacchus, David L.; Vickers, Jack R.; and Foughner, Jerome T.: Wind Tunnel Investigation of Space Shuttle Solid Rocket Booster Drogue Parachutes and Deployment Concepts. AIAA Paper 75-1366, November 1975.

68. Ira T. Holt: Design and Development of a Heavy Duty 76-foot Ribbon Parachute. Proceedings of Joint DOD, AIAA Aerodynamic Decelerations Systems Conference, September, 1968, FTC-TR-69-11, April 1969.

69. Maydrew, R. C.; and Johnson, D. W.: Supersonic and Transonic Deployment of Ribbon Parachutes at Low Altitudes. Journal of Aircraft, Volume 9, No. 7, July 1972.

70. Bohon, Herman L.; and Miserentino, Robert: Attached Inflatable Decelerator Performance Evaluation and Mission-Application Study. AIAA paper no. 70-1163, September 1970.

71. Mikulas, Martin M., Jr.; and Bohon, Herman L.: Summary of the Development of Attached Inflatable Decelerators. AIAA paper no. 68-929, September, 1968.

72. Deveikis, William D.; and Sawyer, James Wayne: Static Aerodynamic Characteristics, Pressure Distributions, and Ram-Air Inflation of Attached Inflatable Decelerator Models at Mach 3.0. NASA TN D-5816, May 1970.

73. Bohon, Herman L.; and Miserentino, Robert: Deployment and Performance Characteristics of 5-foot-diameter (1.5m) Attached Inflatable Decelerators from Mach Number 2.2 to 4.4. NASA TN D-5840, August 1970.

74. Willis, Conrad M.; and Mikulas, Martin M., Jr.: Static Structural Tests of a 1.5-meter-diameter Fabric Attached Inflatable Decelerator. NASA TN D-6929, October 1972.

75. Bohon, Herman L.; and Sawyer, James Wayne: Deployment and Performance Characteristics of 1.5-meter Supersonic Attached Inflatable Decelerators. . NASA TN D-7550, July 1974.

76. Corliss, William R., The Viking Mission to Mars. NASA SP-334, 1974.

77. Cooley, C. G.; and Lewis, J.G.: Viking Lander System – Primary Mission Performance Report. NASA CR-145148, 1977.

78. Scientific Results of the Viking Project. Journal of Geophysical Research, Volume 82, No. 28, September 30, 1977, pp. 3959-4680.

79. Foughner, Jerome T., Jr.: Viking Mars Mission Support Investigations in the Langley Transonic Dynamics Tunnel. NASA TM 80234, May 1980.

80. Steinberg, Sy; Siemers, Paul M., III; and Slayman, Robert G.: Development of the Viking Parachute Configuration by Wind-Tunnel Investigation. Journal of Spacecraft, Volume 11, No. 2, February 1974, pp. 101-107.

81. Seiff, Alvin; and Kirk, Donn B.: Structure of the Atmosphere of Mars in Summer at Mid-Lattitudes. Journal of Geophysical Research, Volume 82, No. 28, September 30, 1977, pp. 4364-4378

82. O'Neil, W. J. and Mitchell, R. T., "Galileo Mission Overview," AIAA Paper 83-0096, January 1983.

83. Vojvodich, N. S., Drean, R. J., Schaupp, R. W., and Farless, D. L.; "Galileo Atmospheric Entry Probe Mission Description," AIAA Paper 83-0100, January 1983.

84. Corridan, Robert E., Givens, John G., and Kepley, Bryce M.; Transonic Wind-Tunnel Investigation of the Galileo Probe Parachute Configuration, AIAA Paper 84-0823, 1984.

85. McMenamin, H. J., Pochettino, L. R.; Galileo Parachute System Modification Program. AIAA Paper 84-0824, April 1986.

86. Science Magazine, Volume 272, pp. 781-920 (May 10, 1996 issue).

Planetary-probe testing

87. Greene, George C.; Keafer, Lloyd S., Jr.; Marple, Charles G.; and Foughner, Jerome T., Jr.: Flow-Field

Measurements Around a Mars Lander Model Using Hot-Film Anemometers Under Simulated Mars Surface Conditions. NASA TN D-6820, 1972

88. Chamberlain, T.E.; Cole, H. L.; Dutton, R. G.; Green, G. C.; and Tillman, J. E.: Atmospheric Measurements on Mars: The Viking Meteorology Experiment. Bulletin of the American Meteorological Society, Volume 57, No. 9, September 1976, pp.1094-1104

89. Hess, S. L.; Henry, R. M.; Leovy, C. B.; Ryan, J. A.; Tillman, J. E.: Meteorological Results From the Surface of Mars: Viking 1 and 2. Journal of Geophysical Research, Volume 82, No. 28, September 30, 1977, pp. 4559-4574.

Table 1- TDT space-related tests.

Test #	Test Title	Dates	Model	Mount	Description	Category
12	Scout	10/5/60 - 10/18/60	LV	F	15%-scale, Ground wind loads, with service tower, no turntable, R-12/Air	LVGWL
13	Rigid AVCO Drag Brake	10/19/60 - 11/2/60	PD	S	1/12-scale, Simple representation of proposed reentry brake concept, loads data? No data avail.	AR
18	Saturn I Block I (SA-1)	3/6/61 -3/23/61	LV	F	7.5%-scale, Ground wind loads, no turntable, no service tower, steady pressure, R-12/Air	LVGWL
20	Parawing	5/23/61 - 6/13/61	PW		Parawing recovery system	AR
21	Parawing	6/20/61 - 7/14/61	PW	S	Parawing recovery system	AR
22	Parawing	7/17/61 - 8/4/61	PW	FP	Parawing recovery system	AR
23	Scout Missile and Tower	8/4/61 - 8/24/61	LV	F	15%-scale, Ground wind loads, no turntable, R-12/Air	LVGWL
24	Saturn-Apollo Pressure Models	8/24/61 - 9/14/61	LV	S	8% and 1.6%-scale, Buffet pressure measurements, air and Freon, different size models	LVFD
28	Jupiter Missile	10/9/61 - 10/23/61	LV	F	1/5-scale, Ground wind loads, no turntable, R-12/Air	LVGWL
31	Saturn-Apollo Pressure Models	11/7/61 - 11/20/61	LV	S	8% and 1.6%-scale, Buffet pressure measurements, air and Freon, different size models	LVFD
37	Wind Induced Loads Research Model	2/27/62 - 3/12/62	LV	F	Ground wind loads, generic model	LVGWL
38	Project "Fire" Buffet Model	3/12/62 - 4/3/62	LV	S	1/6-Scale, Buffet(unsteady pressures) and air loads (steady pressures) data	LVFD
40	Smokestack Flutter	4/5/62 - 4/16/62	LV	F	Ground wind loads, generic model, air	LVGWL
46	Parawing deployment test	10/8/62 - 10/31/62	PW	HR	1/8 scale model	AR
48	Saturn	11/19/62 - 12/7/62	LV	S	8%-scale, SD-1 model, Apollo and Jupiter noses	LVFD
49	Drougue Chute Deployment for Apollo Command Module	12/10/62-12/14/62	PD	P	Parachute recovery system	AR
52	Titan III	1/15/63 - 2/15/63	LV	FT	7.5%-scale, Ground wind loads, with tower, first test with floor turntable, R-12/Air	LVGWL
53	Saturn I Block II (SA-5)	2/18/63 - 3/6/63	LV	FT	7%-scale, Ground wind loads, with LC 37B umbilical tower, Jupiter & Apollo payload, R-12/Air	LVGWL
55	Saturn-V	3/11/63 - 3/29/63	LV	FT	3%-scale, Ground wind loads, with tower, R-12/Air, sub-critical Reynolds number	LVGWL
56	Saturn-V	3/11/63 - 3/29/63	LV	FT	3%-scale, Ground wind loads, with tower, R-12/Air, sub-critical Reynolds number	LVGWL
60	Saturn-Apollo + hot-wire probes	5/17/63 - 6/6/63	LV	S	SD-1 model, Apollo & Jupiter noses, aerodynamic damping and buffet	LVFD
62	Saturn V	7/15/63 - 8/20/63	LV	FT	3%-scale, Ground wind loads, with tower, R-12/Air, sub-critical Reynolds number	LVGWL
65	Saturn IB	10/23/63 - 11/21/63	LV	FT	5.5%-scale, Ground wind loads, with LC-34 and LC-37B, Apollo spacecraft payload, R-12/Air	LVGWL
66	Launch Escape Canard Model	11/24/63 - 12/6/63	O	S	Full-scale forebody of canard launch escape vehicle	LVFD
67	Apollo Parawing	12/9/63 - 1/3/64	PW	S & C	Parawing recovery system, sting and cables	AR
71	Saturn IB	3/25/64 - 4/7/64	LV	FT	5.5%-scale, Ground wind loads, LC-34 and -37B, space station payload, R-12/Air, model destroyed	LVGWL
72	Titan II - Gemini	4/15/64 - 5/15/64	LV	FT	7.5%-scale, Ground wind loads, dynamically-scaled erector tower, R-12/Air	LVGWL
73	Parawing	6/1/64 - 6/7/64	PW	S		AR
74	Parawing Deployment	6/8/64 - 7/2/64	PW	HR	With capsule, bar mounted	AR
79	Saturn V	9/17/64 - 11/10/64	LV	FT	3%-scale, Ground wind loads, with tower, R-12/Air, sub-critical Reynolds number	LVGWL
82	Parawing + Capsule	1/4/65 - 1/15/65	PW		Spacecraft recovery system	AR
88	Saturn IB	3/15/65 - 4/30/65	LV	FT	5.5%-scale, Ground wind loads, Apollo and generalized payloads, LC-34 and -37B, R-12/Air	LVGWL
94	Martin G.W.L Cylinder (2-D)	6/30/65 - 9/17/65	O	F	2-D oscillating cylinder, vortex shedding at high Reynolds numbers	LVGWL
95	Titan III	9/20/65 - 10/27/65	LV	FT	7.5%-scale, Ground wind loads, dynamically-scaled transporter/tower, R-12/Air	LVGWL
102	PSTL 1 Saturn Apollo Model	2/28/66 - 3/25/66	LV	S	Buffet pressure measurements, rigid model	LVFD
106	Saturn-V	5/2/66 - 6/3/66	LV	FT	3%-scale, Ground wind loads, with and without service tower	LVGWL
119	Barish Sail Wing Test	3/6/67 - 3/20/67	PD	FP	1/6-scale, Aerodynamic decelerator concept, Stability and loads during deployment	AR
123	Turntable and MET Tower	5/5/67 - 5/16/67	LV	FT	Ground wind loads and response, flow field measurements	LVGWL
	(+ vertical rake)	5/26/67 - 6/1/67	LV	FT		
	Saturn-V	6/6/67 - 6/14/67	LV	FT	3%-scale	
	(+ vertical rake)	6/15/67 - 6/19/67	LV	FT		
	Turntable and MET Tower	6/19/67 - 6/21/67	LV	FT		
124	Paravulcoon	5/17/67 - 5/25/67	LV	S	Test of space vehicle terminal recovery system (balloon), sting mount	LVFD
130	Bulbous Nose Pressure Distribution Models (2)	12/20/67 - 1/29/68	LV	S	Steady-pressure measurements, large and small bulbous nose rigid models	LVFD
148	Saturn Apollo (command module) (+ explosive charges)	2/28/69 - 3/27/69	LV	FP	Pressure means. on Apollo SC, TNT charges simulated booster explosion	LVFD
149	Attached Inflator Decelerator Model	3/28/69 - 4/11/69	PD	S	Atmospheric decelerator test	AR
150	Reentry Vehicles (2)(Martin SV-5D)	4/14/69 - 5/2/69	FS	FP	Ablation surface roughness effects on stability derivatives. Used a flight test vehicle and smooth model	AF
157	Shuttle concept stall flutter/buffet wings (2)	8/29/69 - 9/4/69	SS	SW	Candidate wing designs, high angle of attack, stall flutter, buffeting (Straight and clipped delta wings)	AF
158	Shuttle concept stall flutter/buffet wings (2)	9/29/69 - 10/1/69	SS	SW	Candidate wing designs, high angle of attack, stall flutter, buffeting (Straight and clipped delta wings)	AF
180	Viking	10/22/70 - 11/9/70	PP	FT	45%-scale, flow-field measurements around lander, meteorology system development	PP
181	Viking	11/10/70 - 11/16/70	PP	FT	45%-scale, convective heat-transfer test to establish shielding needed for RTG's	PP
182	Saturn-V	11/17/70 - 12/10/70	LV	FT	3%-scale, Ground wind loads, Skylab payload, with LC-39B tower, R-12/Air	LVGWL
186	Space Shuttle Booster Wing Concept (with tip fin)	2/15/71 - 2/23/71	SS	SW	0.05-scale, Candidate wing design, high angle of attack, stall flutter, buffeting, tip fin effects	AF
190	Viking Decelerator (Martin Marrietta)	4/21/71 - 4/28/71	PD	FP	10%-scale, parachute environment and performance, parametric testing	AR
193	Viking (Martin)	6/29/71 - 7/1/71	PP	S	19%-scale, pressure measurements on lander/base cover, stag. press. sensor location optimization	AR
200	Saturn IB	10/19/71 - 11/12/71	LV	FT	5.5%-scale, Ground wind loads, Apollo spacecraft payload, LC-39B tower, Skylab, R-12/Air	LVGWL
204	Viking Separation	2/7/72 - 2/29/72	PP	S	10% scale, loads measurements for aeroshell-lander/basecover separation during aeroshell jettison	AR
210	Space Shuttle	10/16/72 - 11/16/72	LV	FT	3%-scale, Ground wind loads, preliminary Space Shuttle design, R-12/Air	LVGWL
243	Space Shuttle SRB Parachutes	7/12/74 - 7/29/74	PD	C & F	0.125-scale, Solid rocket booster drogue parachutes and deployment concepts	AR
246	Space Shuttle V-tail and Wing	8/19/74 - 9/13/74	FS/SS	SW	0.14-scale, Vertical fin/rudder flutter, buffet and buzz. Also 0.14-scale Wing-elevon model - flutter	AF
258	Space Shuttle V-tail	4/2/75 - 4/10/75	FS	SW	0.14-scale fin-rudder model, flutter and buffet, simulated deployed speed brake(split rudder) with wedge	AF
263	Viking	7/23/75 - 8/11/75	PP	FT	37.5%-scale, meteorology science experiments - system calibration and lander flow field effects	PP
266	Space Shuttle Orbiter	10/16/75 - 11/7/75	FS	C	0.055-scale, Stability (*rigid) model on active cable-mount system, Cable stability, buffet and stab. derivatives	AF
275	Space Shuttle SRB Parachutes	3/24/76 - 4/2/76	PD	FP & C	0.125-scale, SRB Drogue and main parachute systems	AR
300	Space Shuttle Orbiter	5/9/78 - 5/29/78	FS	C	0.055-scale dynamically scaled model on active cable-mount system, flutter and buffet loads	AF
306	Space Shuttle	7/30/78 - 8/24/78	LV	FT	4.6%-scale, Ground wind loads, final shuttle configuration, with tower, R-12/Air, tower destroyed	LVGWL
308	Space Shuttle Launch Configuration	9/15/78 - 10/17/78	LV	S	0.055-scale all-up (orbiter, external tank, and SRB's) configuration, flutter and buffet loads	AF
321	Space Shuttle V-tail	8/29/79 - 9/27/79	FS	SW	Shuttle test OS-30, 0.14-scale fin model, flutter, buffet, speed brake (split rudder) deployed	AF
363	Galileo Parachute	4/13/83 - 4/22/83	PD	FP	25% and 50%-scale, parachute static and deployment testing for development of Jupiter probe system	AR
407	72° Delta Wing Flutter	7/2/87 -7/6/87	SS	SW	Flutter research related to NASP	AF
410	72° Delta Wing Flutter II	8/20/87 - 8/25/87	SS	SW	Flutter research related to NASP	AF
420	Simple Delta Wing Models (NASP)	3/23/88 -3/29/88	SS	SW	72-degree sweep wings, NASP	AF
423	Atlas-Centaur Large Payload Fairing	6/12/88 - 7/15/88	LV	FT	1/10th-scale, buffeting, enlarged payload fairing	LVFD
424	Delta Wing Flutter	7/17/88 - 7/27/88	SS	SW	NASP related	AF
425	MAMA (Mass and Motion Apparatus)	7/28/88 - 8/2/88	SS	SW	All-movable wing flutter, NASP	AF
431	Aileron Buzz of Generic NASP Configuration	2/14/89 - 2/14/89	SS	SW	Delta wing with large trailing edge control surface, NASP related	AF
432	Delta Wing w/Mass and Motion Apparatus (MAMA)	2/22/89 - 3/9/89	SS	SW	All-movable wing flutter, NASP related	AF
443	ATLAS II (Centaur)	6/18/89 -7/17/89	LV	FT	8.6%-scale, Ground wind loads, with umbilical tower, R-12/Air	LVGWL
446	Composite Aileron Buzz I	8/30/89 - 9/9/89	SS	SW	NASP, large trailing edge control, clipped-delta wing	AF
448	Composite Aileron Buzz II	9/26/89 - 10/7/89	SS	SW	NASP, large trailing edge control, clipped-delta wing	AF
449	MD Panel Flutter	9/23/89 - 10/14/89	O	SW	NASP, panel flutter	AF
454	Balsa Buzz I-b	3/4/90 - 3/17/90	SS	SW	NASP related	AF
458	Panel Flutter II	4/15/90 - 4/28/90	O	SW	NASP engine	AF
460	Composite Buzz III, L=60°, t=6%	7/29/90 - 8/11/90	SS	SW	NASP related	AF
464	Composite Buzz IV, L=72°, t=6%	10/14/90 - 10/20/90	SS	SW	NASP related	AF
466	Panel Flutter III	11/8/90 - 11/17/90	O	SW	NASP related	AF
471	Engine Panel Divergence/Flutter	4/21/92 - 5/30/92	O	SW	NASP, mounted on upstream end of PAPA splitter plate, NASP engine related	AF
476	NASP Flexible Fuselage	11/16/92 - 12/15/92	FS	FP	NASP related, body-freedom flutter (model destroyed, mount divergence)	AF
477	Wright Labs NASP Wing (Honz. Lifting Surface)	1/8/93 - 1/22/93	SS	SW	NASP configuration	AF
481	SWIF II Model	4/9/93 - 4/27/93	SS	SW	All-movable wing flutter, NASP related	AF
490	Wright Labs Fin-Rudder	2/7/94 2/14/94	SS	SW	NASP	AF
495	Engine Lip Divergence/Flutter	6/8/94 - 6/24/94	O	SW	NASP Engine related, classified test	AF
510	Delta II Launch Vehicle , Composite Payload	6/22/95 - 7/6/95	LV	S	16.5%-scale, Buffeting response	LVFD
519	Delta III Launch Vehicle	2/26/96 - 3/12/96	LV	S	9.5%-scale, Buffeting response	LVFD
540	Mars Airplane Aerodynamic Lift Concept Models	8/23/99 - 10/18/99	FS	S	1/4-scale, Performance test of MAP models(4) - loads, pressure distributions, hot film data	AF
541	Mars Airplane Aerodynamic Lift Concept Model (inverted tail)	12/6/99 - 12/14/99	FS	S	1/4-scale, Performance test MAP model - loads, flow viz (flourescent tufts (US))	AF

Model Type
FS = Full Span
LV = Launch Vehicle
O = Other
PD = Parachute/Decelerator
PW = Parawing
PP = Planetary Probe
SS = Semispan

Mount Type
C = Cables
F = Floor (no turntable)
FP = Floor Pedastal/Strut
FT = Floor with turntable
HR = Horizontal Rod (wall-to-wall)
PAPA = Pitch and Plunge Apparatus
S = Sting
SW = Sidewall

Category
AF = Atmospheric Flight
AR = Atmospheric Re-entry
LVFD = Launch Vehicle Flight Dynamics
LVGWL = Launch Vehicle Ground Wind Loads/Dynamics
PP = Planetary Probe